Kinematics of fibrous aggregates

Dissertation
zur Erlangung des Grades

"Doktor der Naturwissenschaften"

am Fachbereich Geowissenschaften
der Johannes Gutenberg Universität
in Mainz

Daniel Köhn
geboren in Karlsruhe

Mainz, März 2000

Tag der mündlichen Prüfung: 7.6.2000

Erklärung:

Ich versichere hiermit die vorliegende Arbeit selbstständig und nur unter der Verwendung der angegebenen Quellen und Hilfsmittel verfaßt zu haben.

Mainz, März 2000

All views presented here are those of the author, Daniel Köhn. All chapters including multiple author chapters are solely written by Daniel Köhn unless stated otherwise. Research and results presented in all chapters including multiple author chapters are the sole work of Daniel Köhn unless stated otherwise. Second, third and fourth authors have either supervised the work, offered study of their samples, helped during field work, introduced the author into computer programs or offered the use of previously developed methods. The computer program ”Fringe Growth” (Appendix) was developed by the author from an existing program ”Vein Growth” (by Bons). About 50% of the program was written by the author (Köhn), 50% is the older version of Bons. Chapter 2 is in press in the Journal of Structural Geology. Chapter 3 has been reviewed for the Journal of Structural Geology with positive advice. Chapter 4 is submitted to the Journal of Metamorphic Geology. Part of this research has been presented by the author at the following Conferences:

- Koehn, D., Bons, P.D. & Passchier, C.W. (1998) Modelling the tracking ability of fibrous crystals. GSA Abstracts w. Prog. 30(7), p. A-197.

- Koehn, D., Passchier, C.W. & Bons, P.D. (1999) Simulation of fibre growth in strain fringes. STSG, Schweizerisches Tektoniktreffen, Lausanne (Switzerland), Feb.

- Koehn, D., Passchier, C.W. & Bons, P.D. (1999) Kinematic analysis of strain fringes. EUG 10, Strasbourg (France), March.

- Koehn, D., Passchier, C.W. (1999) A Classification for Banded-Bedding-Parallel-Veins. Def. mech Conf., Neustadt a.d. Weinstrasse, Germany, 22-24 March.

- Koehn, D., Bons, P.D., Passchier, C.W., Aerden, D.G.A.M., (1999) Interpretation of fibre growth in strain fringes, GSA Abstracts w. Prog.

For

Vera

And the sun toiled across the sky.
Many people have wondered why. Some people think a giant dung beetle pushes it.
As explanations go it lacks a certain technical edge, and has the added drawback that, as certain circumstances may reveal, it is possibly correct.

Terry Pratchett "Pyramids"

There's no single definition of a "best" model, although quasi-religious wars are fought over the question.

Neil Gershenfeld "The Nature of Mathematical Modeling"

Acknowledgements:

First of all I want to thank my supervisor for all his help and patience. I have learned a great deal. I want to thank all the people at the Geological Institute at Mainz University for being a great bunch of people and a nice working group. I want to thank my parents for all their help especially during the last year and my family for their support and love.

I thank the reviewers of the Journal of Structural Geology for their comments and suggestions that helped to improve this work. Parts of the project were made possible by a visit to the Epsilon Earth Processes Simulation Laboratory, Dept. of Earth Sciences, Monash University, Clayton (Melbourne), Australia and by a visit to the University of Salamanca, Salamanca, Spain. Some people are thanked for their hospitality during the visits. This research was funded by the DFG-grant Pa 578/3.

Abstract

This thesis reports on a research into the progressive development of fibrous aggregates, e.g. calcite, quartz and mica crystals in veins and strain fringes. The study is based on microstructural analysis of natural examples and on computer experiments. Natural examples include striped calcite, quartz and mica veins from the Orobic Alps, northern Italy and antitaxial strain fringes of quartz, calcite and chlorite fibres around pyrite and iron-oxide crystals from the Yilgarn Craton and the Hamersley Ranges, West-Australia and from Lourdes in the northern Pyrenees, France. Thin-sections of the veins and strain fringes were studied in detail under an optical microscope to investigate the fibre patterns. To analyse progressive growth of fibrous aggregates in strain fringes, a two-dimensional computer model "Fringe Growth" was developed.

Investigation of fibrous looking elongate crystals in striped bedding-veins from the Orobic Alps, Italy indicate that these crystals do not track the opening trajectory of the veins but are oriented at an angle of up to 80° to the opening direction. These elongate crystals grow into open cracks and outgrow each other due to their crystal anisotropy. Inclusion trails in the veins can be used to determine the opening direction and the sense of shear along the bedding plane. A new classification of striped bedding-veins is being proposed. They are classified according to their internal segmentation into bedding-type (B-type), jog-type (J-type) and orthogonal-type (O-type) veins.

Microstructural analysis of quartz, calcite and chlorite fibres in antitaxial strain fringes indicate that most strain fringes contain complex intergrowth of tracking (displacement-controlled) and non-tracking (face-controlled) fibres. To explain these growth features the computer program "Fringe Growth" was developed. It can be used to model the incremental growth of fibrous crystals in antitaxial strain fringes. "Fringe Growth" is a two-dimensional numerical front-tracking model. Anisotropic growth of crystals is simulated by incremental movement of nodes which are connected by straight line segments that define the grain boundaries. The boundary of the model is the fringe-matrix contact; flow in the matrix cannot be modelled. Numerical experiments were undertaken to examine the progressive development of fibre patterns in detail. The results predict that face-controlled fibres develop on smooth surfaces on the core-object while displacement-controlled fibres are locked to outward-pointing asperities. The surface roughness of a core-object determines if fibres in the fringes will grow displacement- or face-controlled. Displacement-controlled fibres follow points on the core-object so that they record only relative core-object fringe movement and are not directly dependent on the orientation of the

extensional instantaneous stretching axes (ISA) or the orientation of the axis of maximum finite strain.

Computer experiments were performed using "Fringe Growth" to reproduce complex fibre patterns observed in antitaxial strain fringes from Lourdes, France. Relative core-object fringe movements (object-centre paths) were reproduced from thin-sections of the natural examples and these paths and the core-objects were used in the experiments. The resulting fibre patterns are very similar to the natural ones indicating that the fibre growth model is valid in nature. A new advanced classification of fibres is presented based on these experiments. Displacement-controlled and face-controlled fibres are end-members because fibres can switch from displacement- to face-controlled growth and form intermediate fibres. Fringes and core-object often rotate at different rates relative to an external reference frame resulting in relative core-object fringe rotation. This produces characteristic changing fibre curvatures. Once the fibre growth process is known and displacement-controlled fibres can be separated from other fibres, object-centre paths can be established, and these can be used to estimate finite strain in the matrix and the rotation rate of fringes.

Zusammenfassung

In dieser Studie wird die schrittweise Entwicklung von natürlichen Quarz-, Kalzit- und Glimmerfaseraggregaten in Kluftfüllungen und Verformungshöfen untersucht. Die Studie basiert auf mikrostrukturellen Untersuchungen natürlicher Proben, sowie auf Computerexperimenten. Als natürliche Proben wurden gestreifte Kalzit-, Quarz- und Glimmerkluftfüllungen aus den Orobischen Alpen (Italien) und antitaxiale Verformungshöfe mit Quarz-, Kalzit- und Chloritfasern um Pyrit- und Eisenoxidkristalle aus Leonora, Yilgarn Kraton und aus den Hamersley Ranges (Australien) sowie aus Lourdes in den nördlichen Pyrenäen (Frankreich) gewählt. Dünnschliffe der Proben wurden unter einem optischen Mikroskop detailliert untersucht. Um das schrittweise Wachstum der Faseraggregate in Verformungshöfen zu analysieren, wurde ein zweidimensionales Computerprogramm "Fringe Growth" entwickelt.

Die Untersuchungen von faserigen ausgelängten Quarzkristallen in gestreiften Schichtungskluftfüllungen aus den Orobischen Alpen (Italien) ergaben, dass diese Kristalle nicht der Öffnungsrichtung der Kluft folgen, sondern in einem Winkel von bis zu 80° zur Öffnungsrichtung gewachsen sind. Diese ausgelängten Kristalle wachsen in offene Spalten und überwachsen sich gegenseitig je nach Lage der kristallographischen C-Achse. Die Orientierung von Einschlüssen in den Kluftfüllungen ergeben die Öffnungsrichtung der Kluft und den Schersinn entlang der Schichtung. Gestreifte Schichtungskluftfüllungen können aufgrund ihrer internen Segmentierung in Schichtungtyp (B-Typ), Vorsprungtyp (J-Typ) und Orthogonaltyp (O-Typ) unterteilt werden.

Die mikrostrukturelle Analyse von Quarz-, Kalzit- und Chloritfasern in antitaxialen Verformungshöfen zeigt, dass die meisten Verformungshöfe komplex gewachsene Faseraggregate enthalten mit sowohl flächenkontrollierten Fasern, die nicht der Öffnungsrichtung folgen als auch Fasern, die der Öffnungsrichtung folgen. Um deren Wachstum zu untersuchen, wurde das numerische Computerprogramm "Fringe Growth" entwickelt. Mit dem Programm kann das schrittweise Wachstum von Fasern in antitaxialen Verformungshöfen analysiert werden. Das anisotrope Wachstum der Kristalle wird mit der Bewegung von Knotenpunkten simuliert, deren direkte Verbindungen die Kristallgrenzen definieren. Der Kontakt des Verformungshofes zum Nebengestein stellt den Rand des Modells dar. Numerische Experimente wurden durchgeführt, um das schrittweise Faserwachstum genau zu analysieren. Die Ergebnisse zeigen, dass flächenkontrollierte Fasern auf zentralen Objekten mit einer flachen Oberfläche wachsen. Fasern, die der Öffnungsrichtung folgen, folgen vorstehenden Vorsprüngen auf der Objektoberfläche. Die Oberflächenrauhigkeit des zentralen Objektes bestimmt, welche Fasern sich entwickeln. Da Fasern Punkten

auf dem zentralen Objekt folgen, zeigen sie die relative Bewegung und Rotation zwischen Objekt und Verformungshof an. Sie sind damit nicht direkt abhängig von der Lage der Extensionsachse im Nebengestein.
Computerexperimente wurden mit "Fringe Growth" durchgeführt, um komplexe Faseraggregate in natürlichen Verformungshöfen nachzubilden. Es wurden relative Bewegungen zwischen den Verformungshöfen und dem zentralen Objekt ermittelt und für die Simulationen verwendet. Die resultierenden Faseraggregate sind den natürlichen sehr ähnlich, sodass angenommen wird, dass das Wachstumsmodel realistisch ist. Gestützt auf die numerischen Experimente wurde eine erweiterte Klassifikation für Fasern erarbeitet. Flächenkontrollierte Fasern und Fasern, die der Öffnungsrichtung folgen, stellen Randgruppen dar. Fasern können von einem Wachstumsmechanismus zum anderen wechseln und intermediäre Fasern bilden. Die Verformungshöfe und die zentralen Objekte rotieren im Verhältniss zu einer externen Referenzachse häufig mit verschiedenen Geschwindigkeiten, sodass sie auch relativ zueinander rotieren. Dadurch entwickeln sich charakteristische Fasern mit variierender Krümmung. Ist der Wachstumsprozess der Fasern bekannt, kann man aus öffnungsrichtungkontrollierten Fasern die Öffnungsrichtung der Verformungshöfe und deren relative Rotation zum zentralen Objekt bestimmen (Objekt-Zentrum Pfade) und aus diesen die finite Verformung des Nebengesteins und die Rotationsrate der Verformungshöfe berechnen.

Index

page

1. Introduction: Problems and aims

In the first Chapter of this thesis a general introduction on fibrous aggregates and their use in structural geology is given. Special emphasis was laid on fibre growth hypotheses and structural analysis using fibres in veins and strain fringes. Major problems of existing theories are identified and aims and methods of the study are presented.

1.1. Background and previous work on fibrous aggregates

1.1.1. General introduction

In geology, fibrous aggregates are aggregates of crystals with a high length to width ratio or a "rod-like" shape (reviews in Ramsay and Huber, 1983; Passchier and Trouw, 1996). If these fibres occur in syntectonic veins and strain fringes they are of great importance to structural geologists since they are thought to contain information about progressive deformation of the host-rock (Mügge, 1928; Pabst, 1931; Zwart and Oele, 1966; Elliot, 1972; Durney and Ramsay, 1973; Wickham, 1973; Ramsay, 1980; Cox and Etheridge, 1983; Casey et al., 1983; Van Der Pluijm, 1984; Beutner and Diegel, 1985; Ellis, 1986; Cox, 1987; Etchecopar and Malavielle, 1987; Spencer, 1991; Urai et al., 1991; Fisher and Brantley, 1992; Aerden, 1996; Kanagawa, 1996; Bons and Jessell, 1997). This is due to the fact that these fibres grow while the host-rock is being deformed so that fibre length and orientation might reflect strain and vorticity of the host-rock. Different hypotheses and methods associated with the development of fibrous aggregates and their use to reconstruct progressive deformation are described in detail in sections 1.1.2. and 1.1.3. Veins and strain fringes as discussed in this thesis are dilatation sites in natural rocks where minerals are precipitated from an aquaeous solution. Veins are isolated elongate dilatation sites, while strain fringes develop next to a rigid object (core-object) embedded in a weaker deforming matrix (Fig. 1.1). Core-objects together with their strain fringes are termed fringe structures in this study.

1.1.1.1. Classification of veins and strain fringes

Veins are classified into antitaxial, syntaxial, composite or ataxial types depending on the location of the crystal growth surface (reviews in Ramsay and Huber, 1983; Passchier and Trouw, 1996). In veins antitaxial growth takes place at the vein wall-rock contact and syntaxial growth at the vein centre. Composite growth is a mixture of antitaxial and syntaxial growth and ataxial growth is defined as growth at random locations within a vein (Passchier and Trouw, 1996). In strain fringes, antitaxial growth takes place at the rigid-object fringe contact and syntaxial growth at the contact of the

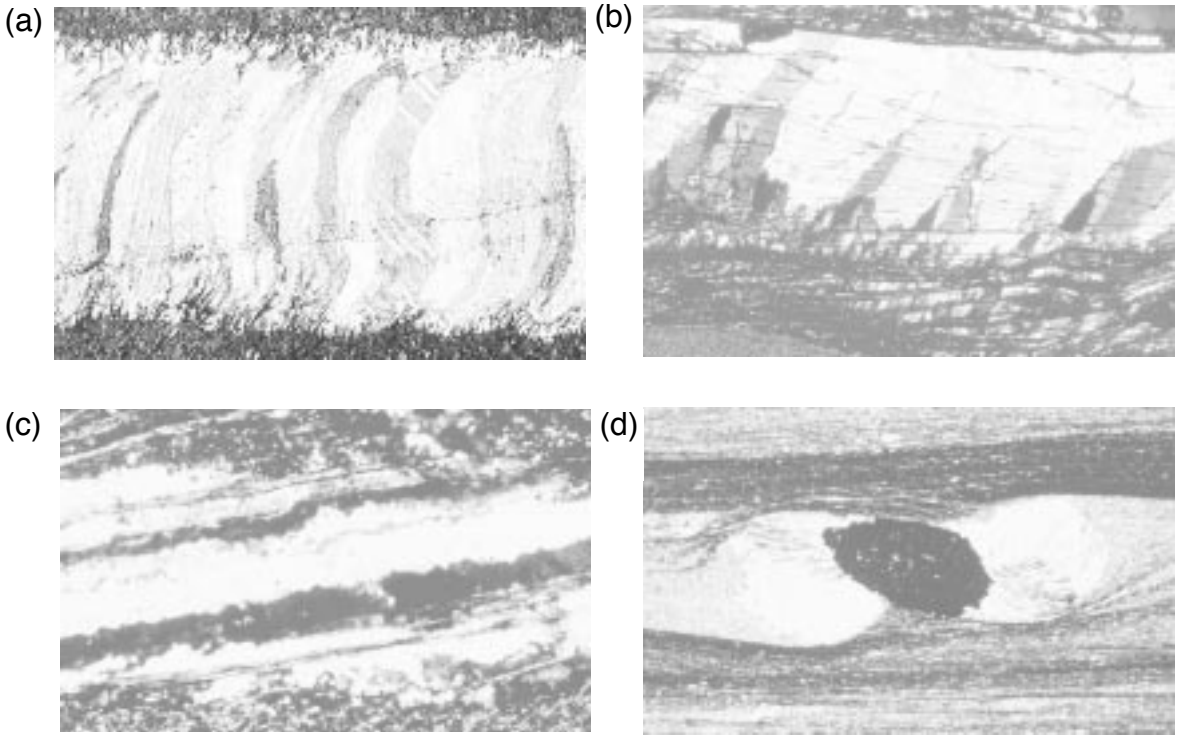

Fig. 1.1 (a) Micrograph of a fibrous vein from Sestri Levante, Italy. The vein is made up of quartz and calcite crystals. Width of view is 4 mm. (b) Micrograph of a vein from the Orobic Alps, Italy with elongate quartz crystals. Width of view is 15 mm. (c) Micrograph of slicken-fibres from the Orobic Alps, Italy. Width of view is 0.1 mm. (d) Micrograph showing a fringe structure from Lourdes, France. Quartz, calcite and chlorite crystals grow in a fibrous habit around an elongate pyrite core-object. Width of view is 20 mm.

fringe with the matrix (reviews in Ramsay and Huber, 1983; Passchier and Trouw, 1996). During syntaxial growth crystals grow from the wall-rock (veins) or from the rigid object (fringe structures) and vein or fringe mineralogy is the same as that of the host-rock (veins) or that of the rigid object (fringe structures). Antitaxial growth implies that the vein material is separated from the host-rock (veins) or rigid object (fringe structures) by the growth surface (although not necessarily detached). There is no overgrowth on the host-rock (veins) nor on the rigid object (fringe structures) (Fig. 1.2). Antitaxial growth in veins probably requires the formation of new nuclei at the time of "birth" of the vein. Crystals in antitaxial fringes, however, can grow syntaxially on the host-rock (antitaxially with respect to the rigid object) and no new nucleation is needed.

1.1.1.2. Crystal fabrics

The nomenclature for crystal fabrics in veins and strain fringes is still a matter of discussion (Mügge, 1928; Ramsay and Huber, 1983; Cox, 1987; Urai et al., 1991; Fisher and Brantley, 1992; Passchier and Trouw, 1996; Bons and Jessell, 1997). A

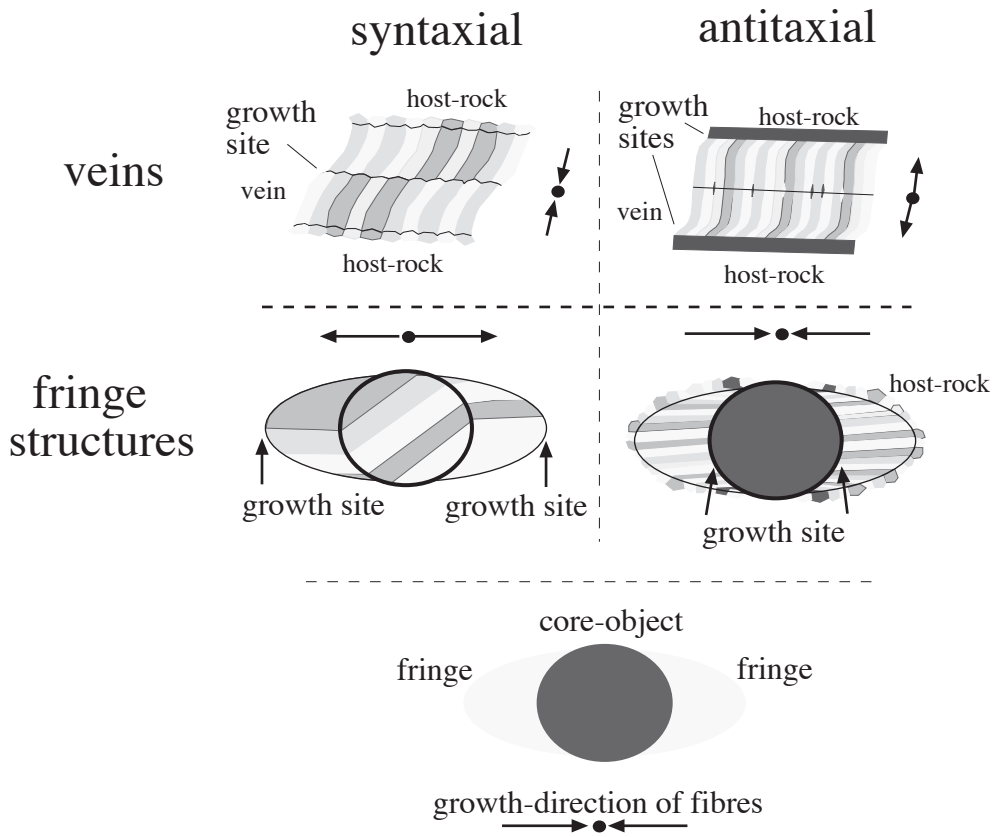

Fig. 1.2 Classification for veins and fringe structures based on the direction of crystal growth with respect to the host-rock (veins) and the core-object (fringe structures).

fibre is a crystal with a high length to width ratio in contrast to a blocky crystal that has a low length to width ratio (Taper, 1918; Mügge, 1928). Fisher and Brantley (1992) and Bons and Jessell (1997) introduced elongate crystals as a separate class of crystal fabric, they lie between fibres and blocky crystals (Fig. 1.3). Blocky crystals and fibres are the end-members of a continuum and elongate crystals are between these two.

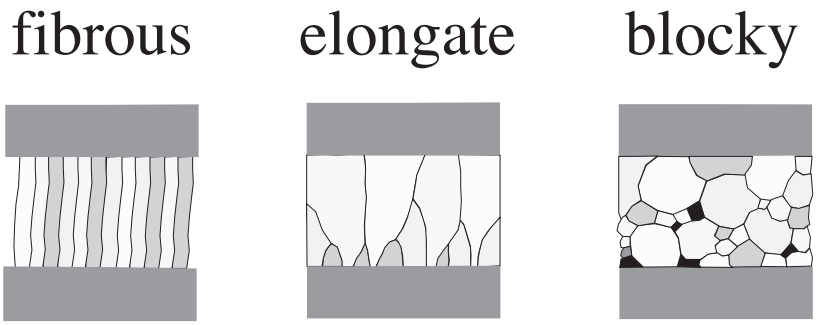

Fig. 1.3 Illustration of three crystal textures in veins that form a continuum where fibrous and blocky crystals are end-members.

Stretched crystals are a special kind of fibre (Ramsay and Huber, 1983). They commonly have serrated grain boundaries and show multiple internal fracture surfaces, which are interpreted to be an effect of ataxial growth (Ramsay and Huber, 1983). Elongate crystals will have a single growth surface between the host-rock and

the vein, whereas streched crystals grow at changing locations within the crystals themselves.

1.1.1.3. Vein- and fringe-forming processes

Several studies have tried to relate the crystal shape of fibres, elongate or stretched crystals to a vein or fringe forming process (e.g. Mügge, 1928; Fisher and Brantley, 1992; Bons and Jessell, 1997). Three processes have to operate together in order for crystals to grow in a vein or strain fringe (Fisher and Brantley, 1992; Bons and Jessell, 1997; Hilgers et al., in press): (1) dilatation of the vein or strain fringe, (2) transport of material to the vein or strain fringe and (3) precipitation of material and growth of crystals in the vein or strain fringe. Process (1) is due to deformation of the matrix so that fractures develop and dissolution precipitation processes take place. Process (2) can be either transport through a stationary fluid by diffusional transport or flow with a fluid through fractures or pores. Process (3) can be due to differences in pressure, temperature or chemistry between host-rock and vein or strain fringe that result in precipitation of material from a solution. The relative rates at which transport, dilatation and precipitation processes operate have a strong influence on the microstructure of veins and strain fringes (Fisher and Brantley, 1992; Bons and Jessell, 1997; Hilgers et al., in press). Mügge (1928) discussed three different cases of crystal growth rate relative to dilatation (for anisotropically growing crystals) (Fig. 1.4): (1) the dilatation rate is faster than the maximum growth rate of crystals (which is rate-controlling), (2) the crystal growth rate can partly keep up with dilatation rate and (3) the dilatation rate is slower than the crystal growth rate and thus rate-controlling. In case (1) facetted blocky crystals will form (with a strong CPO), in case (2) crystal growth will be partly inhibited so that elongate crystals will form (with a CPO (Cox and Etheridge, 1983)) and in case (3) growth will be strongly inhibited so that fibrous crystals will develop (with no CPO (Papst, 1931)).

Two different processes have been proposed for the dilatation of a vein or a strain fringe (Fig. 1.5): (1) continuous opening (Durney and Ramsay, 1973) and (2) the crack-seal mechanism (Ramsay, 1980). Continuous opening is similar to Mügge's case three were minerals are precipitated in a vein or fringe while it is opening so that growth takes place in a grain boundary rather than in a crack. The crack-seal mechanism implies the formation of a distinct open fracture which is sealed by growing crystals and then opens again. Whether or not these two processes form a continuous range where a very narrow crack is similar to a wide grain boundary is a matter of discussion (Bons and Jessell, 1997; Hilgers et al., in press). A wide grain boundary can probably still support a differential stress in contrast to an open fluid filled fracture. The present literature gives no reliable criteria to attribute a certain

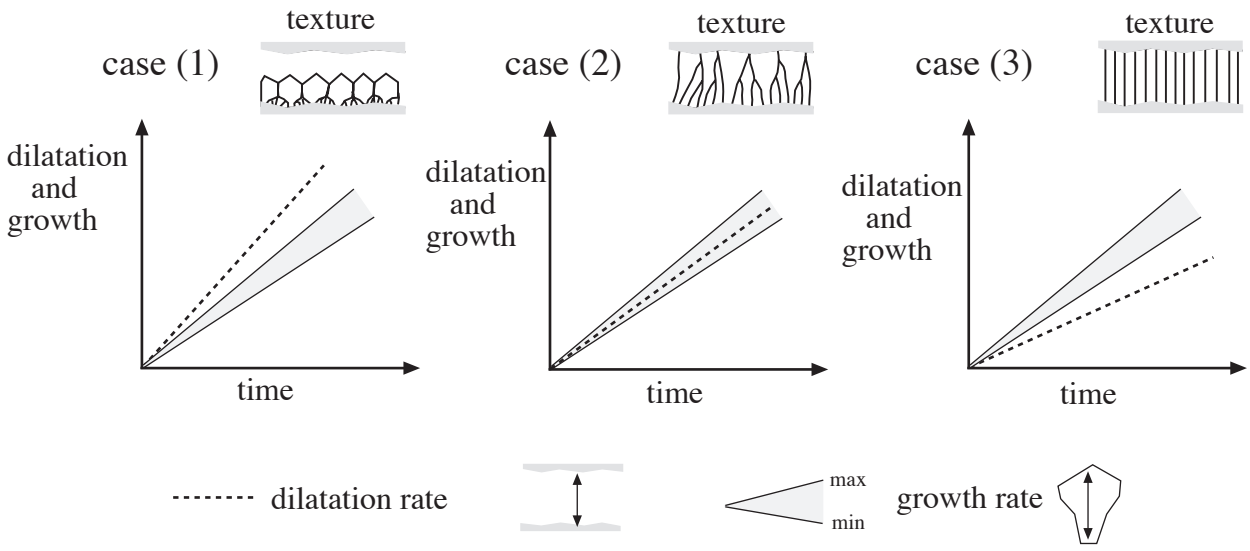

Fig. 1.4 Three cases of different dilatation rate of veins relative to growth rate of crystals after Mügge (1928). Dilatation is measured perpendicular to the wall-rock. Crystal growth rate is measured as length of crystals perpendicular to the wall-rock per time unit and is plotted for free crystal growth. Crystals grow anisotropically so that they have a maximum and a minimum growth rate depending on their crystallographic orientation with respect to the growth surface.

crystal shape to a vein or fringe forming process. Elongate or blocky crystals as well as stretched crystals are probably formed by the crack-seal mechanism since the crystals did grow at least partly into an open space or show distinct internal fracture surfaces (stretched crystals) (Ramsay and Huber, 1983; Cox, 1987; Bons and Jessell,

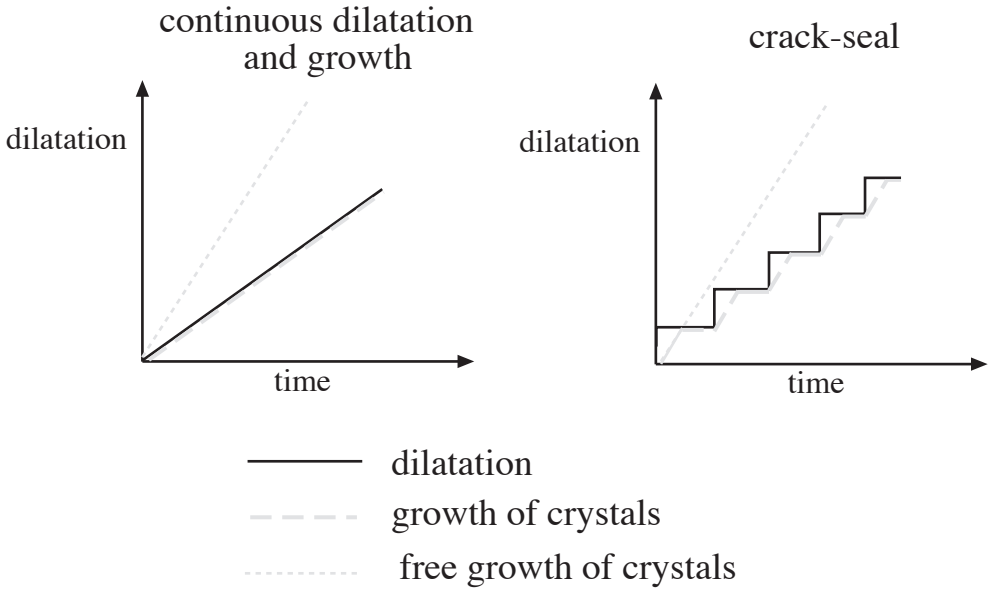

Fig. 1.5 Plots of dilatation rate and growth rate to illustrate the differences between continuous dilatation and crack-seal (after Passchier and Trouw, 1996).

1997). Fibrous crystals may form by both processes, continuous growth and crack-seal growth in narrow cracks (Hilgers et al., in press). If veins contain inclusion bands

of solid inclusions they are thought to have developed by the crack-seal process, where single inclusion bands are thought to have formed during single fracture events (Ramsay, 1980; Ramsay and Huber, 1983; Cox, 1987; Fisher and Brantley, 1992). This has been at least partly challenged by experiments of Li and Means (1995) and Means and Li (1995a,b) which showed that inclusion bands can develop during continuous growth of crystals if impurities are trapped at the growth surface during growth.

Irrespective of the fibre-forming process, fibres have been used to determine progressive deformation histories of host-rocks as noted above. Hypotheses on fibre growth and different methods which are commonly used for structural analysis of fibrous aggregates are discussed in detail in the following sections.

1.1.2. Fibre growth hypotheses

If fibres are curved without showing evidence for internal deformation (White and Wilson, 1978; Williams and Urai, 1989) they may record a change in the extension direction of a vein or strain fringe and track the displacement of two once adjacent points (Elliot, 1972; Durney and Ramsay, 1973; Wickham, 1973; Ramsay and Huber, 1993; Ellis, 1986; Urai et al., 1991; Spencer, 1991). This ”tracking hypothesis” of fibres

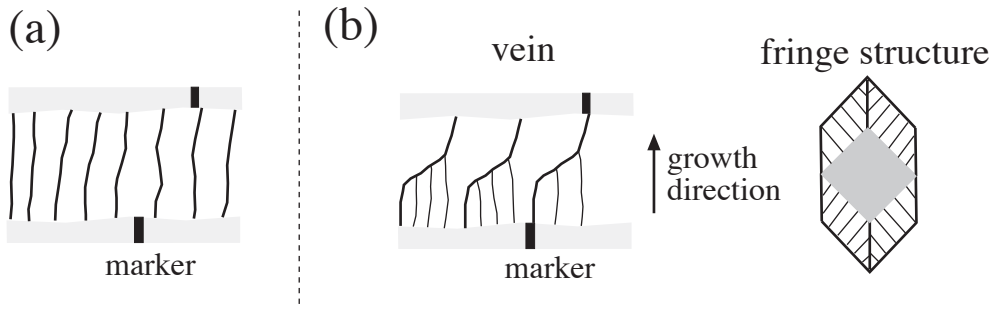

Fig. 1.6 Not all fibres in veins and strain fringes track the opening trajectory because (a) fibres do not connect markers on each side of some veins and (b) fibres grow in different directions in some veins and fringe structures.

has been challenged by two observations of natural fibre patterns: (1) fibres do not always connect markers on each side of a vein (Van der Pluijm, 1984; Cox, 1987; Urai et al., 1991) and (2) different fibres in a single vein or fringe may grow in different directions (Papst, 1931; Ramsay and Huber, 1983) (Fig. 1.6). Fibres growing in different directions are especially common in fringe structures. In order to explain this, fibres in strain fringes have been classified into face-controlled and displacement-controlled fibres (reviews in Ramsay and Huber, 1983; Passchier and Trouw, 1996). Face-controlled fibres grow perpendicular to the face of a core-object while displacement-controlled fibres are thought to follow the opening trajectory of a fringe. This classification has been extended to veins (Urai et al., 1991; Hilgers et al., in

press) where displacement-controlled fibres are termed tracking fibres, face-controlled fibres are termed non-tracking fibres and partial-tracking fibres are defined as an intermediate class between tracking and non-tracking end-members. Geologists are generally interested in tracking- or displacement-controlled fibres since these can be used to reconstruct progressive deformation of the host-rock (Elliot, 1972; Wickham, 1973; Durney and Ramsay, 1973; Ramsay and Huber, 1983; Beutner and Diegel, 1985; Ellis, 1986).

Two different fibre growth hypotheses can be found in the literature: (1) fibre growth parallel to the least stress (Durney and Ramsay, 1973) and (2) fibres following asperities on the wall-rock (Urai et al., 1991) or core-object. Hypothesis (1) states that fibres may grow parallel to the least stress because crystals will have to overcome the smallest force if they grow in that direction (Durney and Ramsay, 1973). Hypthesis (2) states that tracking fibres will follow outward-pointing asperities (Urai et al., 1991) on the host-rock of a vein if a newly-formed crack is sufficiently small with respect to the

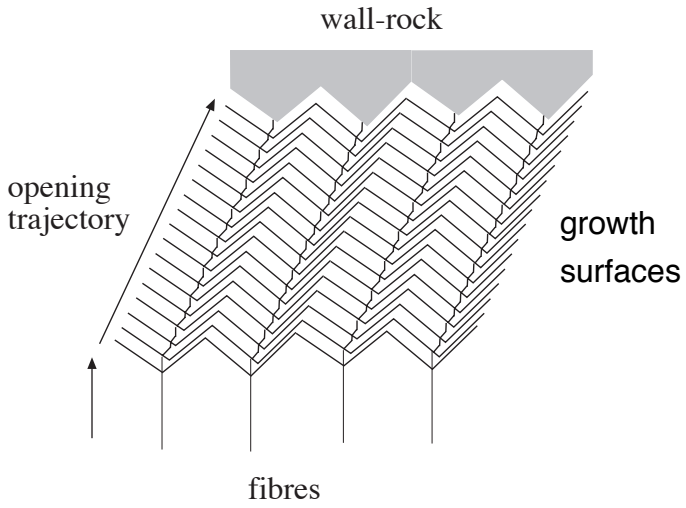

Fig. 1.7 Fibre tracking hypothesis after Urai et al. (1991). Fibres grow isotropically in this example. They are locked to outward pointing asperities on the wall-rock. If the opening trajectory of the vein changes, fibres grow first straight. After the next opening event they will grow perpendicular to the side of an asperity so that they grow back towards its tip which results in fibre boundaries that follow the opening trajectory.

size of the asperity and if crystals can fill this crack before it opens again. A simple geometrical consideration shows that fibre boundaries will in that case be locked to outward pointing asperities because their growth surface is a cast of the host-rock with similar asperities (Fig. 1.7). This is discussed in detail in Chapter 3 of this thesis. The hypothesis that fibres grow in the direction of the least stress cannot explain the occurence of non-tracking, partial-tracking or face-controlled fibres but may only work for displacement-controlled or tracking fibres. The fibre growth hypothesis of Urai et

al. (1991) can explain the occurence of different fibres in one vein/fringe. This has been shown by Hilgers et al. (1997), Bons (in press.) and Hilgers et al. (in press) with numerical experiments on fibre growth in veins.

1.1.3. Fibres in structural analysis

Fibres in veins and strain fringes have been used for structural analysis based on different assumptions which are related to the described growth or tracking hypotheses. Special emphasis was put on the evaluation of the orientation and magnitude of the incremental strain ellipse in the host-rock. The following assumptions have been used for fibre analysis: (1) fibres grow parallel to the extensional incremental stretching axis (ISA, the eigenvectors of the non-rotational part of the flow tensor (Means et al. 1980)) (Durney and Ramsay, 1973; Ramsay and Huber, 1983; Ellis, 1986), (2) fibres grow parallel to the incremental finite strain axis (Beutner and Diegel, 1985) and (3) fibres follow points on the core-object in fringe structures and on the wall-rock in veins (Etchecopar and Malavielle, 1987; Urai et al., 1991; Aerden, 1996). An analysis based on these three assumptions will lead to the same results if progressive deformation is coaxial and if fringes, core-objects and

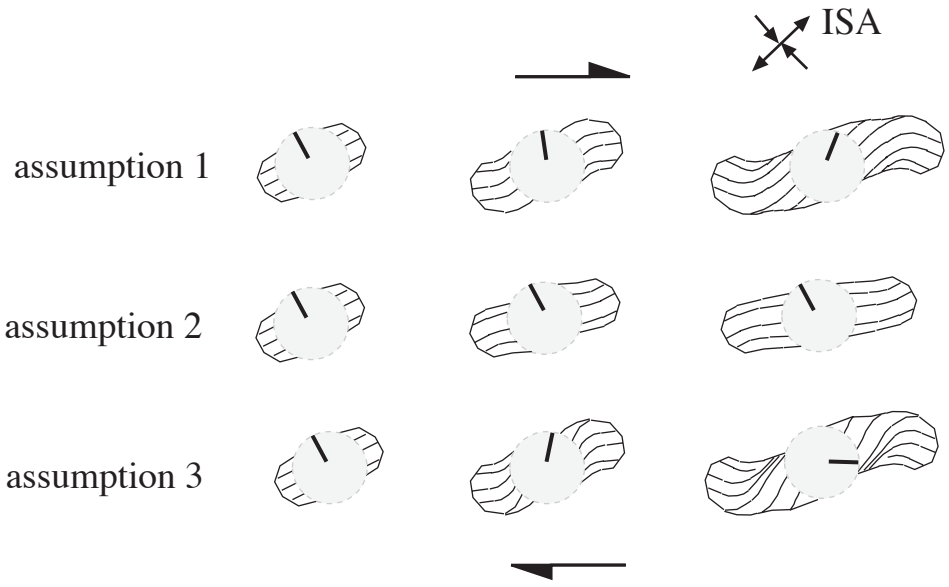

Fig. 1.8 Fibre patterns that develop during non-coaxial progressive deformation based on the three different assumptions discussed in the main text. (1) Fringes and core-object rotate at the same rate with respect to ISA and fibres grow parallel to extensional ISA. (2) Fringes and core-object do not rotate with respect to ISA and fibres grow parallel to the axis of maximum finite strain. (3) The core-object rotates twice as fast as its fringes with respect to ISA so that the core-object rotates relative to its fringes, and fibres follow points on the core-object.

veins are not rotating with respect to ISA (Aerden, 1996). However, if fringes, core-objects and veins are rotating with respect to ISA, for example during non-coaxial

progressive deformation, the three assumptions will lead to different results (Fig. 1.8). This is due to the fact that (a) the long axis of the finite strain ellipse is not parallel to the extensional ISA during non-coaxial deformation (Ramsay, 1967; Means, 1979; Means et al., 1980) and (b) if fibres follow points on the core-object or vein wall they will only record relative movement between once adjacent points and not necessarily the orientation of the extensional ISA in all cases (Casey et al., 1983; Ellis, 1986; Aerden, 1996). Because of point (b) it is important to separate assumption 1 from assumption 3 even though some geologists (Wickham, 1973; Ramsay and Huber, 1983; Kanagawa, 1996) treat assumption 3 and assumption 1 as being identical. It is therefore necessary to consider the three assumptions in more detail.

Assumption 1, fibres grow parallel to the extensional ISA: the assumption that fibres grow parallel to the extensional ISA is used by most geologists. It is based on two different hypotheses: (1) fibres grow parallel to the least stress (Durney and Ramsay, 1973) or (2) fibres follow outward pointing asperities (Urai et al., 1991). Hypothesis (1) has been discussed in the previous section. It cannot explain the occurence of tracking/displacement-controlled and non-tracking/face-controlled fibres in one vein/fringe. The validity of hypothesis (2) does not necessarily imply that fibres grow parallel to the extensional ISA since for example relative rotation between core-object and fringes does influence fibre patterns (Aerden, 1996). Therefore Ellis (1986) assumed that round core-objects do not rotate relative to their fringes. This was challenged by Aerden (1996) who has shown that core-objects with low aspect ratios do rotate relative to their fringes.

Assumption 2, fibres grow parallel to axis of maximum finite strain: the assumption that fibres grow parallel to the maximum finite strain axis during coaxial and non-coaxial deformation was put forward by Beutner and Diegel (1985). They assumed that core-object and fringes are not rotating with respect to ISA and that fringes are being pulled away from the core-object in the direction of the maximum finite strain axis. As a consequence even the sense of shear determined from fringe structures will be different to a shear sense evaluation based on assumptions 1 and 3 (discussion in Aerden, 1996). Since fringes and core-objects are rigid objects in a weaker matrix it seems unrealistic to assume that they are not rotating with respect to ISA in non-coaxial progressive deformation (Jeffrey, 1922; Ghosh and Ramberg, 1976).

Assumption 3, fibres follow points: the assumption that displacement-controlled fibres follow points on the core-object or the vein wall has been put forward by Elliot (1972), Wickham (1973), Ramsay and Huber (1983), Ellis (1986), Etchecopar and Malavielle (1987) and Aerden (1996). This assumption is in agreement with the tracking hypothesis of Urai et al. (1991).

If assumption 1 is valid, single fibres can be used to determine incremental and finite

strain of the host-rock in non-deformable strain fringes (Wickham, 1973; Durney and Ramsay, 1983) and two fibres in a fringe can be used to determine incremental and finite strain and area changes in deformable strain fringes (Ellis, 1986; Ramsay and Huber, 1983; review in Spencer, 1991). If assumption 3 is valid and core-objects rotate relative to their fringes Aerden's method (Aerden, 1996) has to be used for a structural analysis of non-deformable fibres instead of a single fibre analysis. Assumption 2 is irrealistic as shown previously.

1.2. Remaining problems

1.2.1. Kinematic problems

Apart from the problem of assumption for fibre growth direction, a number of kinematic problems exist in fibre analysis of veins and strain fringes. These can be separated into three groups: (1) the validity of basic growth hypotheses, (2) the reliability of structural analysis using fibres and (3) the rotation of fringe structures and veins during coaxial and non-coaxial flow. Basic growth hypotheses have to be established and tested before a structural analysis can be undertaken because a structural analysis relies directly on a growth hypothesis.

Basic growth hypotheses: the growth hypothesis of Urai et al. (1991) as described in section 1.1.2. was tested for fibres in veins by Hilgers et al. (1997), Bons et al. (in press) and Hilgers et al. (in press) using numerical experiments. It has not been tested by growth experiments nor has it been tested numerically for fibre patterns in strain fringes which commonly show more complex intergrowth structures than fibres in veins. These tests should be undertaken to see if the Urai et al. (1991) hypothesis is valid and can explain all fibre patterns observed in nature.

Structural analysis using fibres: if the growth hypothesis of Urai et al. (1991) is valid this has a number of implications for structural analysis using fibres in strain fringes and veins. Some of these implications have been discussed by Urai et al. (1991), Hilgers et al. (1997), Bons (in press) and Hilgers et al. (in press) for veins and by Aerden (1996) for strain fringes. These authors, however, have not discussed in how far conventional strain analysis can be used or if new methods have to be developed. The growth hypothesis of Urai et al. (1991) becomes more and more accepted but its implication on fibre analysis in strain fringes is not clear.

Rotation of fringe structures and veins during coaxial and non-coaxial flow: the rotational behaviour of fringes and veins during coaxial and non-coaxial flow is incompletely understood. This is especially true for fringe structures since these contain three rigid objects (core-object and two fringes) that might rotate at different rates with respect to ISA and may influence each other (Ghosh and Ramberg, 1976; Ildefonse et al., 1992b). As an extra complication, the two fringes progressively

increase their size and change their shape and this will influence their rotational behaviour. Kanagawa (1996) has tried to address this point using the formulas of Jeffrey (1922) for rigid body rotation. He treated the fringe structure as one rigid object, but this is not in agreement with the commonly observed rotation of the core-object with respect to its fringes (Aerden, 1996). It is important to know how fringe structures and veins rotate with respect to ISA during coaxial and non-coaxial flow in order to obtain estimates on the kinematic vorticity number of flow in the host-rock from fibres and in order to distinguish between single- and polyphase deformation.

1.2.2. Dynamic problems

A number of dynamic problems concerning fibre growth still exist, which can be separated into two different categories: (1) processes of vein and fringe formation and (2) external conditions of vein and fringe formation.

Processes of vein and fringe formation: the main questions concerning the process of formation of veins and fringes are (1) does the material that is precipitated come from a local or distant source, (2) is the material transported by diffusion or fluid flow towards the growth site, (3) does the fringe or vein open by a crack seal process or by a continuous growth process and (4) can the microstructure (fibres, elongate crystals or blocky crystals) be used to determine which process or processes were active? Even though these questions have been discussed by numerous authors (e.g. Mügge, 1928; Cox and Etheridge, 1983; Fisher and Brantley, 1992; Henderson and McCaig, 1996; Bons and Jessell, 1997) there are still a number of uncertainties. For example, can one unequivocally deduct a fringe/vein-forming process solely from the crystal morphology ?

External conditions of vein and fringe formation: a general classification is needed that relates the formation of veins and fringes and their internal textures to external conditions like temperature, differential pressure, bulk strain or chemistry of the host-rock. Some authors have tried to address this issue (e.g. Strömgård, 1973; Cox and Etheridge, 1983; Selkman 1983; Fisher and Brantley, 1992). It would be interesting to know what external conditions are needed for a vein or a fringe to form. In that case one could constrain the external conditions that existed during deformation of the host-rock if it contains veins or fringes with specific morphology (e.g. fibres).

1.3. Aims and methods

The aims of this study were (a) to investigate progressive fibre growth in veins and strain fringes in order to obtain a better understanding of the growth process of fibrous aggregates and (b) to revise the use of fibres for structural analysis. In order to achieve these aims the following methods were used: (1) investigation of natural

fibrous aggregates to understand the fibre growth process, (2) systematic numerical experiments on fibre growth, (3) numerical experiments to reproduce natural fibre patterns and (4) discussion of implications of results from methods 1-3 on structural analysis of fibrous aggregates.

Natural fibres: for the investigation of natural fibrous aggregates veins were used from the Orobic Alps (Italy) and strain fringes from Leonora (Yilgarn Craton, Australia), Hamersley Ranges (Australia) and Lourdes (France). Chapter 2 describes striped bedding-veins (from the Orobic Alps) that contain elongate and fibrous quartz and calcite crystals and solid inclusion bands. Chapters 3 and 4 describe fibrous aggregates in antitaxial strain fringes (from the Yilgarn Craton, Hamersley Ranges and Lourdes). Fibrous aggregates in strain fringes are ideal to study the fibre growth process as they usually contain a large variety of tracking and non-tracking fibres. The aim was to establish the relationship between different fibres, between fibres and the host-rock/core-object and between fibre growth direction and deformation of the host-rock in order to understand the fibre growth process.

Systematic numerical experiments: for the numerical experiments a computer model "Fringe Growth" was developed to investigate incremental fibre growth and to reproduce natural fibre patterns in antitaxial strain fringes. "Fringe Growth" is based on the model "Vein Growth" by Bons (in press). The program was written in ”C”. The existing ”Vein Growth” code was revised and about 100 new functions have been added (code ”Fringe Growth” consists now of about 240 functions) so that about 50% of the code was written anew. "Fringe Growth" and "Vein Growth" both use the fibre growth model of Urai et al. (1991) which has the potential to explain complex fibre patterns found in antitaxial strain fringes and veins. Systematic computer experiments were undertaken with "Fringe Growth" (Chapter 3) to study the effects of core-object surface morphology, core-object shape and variations in the opening trajectory (object-centre path) on the morphology of fibre patterns in fringes.

Numerical experiments to reproduce natural fibrous aggregates: additional numerical experiments with "Fringe Growth" were undertaken to reproduce fibre patterns in strain fringes from the Yilgarn Craton (Chapter 3) and Lourdes (Chapter 4). These strain fringes contain complex intergrowth patterns of fibres which were investigated in detail in order to test the growth hypothesis of Urai et al. (1991) and in order to investigate how such complex fibre patterns develop incrementally and how they can be used for structural analysis. Special emphasis was put on investigation of progressive fibre growth around core-objects of different shape.

Implications for structural analysis: based on the computer experiments and the method of Aerden (1996) the validity of common methods of structural analysis using fibres in strain fringes is discussed in Chapters 3 and 4. A new method was developed

and is described in Chapter 4 to interpret antitaxial strain fringes and this method is used for samples from Lourdes. The bulk shear strain of the Lourdes rocks is calculated and rotation of fringes with respect to extensional ISA is estimated.

1.4. Concluding remarks

In this study a kinematic approach is used to investigate fibrous aggregates. As noted in the previous section dynamic questions are also important. A kinematic approach is used for two reasons: (1) before the dynamics of fibrous crystal growth can be investigated the kinematics of crystal growth should be known and (2) a kinematic approach is already able to clarify how fibres can be used for structural analysis (strain- and vorticity analysis). Dynamic analysis is not so much hampered by possibilities of numerical modelling, which are able to tackle the problem, but by the lack of reliable data on rheology of fibres and wall-rock, and on fluid flow in rocks.

This thesis is structured into five chapters. Chapter 1 contains a general introduction and Chapters 2 to 4 are presented in paper form(with minor changes in layout to fit this thesis). In Chapter 2 striped bedding-veins from the Orobic Alps are described (" Shear sense indicators in Striped Bedding-Veins", in press, Journal of Structural Geology), in Chapter 3 systematic numerical experiments performed with "Fringe Growth 1.3" are described ("Numerical Simulation of Fibre Growth in Antitaxial Strain Fringes", in review, Journal of Structural Geology) and in Chapter 4 numerical experiments with "Fringe Growth 2.0" are described and a new method to interpret fibre patterns in strain fringes is presented ("Computer experiments to investigate complex fibre patterns in natural antitaxial strain fringes", submitted, Journal of Metamorphic Geology). In Chapter 5 general conclusions are presented and suggestions for further research are given. The appendix contains a description and a user manual of the computer program "Fringe Growth" and a CD-ROM with "Fringe Growth 1.3", "Fringe Growth 2.0" and Quicktime movies of progressive fibre growth.

References

Aerden, D.G.A.M., 1996. The pyrite-type strain fringes from Lourdes (France): indicators of Alpine thrust kinematics in the Pyrenees. Journal of Structural Geology 18, 75-91.

Beutner, E.C., Diegel, F.A., 1985. Determination of fold kinematics from syntectonic fibers in pressure shadows, Martinsburg Slate, New Jersey. American Journal of Science 285, 16-50.

Beutner, E.C., Fischer, D.M., Kirkpatrick, J.L., 1988. Kinematics of deformation at a thrust fault ramp (?) from syntectonic fibers in pressure shadows. In: Geometries and Mechanisms of Thrusting, With Special Reference to the Appalachians (edited by Mitra, G. & Wojtal, S.). Special Paper of the Geological Society of America 222, 77-88.

Bons, P.D., Jessell, M.W., 1997. Experimental simulation of the formation of fibrous veins by localised dissolution-precipitation creep. Mineralogical Magazine 61, 53-63.

Casey, M., Dietrich, D., Ramsay, J.G., 1983. Methods for determining deformation history for chocolate tablet boudinage with fibrous crystals. Tectonophysics, 92, 211-239.

Clark, M.B., Fisher, D.M., Chia-Yu, L., 1993. Kinematic analysis of the Hfuehshan Range: A large-scale pop-up structure. Tectonics 12, 205-217.

Cox, S.F., Etheridge, M.A., 1983. Crack-seal fibre growth mechanisms and their significance in the development of oriented layer silicate microstructures. Tectonophysics 92, 147-170.

Cox, S. F., Etheridge, M. A. & Wall, V. J., 1986. The role of fluids in synectonic mass transport and the localization of metamorphic vein-type ore deposits. Ore Geol. Rev. 2 65-86.

Cox, S. F., 1987. Antitaxial crack-seal vein microstructures and their relationship to displacement paths. Journal of Structural Geology 9, 779-787.

Durney, D.W., Ramsay, J.G., 1973. Incremental strains measured by syntectonic crystal growths. In: DeJong, K.A., Scholten, R. (Eds), Gravity and Tectonics, Wiley, New York, 67-95.

Elliot, D., 1972. Deformation paths in structural geology. Bull. geol. Soc. Am. 83, 2621-2638.

Ellis, M.A., 1986. The determination of progressive deformation histories from antitaxial syntectonic crystal fibres. Journal of Structural Geology 8, 701-709.

Etchecopar, A., Malavielle, J., 1987. Computer models of pressure shadows: a method for strain measurement and shear sense determination. Journal of Structural Geology 9,667-677.

Fisher, D.M., 1990. Orientation history and rheology in slates, Kodiak and Afognak Islands, Alaska, Journal of Structural Geology 12, 483-498.

Fisher, D.M., Brantley, S.L., 1992. Models of Quartz Overgrowth and Vein Formation: Deformation and Episodic Fluid Flow in an Ancient Subduction Zone. Journal of Geophysical Research 97, 20043- 20061.

Fisher, D. & Anastasio, D. J., 1994. Kinematic analysis of a large-scale leading edge fold, Lost River Range, Idaho. Journal of Structural Geology 16, 337-354.

Ghosh, S.K., Ramberg, H., 1976. Reorientation of inclusions by combination of pure shear and simple shear. Tectonophysics 34, 1-70.

Hedlund, C.A., Anastasio, D.J., Fisher, D.M. 1994. Kinematics of fault-related folding in a duplex, Lost River Range, Idaho, U.S.A.. Journal of Structural Geology 16, 571-584.

Henderson, I. H. C. & McCaig, A. M. 1996. Fluid pressure and salinity variations in shear zone-related veins, central Pyrenees, France: implications of the fault-valve model. Tectonophysics 262, 321-348.

Hilgers, C., Urai, J.L., Post, A.D., Bons, P.D., 1997. Fibrous vein microstructure: Experimental and numerical simulation. Aardkundige Mededelingen 8, 107-109.

Ildefonse, B., Sokoutis, D., Mancktelow, N.S., 1992. Mechanical interactions between rigid particles in

a deforming ductile matrix. Analogue experiments in simple shear flow. Journal of Structural Geology 10, 1253-1266.

Jeffrey, G.B., 1922. The motion of ellipsoidal particles immersed in a viscous fluid. Proc. R. Soc. Lond. 102, 161-179.

Kanagawa, K., 1996. Simulated Pressure Fringes, Vorticity, and Progressive Deformation. In: De Paor, D. G. (Ed.), Structural Geology and Personal Computers. Computer Methods in the Geosciences 15, 259-283.

Li, T. & Means, W. D. 1995. Experimental antitaxial growth of fibrous crystals 1: technique, fibre character, and implications. GSA Annual Meeting Conf. Abstr.

Means, W.D., 1979. Stress and strain. Springer, Berlin Heidelberg New York.

Means, W.D., Hobbs B.E., Lister G.S., Williams P.F., 1980. Vorticity and non-coaxiality in progressive deformations. Journal of Structural Geology 2, 371-398.

Means, W.D. & Li, T., 1995a. Experimental antitaxial growth of fibrous crystals. II: internal structures. GSA Annual Meeting Conf. Abstr.

Means, W.D. & Li, T., 1995b. Tracking and non-tracking experimental fibrous veins. GSA Annual Meeting Conf. Abstr.

Mügge, O., 1928. Ueber die Entstehung faseriger Minerale und ihrer Aggregationsformen. Neues Jahrbuch für Mineralogie, Geologie und Paläontologie 58A, 303-438.

Pabst, A., 1931. 'Pressure shadows' and the measurement of the orientation in rocks. Journal of the Mineralogical Society of America 16, 55-70.

Passchier, C.W., Trouw, R.A.J., 1996. Microtectonics. Springer, Heidelberg, 289 pp.

Ramsay, J.G., 1967. Folding and fracturing of rocks. McGraw Hill, New York.

Ramsay, J.G., 1980. The crack-seal mechanism of rock deformation. Nature 284,135-139.

Ramsay, J.G., Huber, M.I., 1983. The techniques of modern structural geology, 1: Stain analysis. Academic Press, London.

Sample, J.C., Fisher, D.M., 1986. Duplex accretion and underplating in an ancient accretionary complex, Kodiak Islands, Alaska. Geology 14, 160-163.

Selkman, S. O., 1983. Stress and displacement distributions around pyrite grains. J. Struct. Geol. 5 (1), 47-52.

Spencer, S., 1991. The use of syntectonic fibres to determine strain estimates and deformation paths: an appraisal. Tectonophysics 194, 13-34.

Strömgård, K.-E., 1973. Stress distribution during formation of boudinage and pressure shadows. Tectonophysics 16, 215-248.

Taber, S., 1918. The origin of veinlets in the Silurian and Devonian strata of central New York. Journal of Geology 6, 56-73.

Urai, J.L., Williams, P.F., Van Roermund, H.L.M., 1991. Kinematics of crystal growth in syntectonic fibrous veins. Journal of Structural Geology 13, 823-836.

Van Der Pluijm, B.A., 1984. An unusual 'crack-seal' vein geometry. Journal of Structural Geology 6, 593-597.

White, S.H. and Wilson, C.J.L., 1978. Microstructure of some quartz pressure fringes. Neues Jahrb. Mineral. Geol. Palaeont. 134, 33-51.

Wickham, J.S., 1973. An estimate of strain increments in a naturally deformed carbonate rock. American Journal of Science 237, 23-47.

Wickham, J.S., Anthony, M., 1977. Strain paths and folding of carbonate rocks near Blue Ridge, central Appalachians. Bulletin of the geological Society of America 88, 920-924.

Williams, P. F. & Urai, J. L., 1987. Curved vein fibres: an alternative explanation. Tectonophysics 158, 311-333.

Zwart, H.J. & Oele, J.A., 1966. Rotated magnetite crystals from the Rocroi Massif (Ardennes). Geol. Mijnb. 45, 70-74.

2. Shear sense indicators in Striped Bedding-Veins

in press, Journal of Structural Geology

Daniel KOEHN, Cees W. PASSCHIER
Department of Geology, Johannes Gutenberg Universität, Becherweg 21, 55099 Mainz, Germany,
E-mail: koehn@mail.uni-mainz.de

Abstract

Striped bedding-veins are veins that lie subparallel to bedding and have an internal layering or lineation at a small angle to the veins' long axis. They form during bedding-parallel slip and can be used as shear sense indicators. Solid inclusion trails produce the visible internal layering or lineation and track the opening direction of the veins. Elongate quartz crystals however can be oriented at an angle of up to 80° to the opening direction, are non-tracking, and contain almost no information on the shear sense. The striped bedding-veins can be separated into three types according to the geometry of their internal segmentation. Veins of type B opened parallel to jogs oriented at a low angle to bedding, veins of type J opened parallel to jogs oriented at a high angle to bedding and veins of type O opened orthogonal to bedding and jogs. Striped bedding-veins of types B and J contain crack-seal inclusion bands and displacement parallel inclusion trails. Striped bedding-veins of type O feature only crack-seal inclusion bands. The example of striped bedding-veins presented in this paper from the Orobic Alps of Italy belongs to type B. The lineation in the veins and the orientation of the inclusion bands and inclusion trails, as well as the orientation of steps in the vein wall, can be used to determine the sense of shear and the direction and amount of vein opening or bedding-parallel slip.

2.1. Introduction

In tectonic analysis, it is useful to obtain information on the opening trajectory of veins during deformation, i.e. the path taken by two points in opposite wall-rocks that were originally in contact. Fibrous crystals in veins are commonly used to determine this opening trajectory (Ramsay and Huber, 1983; Urai et al, 1991). As such, they belong to the most important kinematic indicators in rocks. Of special interest are crack-seal veins, which form by a process of periodic fracturing and sealing (Ramsay, 1980), with inclusion bands thought to represent single cracking and sealing events. Studies on crack-seal veins have shown, however, that not all crystals in such veins track the opening trajectory (Ramsay, 1980; Van Der Pluijm, 1984; Cox, 1987; Fisher and Brantley, 1992; Urai et al., 1991). This has been attributed to the fact that growth of some crystals in crack-seal veins is crystal-face controlled, so that crystals growing at different speeds outpace each other (Fisher and Byrne, 1990). Such crystals develop an elongate or blocky form, with variable grain-size and aspect ratios of less than 20:1. In contrast to this anisotropic growth, crystals can also grow isotropically so that fibres develop that do not outgrow each other (Fisher and Brantley, 1992; Bons and Jessell, 1997; Koehn et al., 1998). Such fibres can have a very constant diameter and very high length to width ratio (up to 100:1). Elongate crystals have very poor or no tracking capability (Bons and Jessell, 1997; Koehn et al., 1998) in contrast to isotropically growing fibres.

In crack-seal veins containing elongate or blocky crystals, crack-seal inclusion bands and inclusion trails have been used to determine the opening history of the veins. Crack-seal inclusion bands are arrays of inclusions in a vein reflecting the wall-rock morphology. Inclusion trails are arrays of inclusions assumed to follow the opening trajectory of a vein (Ramsay and Huber, 1983). There are different ideas, however, on the interpretation of these inclusions, especially when the veins are striped and contain both inclusion bands and inclusion trails in different orientation (Nicholson, 1978; Ramsay and Huber, 1983; Cox and Etheridge, 1983; Gaviglio, 1986; Mawer, 1987; Cox, 1987; Labaume et al., 1991; Fisher and Brantley, 1992; de Roo and Weber, 1992; Cosgrove, 1993; Jessell et al., 1994). Of particular interest are striped bedding-veins that have been described from the Alps in Europe (Labaume et al., 1991) and from the Variscan (de Roo and Weber, 1992), the Caledonian (Nicholson, 1978; Cosgrove, 1993), the Appalachian (Stanley, 1990; Ohlmacher and Aydin, 1997) and the Lachlan fold belt (Jessell et al., 1994). These veins are usually found in basins with alternating sandstone and mudstone beds and formed during layer-parallel slip due to folding or thrusting (Jessell et al., 1994; Cooke and Pollard, 1997; Fowler and Winsor, 1997). Metamorphic conditions during growth are up to greenschist facies and fluid pressure was apparently high (Etheridge et al., 1984). This study describes

striped bedding-veins from the Italian Alps and shows how different inclusion bands and inclusion trails can be interpreted, how striped bedding-veins can be classified, and expands on earlier work to show how these veins can be used to determine the direction and amount of bedding-parallel slip during folding or thrusting.

2.2. Regional Geology

The study area lies south of the Insubric Line in the central Orbic Alps of northern Italy, which are part of the Southern Alps (Fig. 2.1). Alpine nappe transport is directed towards the south and Alpine metamorphism is low grade, in contrast to the Central Alps (Laubscher, 1985).

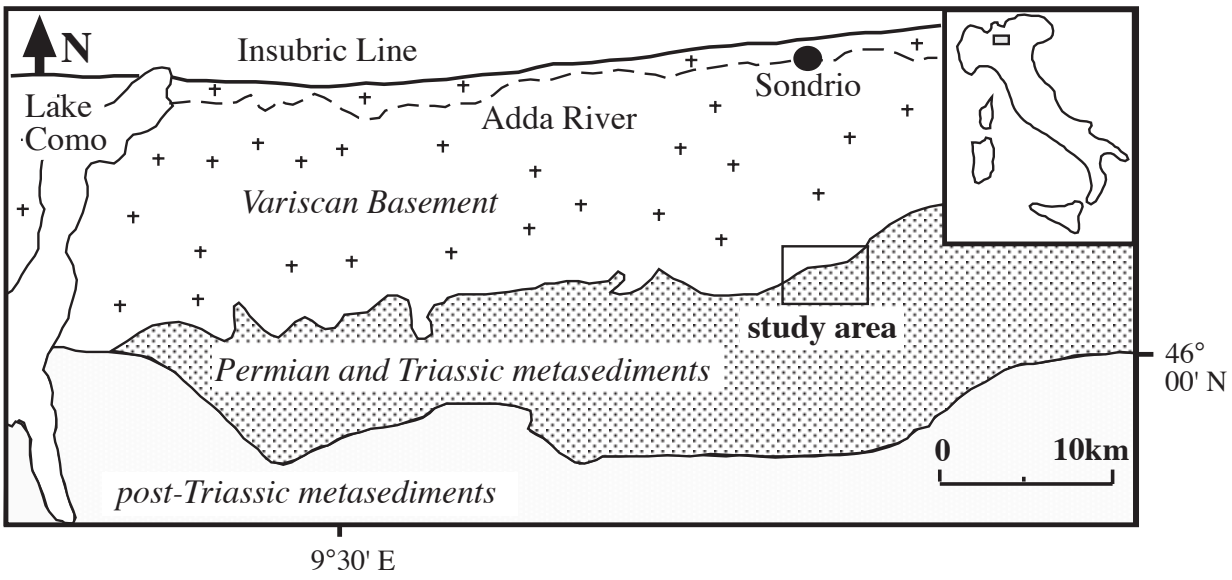

Fig. 2.1 Location of the study-area south of the Insubric Line in the Orobic Alps of northern Italy (modified after Zhang et al., 1994).

A basement consisting of orthogneiss and metasediments was deformed and metamorphosed up to amphibolite facies conditions during the Variscan orogeny. These basement-rocks are unconformably covered by a Permian to Triassic volcano-sedimentary sequence deposited in small fault-controlled basins (Cassinis et al., 1986). The sediments consist of coarse conglomerate at the base followed by the continental Collio Formation and the Verrucano Lombardo Formation. The Collio Formation is made up of an intercalated sequence of alluvial fan and lacustrine sediments, mainly sandstone and siltstone beds with minor conglomerate and felsic volcanics. The sequence varies laterally in thickness and composition. It is overlain unconformably by the Verrucano Lombardo Formation containing conglomerates and coarse grained sandstones. During the Alpine orogeny, normal faults were reactivated as thrusts or strike-slip faults. The whole sequence was folded and developed a

strong S_1 cleavage (Blom and Passchier, 1997; Cassinis et al., 1986).
The study-area is located west of Lake Diavolo (approximately at 9° 52' E and 46° 03' N) (Fig. 2.2). In this area bedding in the Collio Formation is deformed into an open anticline-syncline pair with gently east-west plunging axes, bounded to the north and

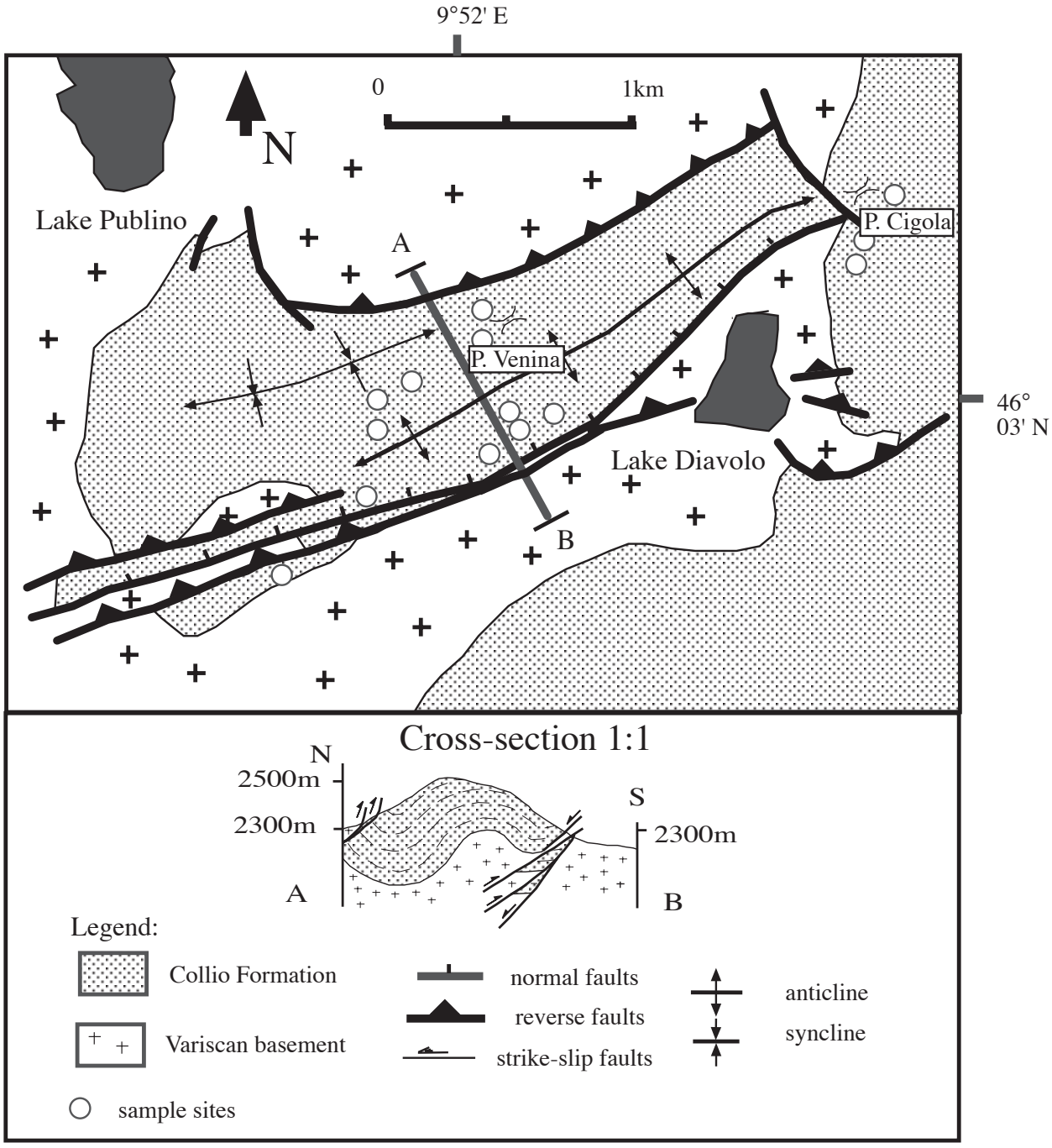

Fig. 2.2 Geological map and cross-section of the study-area. (modified after Zhang et al., 1994 and Blom and Passchier, 1997).

south by reactivated normal faults and south-directed thrusts (Fig. 2.2) (Blom and Passchier, 1997). The folds are upright with a wavelength of about 1 km and have a

strong axial-planar S_1 slaty cleavage. A large number of striped bedding-veins is found in the Collio Formation where sharp contacts exist between mudstone and sandstone layers. They are absent in very fine grained and very coarse grained beds. The sample sites lie mostly along a small trail from the Rifugio Longo cabin along Lake Diavolo towards Passo di Venina. Numerous striped bedding-veins can also be found at the Passo di Cigola, which can be reached from the Rifugio Longo along a trail passing Lake Diavolo.

2.3. Striped bedding-veins and their internal microstructure

2.3.1. Macroscopic appearance of the veins

Striped bedding-veins occur as sheets between sedimentary layers, are striped at a small angle to the vein and contain a lineation (Fig. 2.3). Most of the veins are made up of quartz with minor amounts of calcite, white mica and biotite. The lineation in the

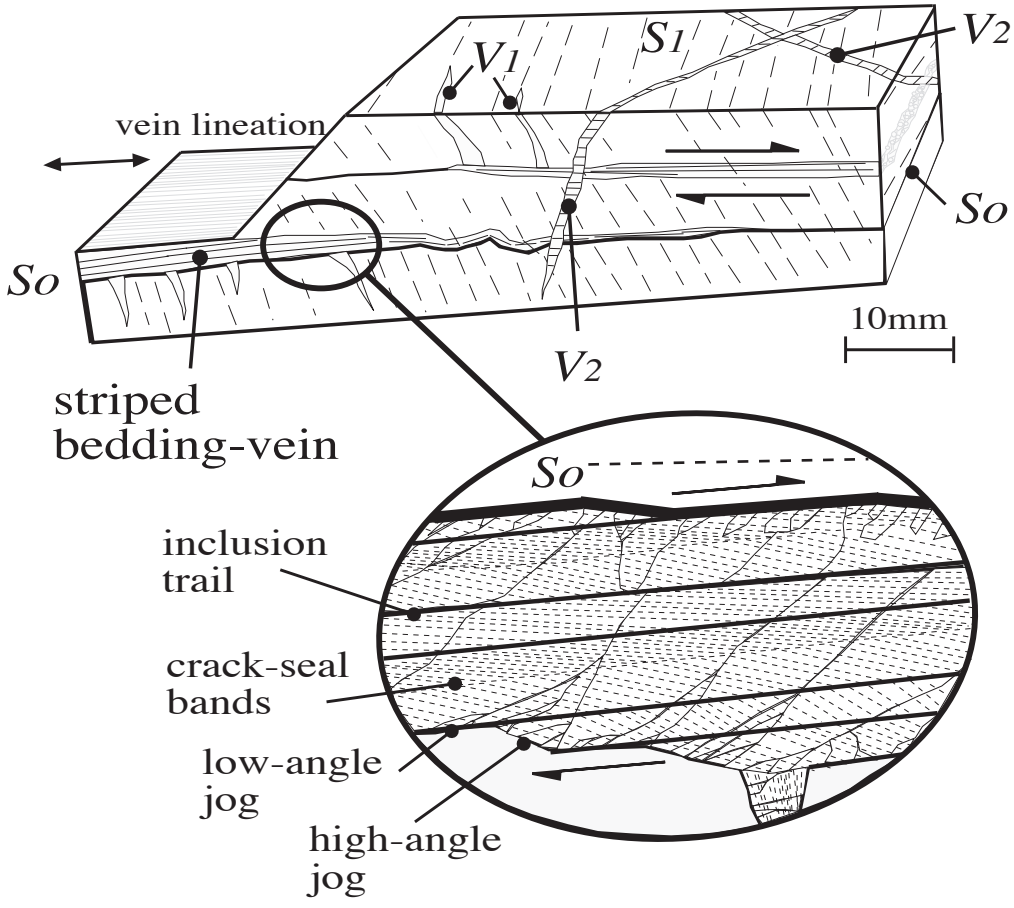

Fig. 2.3 Three different systems of veins can be distinguished in the field: striped bedding-veins; cleavage-parallel veins associated with the striped bedding-veins (V_1); and later vein systems (V_2). Arrows indicate the displacement direction. The inset shows the relative orientation of inclusion trails, crack-seal bands and elongate crystals. The S_1 cleavage is partly cut-off by the striped bedding-veins but some of the cleavage seams cut the veins. V_1-veins are parallel to the cleavage.

veins is parallel to displacement of the vein walls as can be determined by displacement of markers, but lies at a small angle to bedding (less than 10°).
Besides the dominant striped bedding-veins, two other systems of veins can be distinguished in the area, labelled V_1- and V_2-veins. Striped bedding-veins are connected with V_1-veins that are oriented perpendicular to the bedding and parallel to the S_1 cleavage. V_1-veins are widest close to the striped bedding-veins and die out in the wall-rock after 2 to 20 cm (Fig. 2.3). They appear on both sides of the striped bedding-veins. V_2-veins are late and cut all earlier veins. Striped bedding- and V_1-veins are mostly veins with inclusion bands and inclusion trails with elongate or blocky crystals, V_2-veins contain no solid inclusions.
V_1-veins are associated with, and apparently of the same age as, the striped bedding-veins, since each individual V_1-vein lies only on one side of a striped bedding-vein and does not cut it (Fig. 2.3) (Ohlmacher and Aydin, 1997). A variable displacement rate along the striped bedding-veins is a possible explanation for the development of V_1-veins. When a striped bedding-vein is not detached completely from the wall-rock during an opening event, the wall-rock is locally in extension and creates V_1-veins that form along the S_1 pre-existing anisotropy. V_1-veins are filled with elongate crystals and crack-seal inclusion bands, suggesting periodic fracturing of the wall-rock.
Striped bedding-veins are commonly folded due to bedding-parallel shortening and are then cut by the S_1 cleavage. V_1-veins are normally not folded because they are oriented parallel to the S_1 cleavage planes and the S_1 cleavage is invariably associated with the folds. This shows that striped bedding- and V_1-veins formed early during S_1 development. For this study, only non- to weakly folded striped bedding-veins were used, since the internal structure of the veins is destroyed by the dynamic recrystallisation that accompanies folding. Most V_2-veins are later than the main folding event in the area or they developed very late during folding and do not have a consistent orientation with respect to the striped bedding-veins. The internal structure of V_2-veins is not discussed further as they are not associated with the striped bedding-veins that are the subject of this study.

2.3.2. Internal microstructure of the striped bedding-veins

Three different microstructures can be distinguished in the striped bedding-veins: (1) crack-seal inclusion bands (crack-seal bands); (2) inclusion trails; and (3) grain boundaries of crystals (Fig. 2.3). The inclusion trails and the crack-seal bands can be used to determine the opening direction and the amount of opening of the veins. Inclusion trails and crack-seal bands form by different mechanisms and have different orientation with respect to the opening trajectory of veins, as outlined below.

Inclusion trails are always present whereas crack-seal bands, reflecting the wall-rock morphology, are not as common. The crack-seal bands and the inclusion trails are parallel to two different sets of jogs on the initial fracture surface, high-angle and low-angle jogs (Fig. 2.3). The distinction refers to the angle between jogs and the fracture surface. The angle of low-angle jogs is exaggerated in most drawings in this paper for clarity. The two differently oriented sets of jogs form a stair-stepping symmetry. If the initial fracture is not exactly bedding-parallel but one set of jogs is, then the displacement of the vein can be bedding-parallel but the vein itself will make an angle to bedding. If the vein is bedding-parallel then the displacement has to be at an angle to bedding and none of the jogs is bedding-parallel. The striped bedding-veins presented in this study are mostly parallel to bedding, inclusion trails and the displacement are parallel to low-angle jogs and crack-seal inclusion bands are parallel to high-angle jogs (Fig. 2.3).

2.3.2.1. Crack-seal bands

Crack-seal bands in the striped bedding-veins are arrays of inclusions of biotite and white mica with a grainsize of less than 5 μm that lie parallel to high-angle jogs in the vein wall-rock. They cannot be seen macroscopically and are never parallel to bedding or to the lineation in the veins. Single crack-seal bands have exactly the same morphology as the adjacent wall-rock, with small jogs in the wall-rock reflected by identical jogs in the crack-seal bands (Fig. 2.4a). Very pronounced jogs can form planes that are parallel to the inclusion trails (Fig. 2.4a). Crack-seal bands typically lie 6 to 50 μm apart and form sets of up to 200 parallel bands with a very constant spacing. Crack-seal bands are the most important microstructure in the veins since they can be used as shear sense indicators for an accurate reconstruction of vein wall movement.

2.3.2.2. Inclusion trails

Inclusion trails are the dominant structure in all veins in thin-section. They lie at a low angle to the bedding (less than 10°), give the veins their striped appearance and separate sets of crack-seal bands. They consist mainly of white mica and biotite with a grainsize of 5 to 50 μm. They are about 10 to 100 μm thick and appear as straight bands in thin-sections cut parallel to the vein lineation. The inclusion trails normally connect foot-wall and hanging-wall of a vein (Figs. 2.3, 2.4b) but some of the inclusion trails are discontinuous or cannot be followed across the whole vein. The distance between single straight inclusion trails is variable. In sections perpendicular to the vein lineation, the inclusion trails have a wavy and branching appearance and are discontinuous (Fig. 2.4c).

2.3.2.3. Grain boundaries of crystals

Most striped bedding-veins are deformed and crystals show strong undulose extinction, subgrains and evidence for dynamic recrystallization. In weakly to undeformed veins, however, quartz grains without subgrains can be found. These quartz grains still preserve delicate patterns of solid inclusions and are therefore inferred to represent grains that formed when the veins developed.

The striped bedding-veins show two different kinds of undeformed crystals: elongate/blocky crystals and straight fibres, the former of which are dominant. The elongate crystals have the following appearance: close to the wall-rock, small grains with random crystallographic orientation can be found. Only a few of these grains extend further into the vein and form elongate crystals, mainly those that are oriented with the c-axis perpendicular to the wall-rock (Fig. 2.5a). Usually the grain boundaries extend across inclusion trails, but many crystals terminate on relatively thick trails (Fig. 2.5b). Isolated large blocky quartz crystals are present between some of the inclusion trails. These contain no crack-seal bands (Fig. 2.5b) and some show euhedral growth surfaces.

The second kind of crystals are straight quartz or mica fibres (Fig. 2.5c). They are not very common in the striped bedding-veins and are usually found close to the wall-rock. Adjacent fibrous crystals of mica and quartz are of the same length, about 100 μm. The quartz fibres are approximately 5 μm thick, the mica fibres about 1 μm, and both are oriented with their long axis parallel to the inclusion trails.

2.3.3. Interpretation of the microstructures

2.3.3.1. Crack-seal bands

Crack-seal bands are interpreted to represent single cracking events during the formation of the crack-seal veins (Ramsay, 1980; Ramsay and Huber, 1983). This is envisaged as follows. When a vein cracks along the contact with the wall-rock, it provides space for the growth of new crystals. During the sealing period the crack is filled both from the wall-rock and vein sides, from the former dominantly by small micas, from the latter by quartz (Fig. 2.6). This may be due to the fact that the wall-rock is a slate and the vein consists mainly of quartz. When the space is filled, the vein opens again along the contact with the wall-rock, and the new grown micas and small parts of the wall-rock are detached from the wall-rock and become part of the vein forming the crack-seal bands (Cox, 1987).

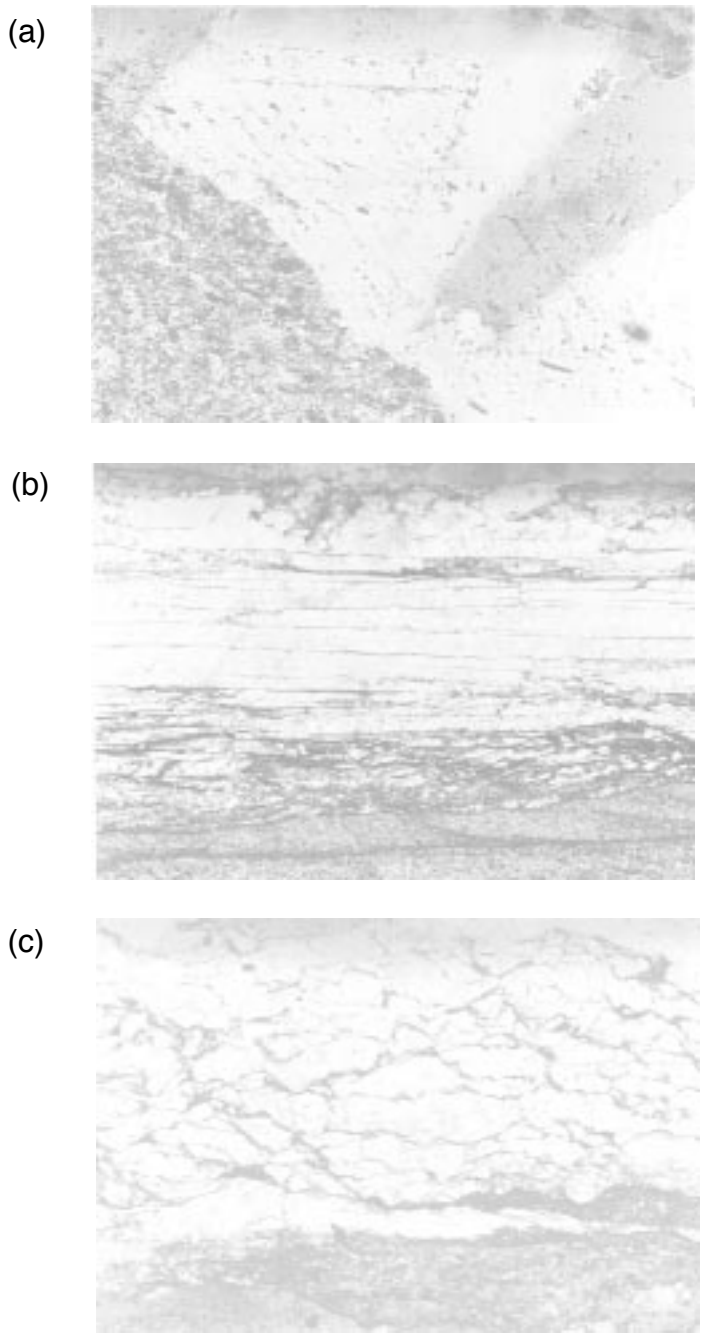

Fig. 2.4 (a) Crack-seal inclusion bands reflecting the morphology of the wall-rock. The vein is cut parallel to the vein lineation. The displacement is parallel to the lines connecting jogs in inclusion bands, i.e. parallel to the lower side of the image. Grain boundaries of crystals that can be seen at the upper right-hand side of the image do not track the opening of the vein. Width of view is 0.15 mm. Crossed polars. (b) Part of a striped bedding-vein cut parallel to the vein lineation. The wall-rock is located in the lower part of the image, the vein in the upper. Shear sense is sinistral. Bedding is horizontal. The inclusion trails are the dominant microstructure in the veins and form straight bands. Width of view is 20 mm. Plain polarized light. (c) Striped bedding-vein cut perpendicular to the vein lineation. The wall-rock is located in the lower part of the image, the vein in the upper. Bedding is horizontal. The inclusion trails are wavy and branching. Width of view is 3 mm. Plain polarized light.

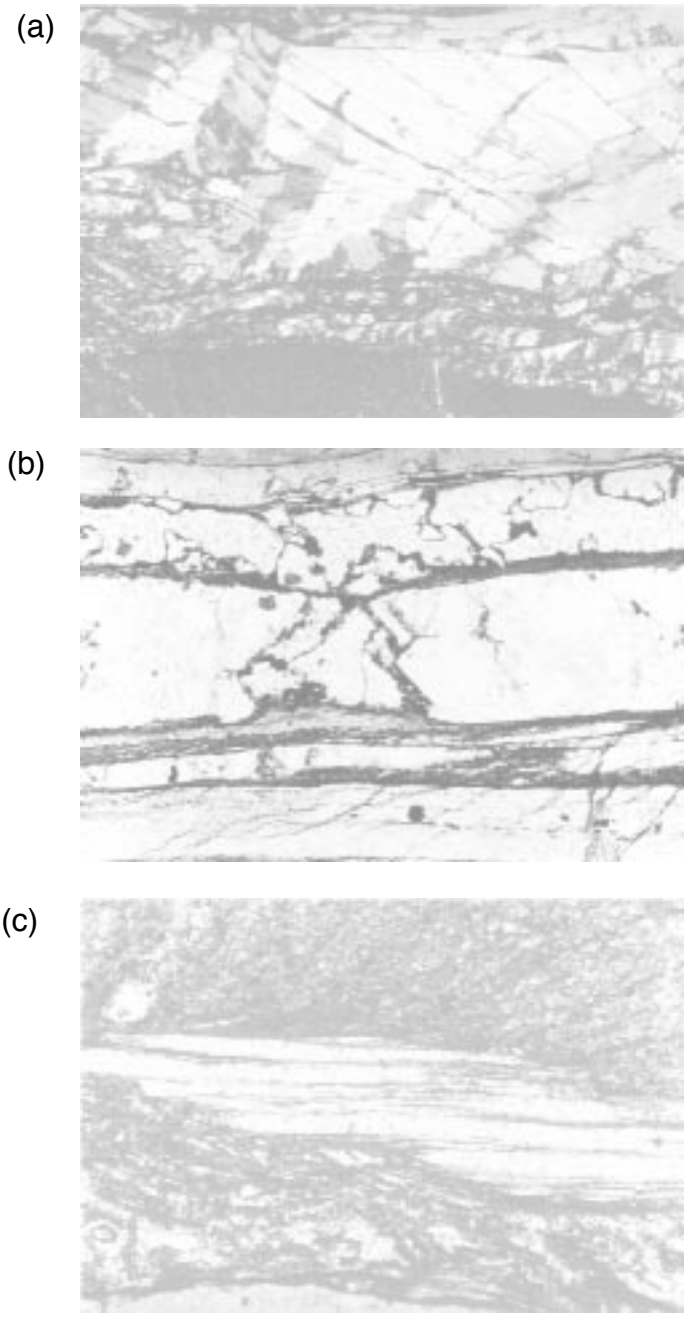

Fig. 2.5 (a) Elongate non-tracking crystals in a striped bedding-vein cut parallel to the vein lineation. The displacement is dextral parallel to the lower side of the picture. Crack-seal bands run from upper left to lower right, inclusion bands from left to right. Width of view is 10 mm. Crossed polars. (b) Single crystals and open voids in a striped bedding-vein between two inclusion trails. Crystal growth was hampered by the inclusion trails. Width of view is 2mm. Plain polarized light. (c) Part of a vein with straight fibres, with fibrous growth of biotite and quartz cut parallel to the vein lineation. Displacement is dextral, parallel to the biotite fibres. Bedding is horizontal. These structures superficially resemble striped bedding-veins with inclusion trails, but here biotite grows with a straight fibrous habit next to straight fibrous quartz. No crack-seal inclusions or elongate crystals develop. Width of view is 0.1 mm. Plain polarized light.

2.3.3.2. Inclusion trails

Inclusion trails are interpreted to develop along low-angle jogs in the vein, parallel to the movement direction of the vein. Contrary to crack-seal bands, inclusion trails contain larger fragments of the wall-rock. Apparently, these fragments are sheared off the vein wall during an opening event parallel to the inclusion trails. The fracture that develops during an opening event parallel to the inclusion trails is a shear fracture whereas the fracture parallel to the crack-seal bands is mostly extensional. Along a shear fracture, pieces of wall-rock can be plucked off and included in the vein (Fig. 2.6). They then form part of the inclusion trails, so that inclusion trails are thicker and more pronounced than crack-seal bands. Because of this mechanism, the distance from one side of the vein to the other measured along one inclusion trail must equal the total amount of movement during layer-parallel slip.

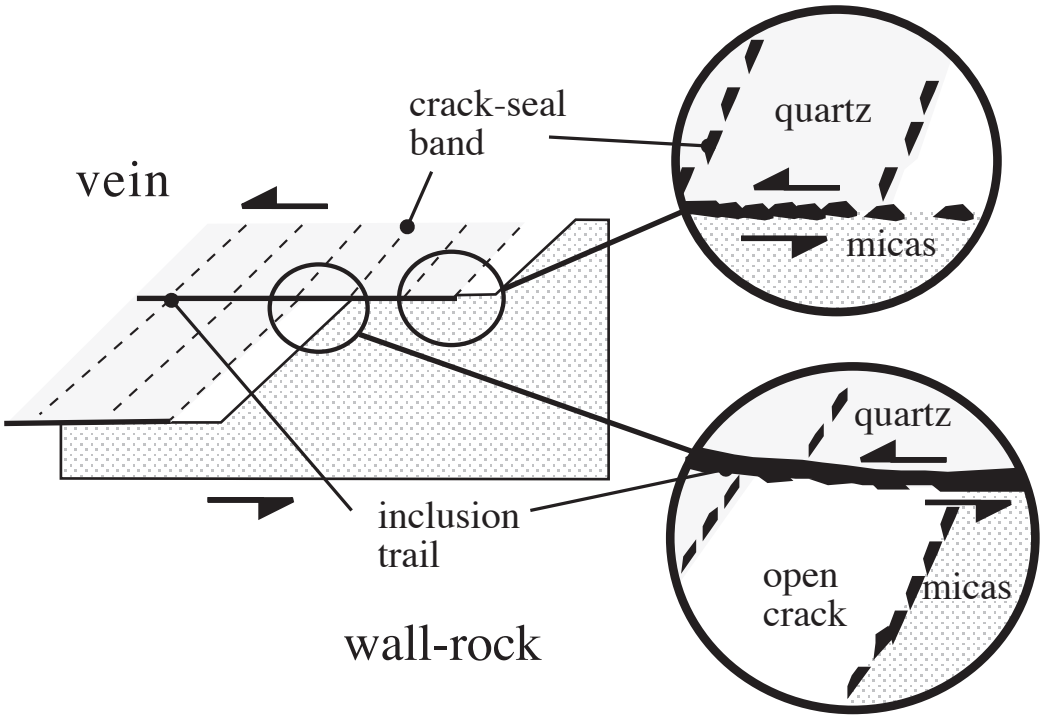

Fig. 2.6 Schematic illustration of the development of crack-seal bands and inclusion trails. After a cracking event, a fluid-filled space opens and micas grow on the wall-rock and on the inclusion trails while quartz grows on crystals in the vein. Quartz outgrows the micas and seals the void. Micas are detached from the wall-rock during subsequent cracking events and form the crack-seal bands. Detached micas and slivers of the wall-rock form the inclusion trails. Arrows show the displacement during vein opening.

2.3.3.3. Grain boundaries

The crystal microstructure in striped bedding-veins is interpreted as follows. The elongate crystals in the striped bedding-veins apparently nucleate in a part of the vein where single crystals are small and have a random crystallographic orientation. The

site of nucleation is commonly close to the wall-rock but can be inside the vein as well. Away from the site of nucleation the crystals start to outgrow each other. Those crystals that are oriented with their fast growth direction perpendicular to the wall tend to become larger and outpace crystals that are less favourably oriented. The surviving larger crystals have an approximately similar lattice preferred orientation and form the elongate crystals that are typical of crack-seal veins. The elongate crystals grow more or less perpendicular to the crack-seal bands, as these reflect the orientation of the growth surface after a cracking event. They are non-tracking, because the parameters controlling the direction of growth are the crystal habit and the angle between the crack-seal bands and the inclusion trails (Fig. 2.7). Thus, their direction of growth is not directly influenced by the direction of vein opening and they cannot be used to determine the opening direction of the vein.

Displacement-parallel straight fibres of mica and quartz may form by a continuous growth mechanism without the formation of cracks or by a crack-seal mechanism with very small cracks. They do track the opening trajectory of the vein, as they are parallel to the inclusion trails (Fig. 2.7).

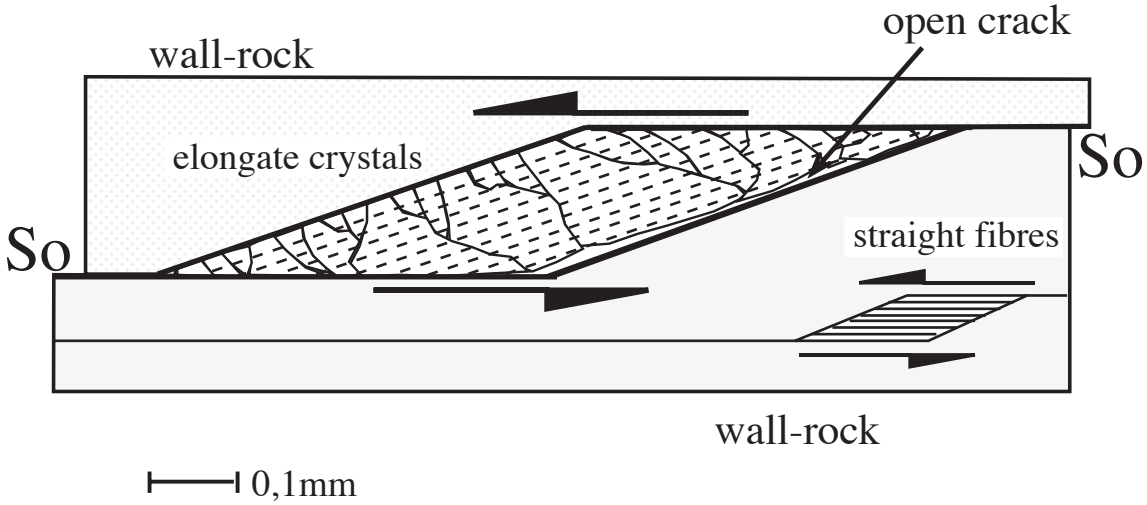

Fig. 2.7 Schematic illustration showing the difference between elongate crystals and straight fibres. Elongate crystals in the vein in the upper part of the wall-rock grow from upper left towards the lower right into an open crack. No straight fibres develop and elongate crystals outgrow each other. The direction of growth is perpendicular to the crack-seal bands (dashed lines) and is not tracking the opening of the vein which is horizontal (see arrows). Straight fibres in the vein at lower right grow parallel to the displacement direction.

2.3.4. Model for the development of the striped bedding-veins

From the observed structures we infer that striped bedding-veins form as follows. A shear fracture develops approximately parallel to bedding with high-angle and low-angle jogs (Fig. 2.8a). Slip along the low-angle jogs at a small angle to bedding results in opening of high-angle jogs oblique to bedding along the fracture. The vein opens

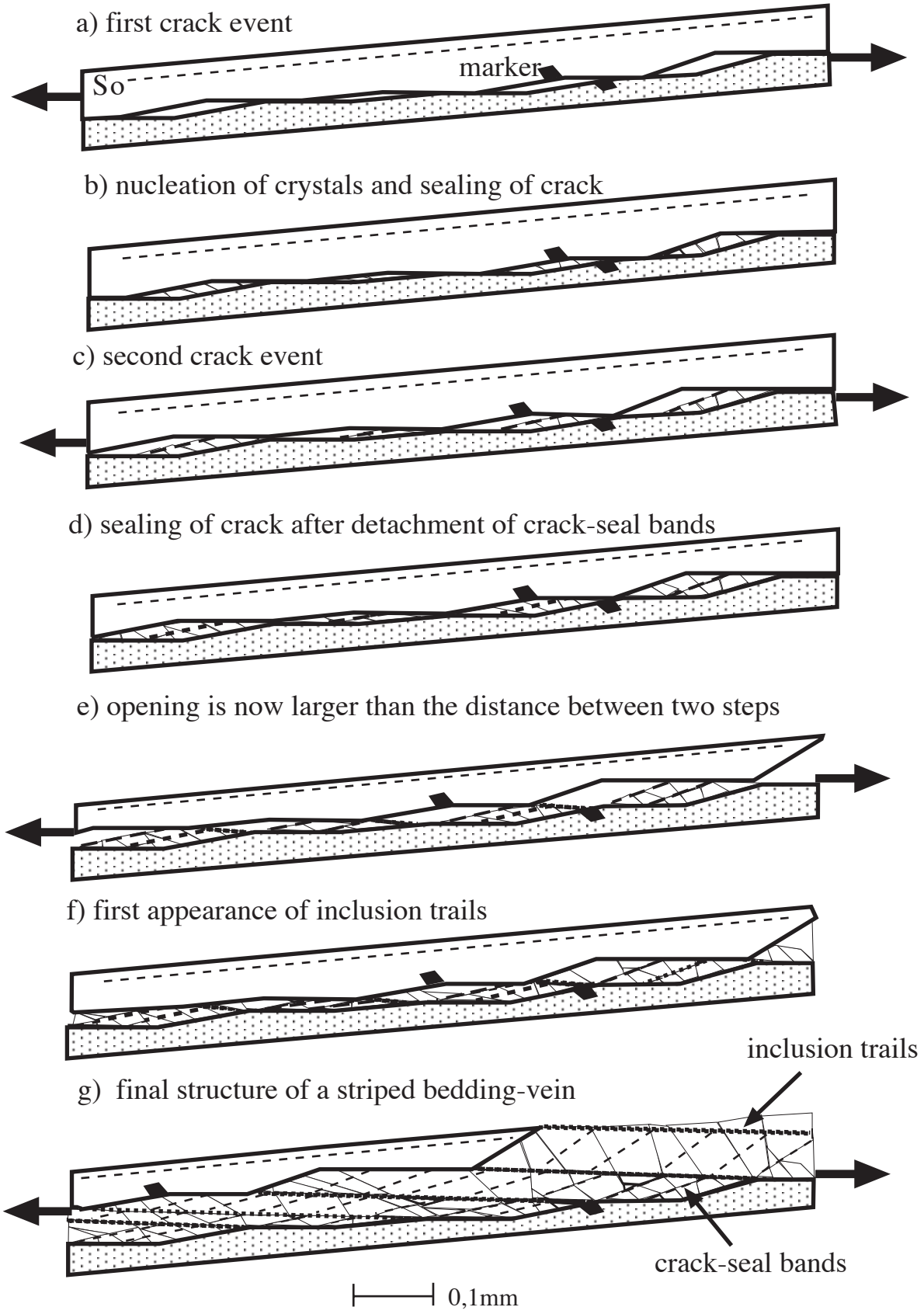

Fig. 2.8 Schematic diagram showing the development of a striped bedding-vein with crack-seal bands and inclusion trails. The vein forms along jogs on the bedding. There is an angle between the bedding and the opening direction, so that either the displacement or the vein are not exactly bedding parallel. This angle is very small in the field so that it cannot be seen macroscopically and sometimes not even with a microscope. The angle is exaggerated in this drawing for clarity.

periodically by cracking and the resulting voids are mainly filled with elongate quartz crystals and minor mica along the vein wall (Fig. 2.8b). During each cracking event, small newly grown micas become detached from the wall-rock and form crack-seal bands (Fig. 2.8c,d). Once the opening vector of the striped bedding-vein exceeds the mean length of the low-angle jogs the vein sectors start to become interconnected (Fig. 2.8e). Detached fragments of the wall-rock and newly grown micas now lie inside the vein and form the inclusion trails (Fig. 2.8f,g).

2.3.5. Nature of the lineation in the striped bedding-veins

Hand specimens of the veins show a well-developed lineation, which in the field seems to be defined by straight (slicken-fibre type) quartz fibres. In fact, it is formed by the inclusion trails that define elongate ribbons, since these are anastomosing in sections cut normal to the vein lineation (Figs. 2.4c, 2.9). The anastomosing nature of the inclusion trails is partly due to the geometry of the initial fracture surface along the bedding plane and partly due to dissolution of parts of the vein during bedding-parallel slip (Stanley, 1990; de Roo and Weber, 1992). Although dissolution can explain part of the geometry in Fig. 2.4c, they are not stylolites formed from planar surfaces, since individual segments can be traced to jog-segments in the wall-rock and branch lines of low-angle and high-angle jogs are not parallel, but anastomosing as well. The dissolution seams visible in the veins are not parallel to the opening trajectory of the veins and are associated with the folding of the veins. The inclusion trails in the veins cannot represent pressure solution seams that developed due to the shear movement because elongate crystals that grow across the inclusion trails are not offset. The jogs shown in Fig. 2.8 in two dimensions may be short segments in three dimensions (Fig. 2.9). Though the lineation looks similar to slicken-fibres, the elongate crystals in the vein are not growing parallel to the inclusion trails, although they are sometimes bounded by them. The rare slicken-fibres with displacement-parallel fibre growth in the striped bedding-veins mentioned above are too small and too short to be seen in hand specimen.

2.4. The role of striped bedding-veins in regional deformation

The striped bedding-veins and their complex internal structures allow reconstruction of the deformation sequence in the study area. The main deformation events are thrusting towards the south, folding of sediments, formation of a pressure-solution cleavage (Blom and Passchier, 1997; Cassinis et al., 1986) and bedding-parallel slip resulting in the formation of the striped bedding-veins. The following observations can be made in the field that constrain the timing of different events. Thrusting must start earlier than folding in the area, since the thrust planes are folded on a 100m scale,

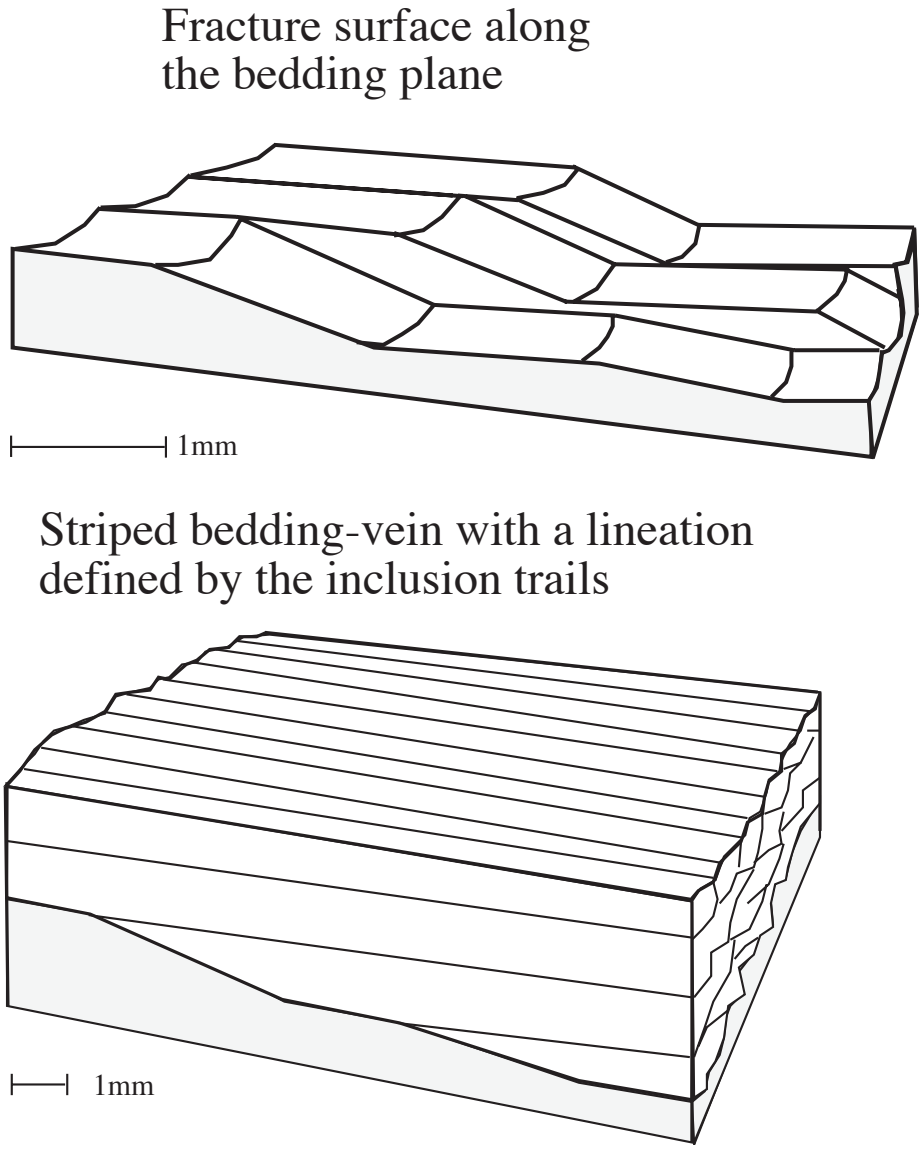

Fig. 2.9 Three-dimensional geometry of a striped bedding-vein with lineations. The direction of movement is dextral, parallel to the vein lineation. The shape of the initial fracture surface determines the form of the inclusion trails and thus the formation of the vein lineation.

where S_1 is the axial-planar cleavage of these folds. The striped bedding-veins cut S_1, and V_1-veins associated with the striped bedding-veins form along S_1, whereas some of the younger pressure solution cleavage seams cut the veins. The cleavage therefore developed over a longer period of time than the veins. The shear sense indicators in the striped bedding-veins, the crack-seal bands (see discussion), show a consistent displacement of the vein hanging-wall towards the south, independent of their location on the limbs of major and minor folds, and the veins tend to wrap over fold hinges in both limbs without a change in thickness. This suggests that the veins are not associated with large scale folding or layer-parallel slip during folding (Jessell

et al., 1994; Fowler and Winsor, 1997; Cooke and Pollard, 1997) but rather with thrusting of sediments towards the south. The large scale folds must have developed later, probably at the same time as cm-scale folds in the veins.

The sequence of deformation is reconstructed as follows. The first alpine event in the study area is the reactivation of normal faults as reverse and strike-slip faults accompanied by newly developed thrust faults. Early layer-parallel shortening resulted in the formation of an early S_1 cleavage. Further thrusting towards the south resulted in layer-parallel slip along bedding planes and the formation of the striped bedding-veins. The latest event in the study area is folding of bedding and veins accompanied by an intensification of the S_1 cleavage.

During large-scale folding, the striped bedding-veins developed parasitic folds with wavelengths of 2 to 5 cm. In the steep limbs of large-scale folds in the Collio Formation, boudinaged striped bedding-veins were observed, which were apparently first shortened, then folded. They rotated from the compressional into the extensional field during folding.

2.5. Discussion

Several different models have been proposed for the development and interpretation of striped bedding-veins and there has been some debate on how to interpret these veins and the inclusion bands within them. Striped bedding-veins are commonly attributed to flexural slip associated with folding, but in the Orobic Alps we found such veins to be associated with thrusting and to predate folding. Microstructures in striped bedding-veins have earlier been described by Jessell et al. (1994), Cox (1987), Cox and Etheridge (1983), Mawer (1987), de Roo and Weber (1992), Labaume et al. (1991) and Gaviglio (1986). Some of these contain both crack-seal bands and inclusion trails, some only crack-seal bands. Jessell et al. (1994) proposed four different models for the interpretation of striped veins containing crack-seal bands and inclusion trails. Model (1) of Jessell et al. (1994) interprets part of the inclusions as pressure solution seams. Model (2) interprets the inclusion trails as shear bands similar to the models of de Roo and Weber (1991) and Labaume et al. (1991). Model (3) suggests opening of the vein parallel to inclusion trails and in model (4) crack-seal bands and inclusion trails are interpreted similarly and the opening of the veins is thought to be parallel to the crack-seal bands. We favour model (3) of Jessell et al. (1994) for striped bedding-veins from the Oropic Alps, since there is no slip along inclusion trails and displacement is not parallel to the crack-seal bands. The inclusion trails can sometimes be the site of pressure solution (Stanley, 1990; De Roo and Weber, 1992), but this effect is thought to be minor in the veins from the Orobic Alps, as explained in section 2.3.5. Jessell et al. (1994) favour model (4), so their

interpretation for striped bedding-veins differs from that of model (3) presented in this paper, with a more than 90° difference in the interpreted opening direction. As a consequence, the sense of shear is also different. The model of Cox (1987), Cox and Etheridge (1983) and Gaviglio (1986) for the development of striped bedding-veins is similar to the interpretation in this paper. These authors distinguish between crack-seal bands and inclusion trails and conclude that the opening direction is parallel to the inclusion trails, which is in agreement with our model. Mawer (1987) presented striped bedding-veins that contain two differently oriented inclusion bands that both reflect the morphology of the wall-rock. They are each interpreted as one set of crack-seal bands and these veins contain no inclusion trails.

Based on our observations, we suggest an alternative general classification for striped bedding-veins. Theoretically, the opening direction of striped bedding-veins is restricted by high- and low-angle jogs on the bedding that have a stair-stepping geometry with two end-member opening directions: parallel to low-angle jogs subparallel to bedding (striped bedding-veins of type B) and parallel to high-angle jogs oblique to bedding (striped bedding-veins of type J). All other opening directions are oblique to bedding and to jogs (striped bedding-veins of type O) (Fig. 2.10). Striped bedding-veins of types B and J have crack-seal bands and inclusion trails, whereas O type striped bedding-veins have crack-seal bands only. Striped bedding-veins from the Orobic Alps, of Jessell et al. (1994), Cox (1987), Cox and Etheridge (1983), de Roo and Weber (1992), Labaume et al. (1991) and Gaviglio (1986) are all of type B whereas the striped bedding-veins of Mawer (1987) are of type O. Veins of J-type are rare, but have been observed in sediments of the southern Pyrenees (Passchier, unpublished data). The distinction is important, since type B and type J veins represent a different shear sense.

The best way to classify striped bedding-veins in our scheme is to make sections parallel to the vein lineation and to identify any inclusion trails that form continuous bands from one side of the vein to the other. If there is no lineation in the veins, they probably contain no inclusion trails at all and are likely to be of type O. Kinematic analysis of the veins can be attempted as follows: The best tool to determine sense of shear is the "sense" of attachment of inclusion trails to the wall-rock (Fig. 2.10). Displacement is parallel to inclusion trails, if present. If only crack-seal bands are present, jogs of similar shape in the bands should be identified and displacement is parallel to the line connecting the jogs (Fig. 2.10). The stair-stepping geometry of jogs in the wall-rock can also be used to determine the shear sense. If the steps in the hanging wall are downwards to the left, the displacement is sinistral for striped bedding-veins of type B and most O-types. O-types approaching J and J-type striped bedding-veins have the opposite sense of shear (Fig. 2.10). If, due to later

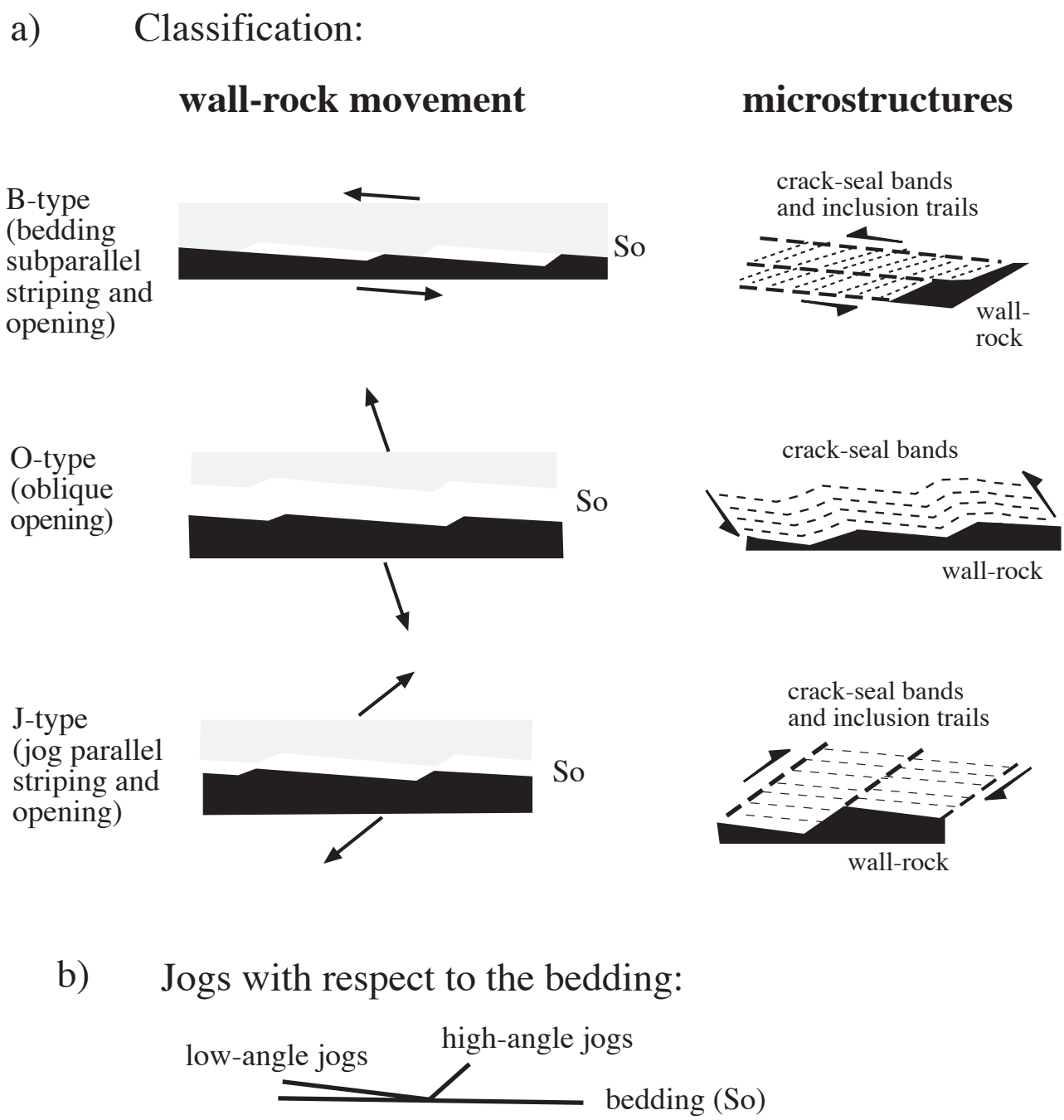

Fig. 2.10 (a) A proposed classification for striped bedding-veins. B-type striped bedding-veins open along low-angle jogs subparallel to the bedding, J-type veins open parallel to high-angle jogs on the bedding and O-type veins open with an angle that lies between B- and J-type veins. O-type striped bedding-veins develop only crack-seal band whereas J- and B-type striped bedding-veins can have both inclusion trails and crack-seal bands. (b) Orientation of low-angle and high-angle jogs with respect to bedding for a striped bedding-vein.

deformation or metamorphic overprint, the original crystals and crack-seal bands have been destroyed, movement direction and shear sense can still be determined from the inclusion trails connecting both wall-rocks. Obviously, either large thin-sections or favourable outcrop surfaces are necessary for such observations.

Cleavage orientation next to the veins cannot be used to determine the shear sense since the orientation of the cleavage with respect to the vein may vary depending on the location of the vein in different fold limbs, as it does in the Orobic Alps.
Finally, the thickness of striped bedding-veins may be used as a measure of finite strain in a rock-pile: with increasing displacement on the veins, their thickness will gradually increase. This means that, if data can be obtained on the shape and size of the jogs, and spacing and number of the inclusion trails, the thickness of the veins can be used to measure the amount of total slip along the vein.

2.6. Conclusion

This study shows how striped bedding-veins can be used to determine the direction and amount of displacement of sedimentary layers during layer-parallel slip. Three types of striped bedding-veins can be distinguished, B,O and J depending on the opening direction. All types may contain crack-seal bands but only B- and J-types contain solid inclusion trails. Steps in the wall-rock, the orientation and form of the inclusion bands and trails, and vein thickness can be used to evaluate the sense of shear and the amount of displacement. Elongate fibrous-looking crystals in striped bedding-veins are not tracking the displacement direction and cannot be used to determine the opening trajectory of the veins.
The vein lineation that is visible in hand specimen is formed by the inclusion trails and can be used to determine the direction of movement. To evaluate the sense of shear one has to look at the orientation of crack-seal bands with respect to inclusion trails in thin-sections that are cut parallel to the vein lineation (Fig. 2.10). It is difficult to determine the sense of shear in hand specimen, as the angle between crack-seal bands and the bedding is commonly very small and obscured by deformation, and it is hard to see stair-stepping in the wall-rock. As a result, it is not easy to establish from which side of the wall-rock the lineation starts. The opening of the veins is parallel to the lineation, but the sense of shear is not always clear. If crack-seal bands are absent, jogs in the wall-rock are the only sense of shear indicators in this type of vein.

Acknowledgements

The authors wish to thank David Durney, Neil Mancktelow and Richard Norris for their careful reviews and their comments that helped to improve the manuscript. The authors also wish to thank Klaus Gessner, Sandra Piazolo and Paul Bons for comments on the manuscript. DK would like to thank Charly Bauermeister and Konrad Koehn for their support in the field and all the people at the Rifugio Longo. Funding for this research was provided by the DFG-grant Pa 578/3.

References

Blom, J.C., Passchier, C.W., 1997. Structures along the Orobic thrust, Central Orobic Alps, Italy. Geologische Rundschau 86, 627-636.

Bons, P.D., Jessell, M.W., 1997. Experimental simulation of the formation of fibrous veins by localised dissolution-precipitation creep. Mineralogical Magazine 61, 53-63.

Cassinis, G., Dal Piaz G.V., Eusebio A., Gosso G., Martinotti G., Massari F., Milano P.F., Pennachioni G., Perello M., Pessina C.M., Roman E., Spalla M.I., Tosetto S., Zerbato M., 1986. Report on a structural and sedimentological analysis in the Uranium province of the Orobic Alps, Italy. Uranium 2, 241-260.

Cooke, M. L., Pollard, D. D., 1997. Bedding-plane slip in initial stages of fault-related folding. Journal of Structural Geology 19, 567-581.

Cosgrove, J.W., 1993. The interplay between fluids, folds and thrusts during the deformation of a sedimentary succession. Journal of Structural Geology 15, 491-500.

Cox, S. F., 1987. Antitaxial crack-seal vein microstructures and their relationship to displacement paths. Journal of Structural Geology 9, 779-787.

Cox, S.F., Etheridge, M.A., 1983. Crack-seal fibre growth mechanisms and their significance in the development of oriented layer silicate microstructures. Tectonophysics 92, 147-170.

de Roo, J.A., Weber, K., 1992. Laminated veins and hydrothermal breccia as markers of low-angle faulting, Rhenish Massif, Germany. Tectonophysics 208, 413-430.

Etheridge, M.A., Wall, V.J., Cox, S.F., 1984. High fluid pressures during regional metamorphism and deformation: implications for mass transport and deformation mechanisms. Journal of Geophysical Research 89, 4344-4358.

Fisher, D.M., Byrne, T., 1990. The Character and Distribution of Mineralized Fractures in the Kodiak Formation, Alaska: Implications for Fluid Flow in an Underthrust Sequence. Journal of Geophysical Research 95, 9069-9080.

Fisher, D.M., Brantley, S.L., 1992. Models of Quartz Overgrowth and Vein Formation: Deformation and Episodic Fluid Flow in an Ancient Subduction Zone. Journal of Geophysical Research 97, 20043- 20061.

Fowler, T. J., Winsor, C. N., 1997. Characteristics and occurrence of bedding-parallel slip surfaces and laminated veins in chevron folds from the Bendigo-Castlemaine goldfields: implications for flexural-slip folding. Journal of Structural Geology 19, 799-815.

Gaviglio, P., 1986. Crack-seal mechanism in a limestone: a factor of deformation in strike-slip faulting. Tectonophysics 131, 247-255.

Jessell, M.W., Willman, C.E., Gray, D.R., 1994. Bedding parallel veins and their relationship to folding. Journal of Structural Geology 16, 753-767.

Koehn, D., Bons, P.D., Passchier, W.C., 1998. Modelling the tracking ability of fibrous crystals, GSA Abstracts with Programs Vol. 30 No. 7, A 197.

Labaume, P., Berty, C., Laurent, P.H., 1991. Syn-diagenetic evolution of shear structures in superficial nappes: an example from the Northern Apennines. Journal of Structural Geology 13, 385-398.

Laubscher, H.P., 1985. Large-scale, thin-skinned thrusting in the southern Alps: Kinematic models. Geological Society of America Bulletin 96, 710-718.

Mawer, C.K., 1987. Mechanics of formation of gold-bearing quartz veins, Nova Scotia, Canada. Tectonophysics 135, 99-119.

Nicholson, R., 1978. Folding and pressure solution in a laminated calcite-quartz vein from the Silurian slates of the Llangollen region of N Wales. Geological Magazine 115, 47-54.

Ohlmacher, G.C., Aydin, A., 1997. Mechanics of vein, fault and solution surface formation in the Appalachian Valley and Ridge, northeastern Tennessee, U.S.A.: implications for fault friction, state of stress and fluid pressure. Journal of Structural Geology 19, 927-944.

Ramsay, J., 1980. The crack-seal mechanism of rock deformation. Nature 284,135-139.

Ramsay, J.G., Huber, M.I., 1983. The techniques of modern structural geology, 1: Strain analysis. Academic Press, London.

Stanley, R.S., 1990. The evolution of mesoscopic imbricate thrust faults--an example from the Vermont Foreland, U.S.A.. Journal of Structural Geology 12, 227-241.

Urai, J.L., Williams, P.F., Van Roermund, H.L.M., 1991. Kinematics of crystal growth in syntectonic fibrous veins. Journal of Structural Geology 13, 823-836.

Van Der Pluijm, B.A., 1984. An unusual 'crack-seal' vein geometry. Journal of Structural Geology 6, 593-597.

Zhang J.S., Passchier C.W., Slack J.F., Fliervoet T.F., Boorder H. de, 1994. Cryptocrystalline Permian tourmalinites of possible metasomatic origin in the Orobic Alps, northern Italy. Economic Geology 89, 391-396.

3. Numerical Simulation of Fibre Growth in Antitaxial Strain Fringes

in review, Journal of Structural Geology

Daniel KOEHN*, Chris HILGERS°, Paul D. BONS*, Cees W. PASSCHIER*

*Institut für Geowissenschaften, Tectonophysics, Johannes Gutenberg Universität, Becherweg 21, 55099 Mainz, Germany, E-mail: koehn@mail.uni-mainz.de
°Geologie-Endogene Dynamik, RWTH Aachen, Lochnerstrasse 4-20, 52056 Aachen, Germany

Abstract

A two-dimensional computer model ("Fringe Growth") is presented that is used to simulate the incremental growth of crystal fibres in undeformed antitaxial strain fringes. The user can define the shape of a core-object (e.g. a pyrite crystal), the growth velocity and anisotropy of growing crystals, the rotation of fringes and core-object with respect to a horizontal datum and with respect to each other, and the opening velocity of fringes. Growth is simulated by movement of nodes connecting line segments that define the grain boundaries.

Modelling results predict that face-controlled strain fringes will grow around smooth core-objects and strain fringes with displacement-controlled and face-controlled fibres around core-objects with rough surfaces. The surface roughness of the core-object determines if fibres in the fringes track the opening trajectory, since fibres follow asperities on the surface of the core-object. Rotation of the core-object and the fringes with respect to an external reference frame and with respect to each other influences the geometry of the fibres. Our modelling results indicate that fibre growth direction is not directly dependent on the orientation of the extensional instantaneous stretching axes or the finite maximum strain axes.

3.1. Introduction

Rigid objects in a matrix deformed by non-coaxial or coaxial progressive deformation cause perturbations of the stress field and flow pattern. Increased pressure solution may occur adjacent to the rigid object on the side of the shortening instantaneous stretching axes (ISA), while new crystals may grow on the side of the extensional ISA and form strain fringes (Mügge, 1928; Pabst, 1931). For over 70 years, geologists have attempted to use crystal fibres in strain fringes that lie on both sides of a rigid core-object such as a pyrite crystal to evaluate the deformation history in the host-rock (Mügge, 1928; Pabst, 1931; Durney and Ramsay, 1973; Cox and Etheridge, 1983; Beutner and Diegel, 1985; Ellis, 1986; Etchecopar and Malavielle, 1987; Aerden, 1996; Kanagawa, 1996). Despite much progress in this field, the methods used are still based on assumptions which have not been tested experimentally. We developed a method to test assumptions of fringe growth in numerical experiments in order to improve the reliability of these structures as providers of kinematic data. The basic assumptions and problems of existing models are outlined below.

Fibre growth in fringes takes place either syntaxially at the matrix-fringe interface or antitaxially at the interface of the core-object and the fringe, and fibres may or may not deform during ongoing deformation (reviews in Ramsay and Huber, 1983; Passchier and Trouw, 1996). This study deals with undeformed antitaxial strain fringes that are most common in nature. Figure 3.1 shows examples of such antitaxial non-deforming strain fringes. The core-object can be a spherical framboidal pyrite (Fig. 3.1a) or an angular iron-oxide object (Fig. 3.1b). Both examples are inferred to have developed during progressive non-coaxial deformation with a dextral shear sense (Passchier and Trouw, 1996). Two models have been proposed in the literature for the development of antitaxial strain fringes, and according to these models the fibres in the fringes may grow in a direction controlled by the orientation of the surface of the core-object (face-controlled growth) or they may grow parallel to the opening trajectory of the fringe irrespective of core-object orientation (displacement-controlled growth) (reviews in Ramsay and Huber, 1983; Passchier and Trouw, 1996).

Strain fringes that are inferred to be displacement-controlled have been used to evaluate incremental and finite strain histories (Durney and Ramsay, 1973; Beutner and Diegel, 1985; Ellis, 1986; Etchecopar and Malavielle, 1987; Aerden, 1996; Kanagawa, 1996). Several authors have stated that single displacement-controlled fibres can be used to evaluate the incremental orientation of the extensional ISA with respect to an external reference frame (e.g. the Earth's surface) (Durney and Ramsay, 1973; Ramsay and Huber, 1983; Beutner and Diegel, 1985; Ellis, 1986; Etchecopar and Malavielle, 1987; Aerden, 1996). Aerden (1996) has shown that this assumption

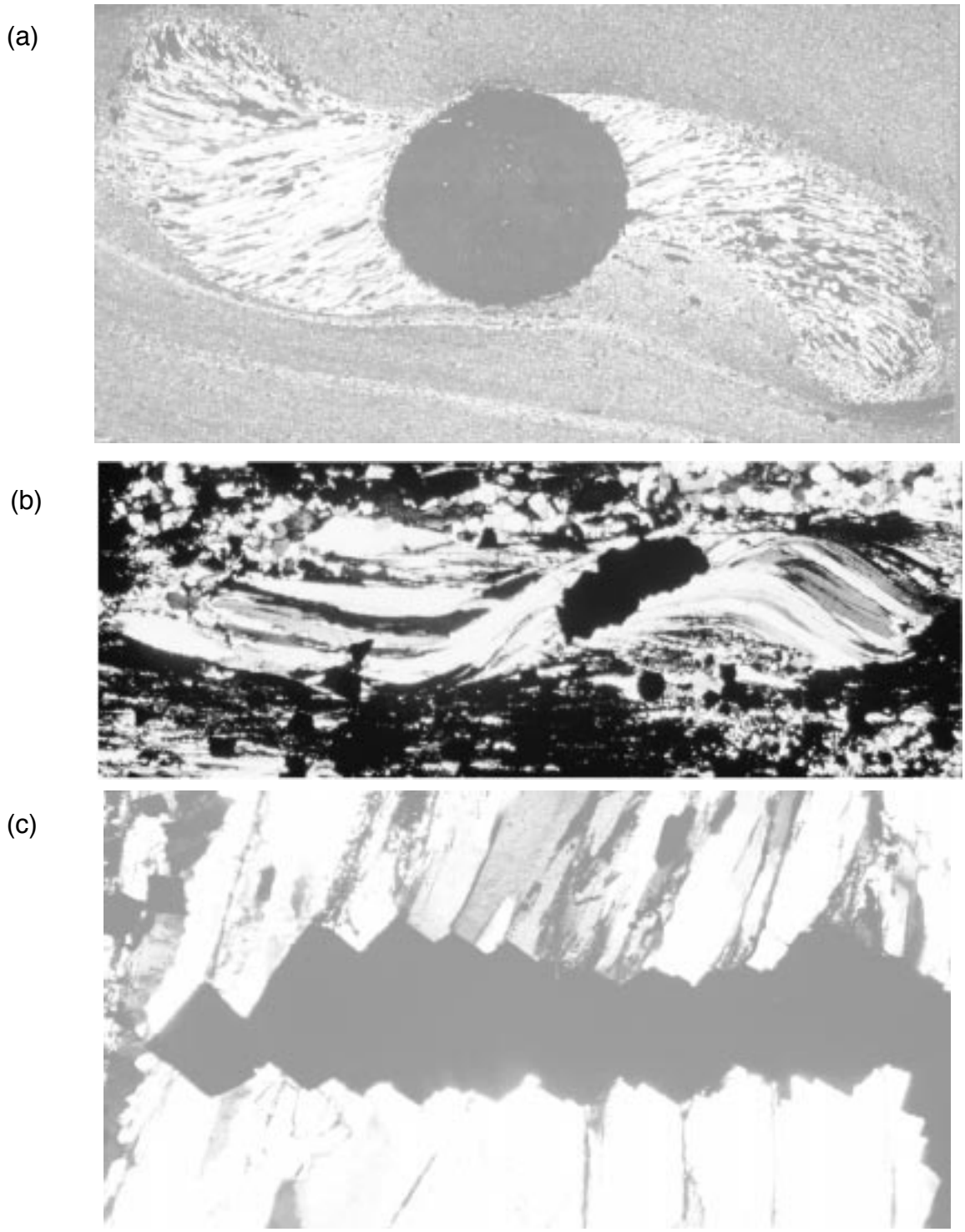

Fig. 3.1 (a) Micrograph of quartz fringes adjacent to a framboidal pyrite that developed during progressive non-coaxial deformation with a dextral shear sense, Leonora, Yilgarn Craton, Australia. Width of view is 20mm. (b) Micrograph of quartz strain fringes adjacent to an elongate iron oxide core-object from the Hamersley Ranges, Australia that developed during progressive non-coaxial deformation with a dextral shear sense. Width of view is 8mm. (c) Micrograph of quartz fibres adjacent to a rough iron oxide core-object from the Hamersley Ranges, Australia. Fibre boundaries are locked to outward-pointing asperities on the core-object surface. Width of view is 3mm.

is only valid for fibres in a plane cut parallel to the extensional ISA for coaxial progressive deformation if the core-object is not rotating with respect to its fringes. Rotation of the core-object with respect to its fringes will influence the geometry of fibres so that their long axis is no longer parallel to the extensional ISA (Aerden, 1996). The core-object in strain fringes will rotate with respect to ISA during (1) coaxial progressive deformation if it is elongate and not aligned with its long axis parallel to the extensional ISA or (2) non-coaxial progressive deformation (Ghosh and Ramberg, 1976; Aerden, 1996).

Non-coaxial progressive deformation produces complex fibre and fringe geometries which are difficult to interpret (Etchecopar and Malavielle, 1987; Aerden, 1996; Kanagawa, 1996; reviews in Passchier and Trouw, 1996). If the Earth's surface is used as an external reference frame during non-coaxial progressive deformation, the finite strain axes, fringes and core-object may all rotate with respect to this reference frame (Aerden, 1996; Passchier and Trouw, 1996) (Fig. 3.2). The orientation of the extensional ISA cannot be easily determined from strain fringes in this case, since the influence of the fringe- or object-rotation on fibre geometry is not clear.

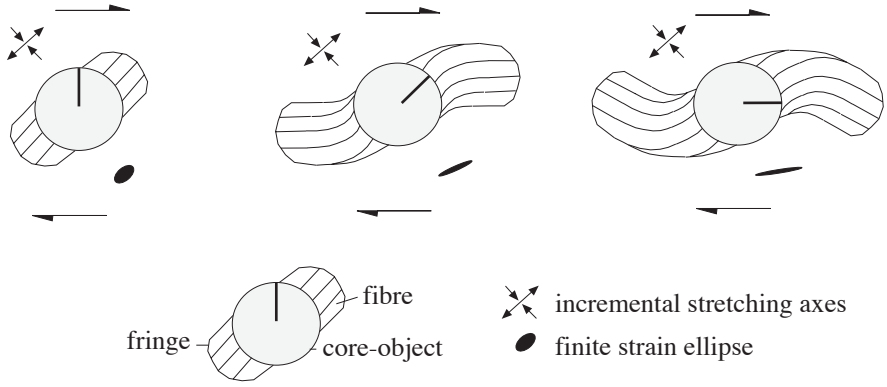

Fig. 3.2 Schematic illustration of the development of a fibrous strain fringe in simple shear, after Aerden (1996) and Passchier and Trouw (1996). Both the fringes and the core-object rotate with respect to ISA and the flow plane.

Nevertheless, several authors use specific assumptions to interpret matrix deformation from strain fringes (Beutner and Diegel, 1985; Ellis, 1986; Etchecopar and Malavielle, 1987; Aerden, 1996; Kanagawa, 1996). Beutner and Diegel (1985) do not consider fringe and core-object rotation with respect to an external reference frame; Ellis (1986) treats fringes and core-object as one rotating complex with respect to an external reference frame. Etchecopar and Malavielle (1987) and Kanagawa (1996) include different rotational behaviour of fringes and core-object in their methods. Aerden (1996) developed a method that can determine the rotation of fringes and core-object. He tried to trace sudden changes in the orientation of the extensional ISA with respect to an external reference frame, which he interprets in

terms of polyphase deformation.

The methods described above are based on different assumptions regarding the mechanism of fibre growth. In order to interpret strain fringes in a reliable way it is necessary to test these assumptions and to explain why fibres grow face- or displacement-controlled. Urai et al. (1991) developed a model that links growth of fibres to the presence of asperities on the surface of a core-object. They pointed out that when a polycrystalline fringe is pulled away from a core-object with asperities, the growth surface will be an irregularly shaped cast of the core-object. A simple geometrical consideration shows what happens if fibres grow equally fast and fill small "cracks" formed when fringe and core-object are pulled apart by several small steps: fibre boundaries will end up "fixed" to the tips of embayments in the irregular growth surface that point in the direction of the fringe. Therefore, the fibres are effectively "fixed" to the tips of asperities that fit in the embayments (Fig. 3.3). We developed a

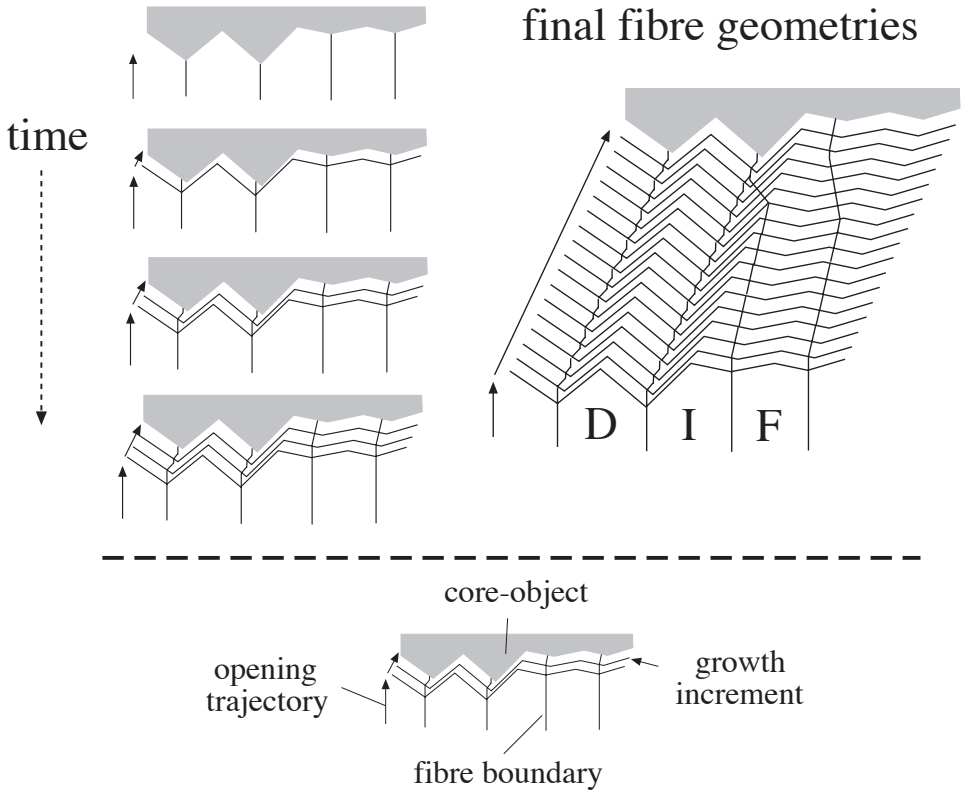

Fig. 3.3 Figure showing the tracking capability of outward-pointing asperities after Urai et al. (1991). D=displacement-controlled fibre, I=intermediate fibre, F=face-controlled fibre. Fibres grow isotropically so that fibre boundaries are oriented perpendicular to the growth surfaces. If the opening path of the core-object is not perpendicular to the enveloping surface of the core-object, fibre boundaries will first grow straight. They are now oriented at one side of the asperity and will grow back towards its tip if the asperity is pronounced enough. This process will produce tracking fibre boundaries.

computer program "Fringe Growth" based on the theory of Urai et al. (1991) to model

the growth of fibrous crystals in antitaxial strain fringes. The program can model differently shaped core-objects with different surface roughness to investigate the growth of face-controlled and displacement-controlled fibres during progressive coaxial deformation with straight fringe opening paths. We also tried to mimick progressive non-coaxial deformation using curved fringe opening paths and rotation of the core-object with respect to the fringes. We investigated the progressive fibre growth patterns during these experiments to test if the growth hypothesis of Urai et al. (1991) can explain fibre patterns examined in natural non-deforming antitaxial strain fringes. We discuss the implications of this growth hypothesis on commonly used kinematic analysis of antitaxial strain fringes.

3.2. The computer model

The computer model "Fringe Growth" is based on the algorithm of the model "Vein Growth" by Paul Bons (Bons, in press) and is written in "C" for Macintosh. "Fringe Growth" simulates two dimensional growth of fibrous grains in one of the two fringes adjacent to a rigid core-object. The horizontal and vertical axes of the computer screen are used as an internal reference frame (Fig. 3.4). The fringe is fixed in this

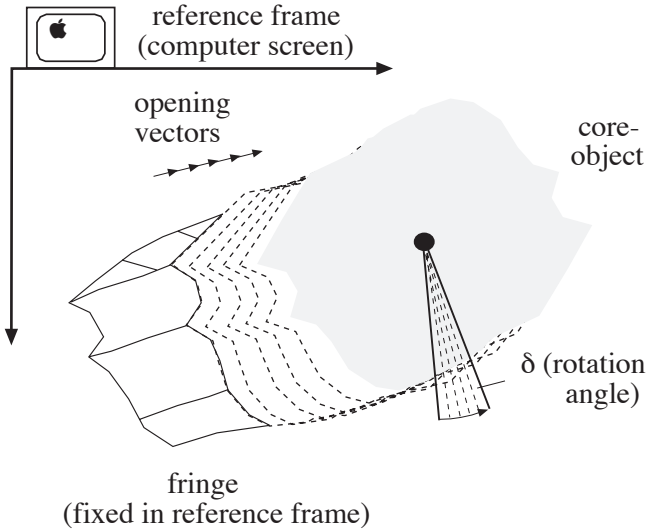

Fig. 3.4 Diagram showing how the core-object is moved in the "Fringe Growth" program. The fringe is fixed in an internal reference frame (the computer screen). The opening vector defines the magnitude and direction of the core-object movement. The rotation angle δ describes rotation of core-object around its centre relative to the computer's reference frame and to the fringe.

reference frame and only the core-object can move and rotate with respect to the fringe. Fibrous grains that build the fringe grow towards the core-object at the object-fringe interface so that the fringes are of the antitaxial type (Fig. 3.5). The growth rate of the crystals, the opening rate and opening direction of the fringe and the rotation of

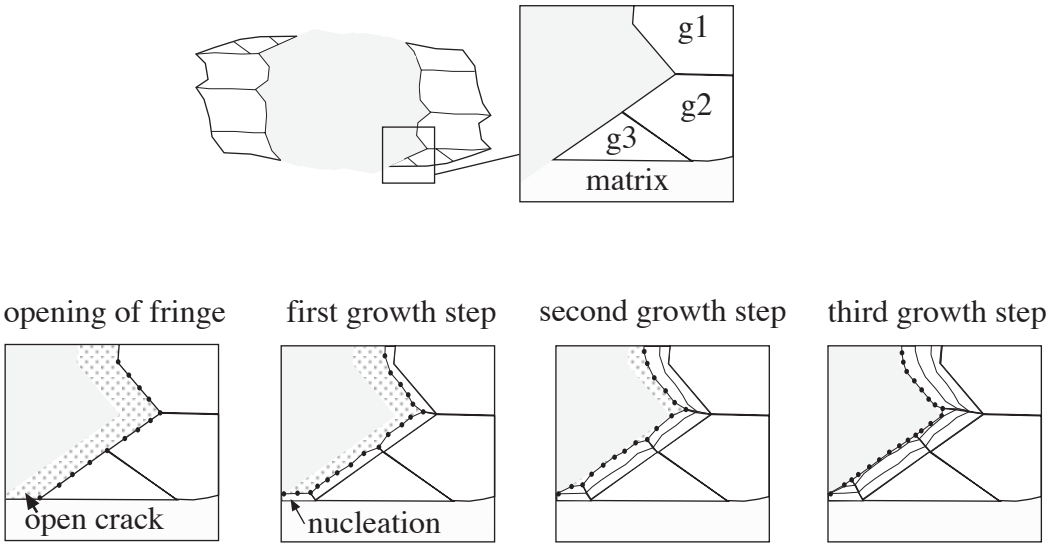

Fig. 3.5 Schematic illustration of the way in which fibres grow in the computer program. g1,g2 and g3 are fibres in the fringe. Once the fringe opens (movement of the core-object) nodes on the grain boundaries will move resulting in fibre growth towards the core-object until the free space is filled. A new nucleus is inserted next to the rim of the fringe after the fringe has opened.

the core-object around its centre are independent of each other and can be defined by the user. The model is only simulating the fibre growth process; the matrix around the strain fringe is not included in the simulations. The contact of the fringe to the matrix is the boundary of the model. Once grains have nucleated on this boundary, the boundary remains stable since the fringes are not deforming. Any core-object shape can be created by the user from digitised drawings. Four pre-defined shapes are available: smooth square, rough square, smooth round and rough round core-objects. The program inserts the first grains with a user-defined width at the rim of the core-object where the fringe opens. A growth-anisotropy of the crystals in the fringe can be defined by a two dimensional crystal growth file (Bons, in press; Appendix). The growth anisotropy defines the crystal growth habit or euhedral shape. For our simulations we use a prismatic mineral growth file (Bons, in press; Appendix).

3.2.1. Growth of fibrous grains

The grains in the fringe, the fringe itself and the core-object are polygons defined by a number of nodes (Fig. 3.5). These polygons are all connected with each other. Triple junction nodes connect three neighbouring nodes and are on the vertices of three polygons; double junction nodes connect two neighbouring nodes and lie between two neighbouring polygons. During runtime, nodes are moved by small increments that are calculated from the maximum growth velocity defined by the user and from the orientation of the growth surface with respect to the crystallographic orientation of the grain (Fig. 3.5). A detailed description of the growth algorithm is

given in Bons (in press; Appendix). If the distance between two nodes is below a user-defined critical value, one node is removed; if the distance is above this critical value an extra node is added. This keeps the user defined distance between nodes roughly constant. Following an opening step of the fringe, nodes of growing grains are unlocked and grow until they reach the core-object (Fig. 3.5). Then they are locked until the fringe opens again. Nucleation of new grains takes place at the contact of the fringe with the matrix (the boundary of the model) (Fig. 3.5). The program will insert a new nucleus if the grain next to the fringe has reached a user-defined width. Sometimes large new sections of a fringe can open at once, especially if the core-object has pronounced corners. If there is enough space for more than one nucleus, the program will keep on nucleating crystals until the free space is filled.

3.2.2. Movement of the core-object

In our model, fringes are fixed in the internal reference frame and fibre-geometry in a developing fringe is completely defined by movement of the core-object. This movement has two components: (1) displacement of its centre away from the fringe and (2) rotation around the object centre. Both are varied in our experiments. The movement of the centre of the core-object away from the fixed fringe is described by the magnitude and direction of the opening vector per time increment (Fig. 3.4) as defined by the user and is termed the object-centre path. The computer screen is used as a reference frame for the direction of the opening vector. The user can change the magnitude and direction of the opening vector and can also define a permutation angle by which the direction of the opening vector will change at each opening increment. This produces curved object-centre paths. The core-object can rotate by user-defined amounts around its centre with respect to the computer's reference frame. Anticlockwise core-object rotation is positive and clockwise rotation negative. The program saves a picture of the growing fringe for every user-defined number of growth steps, so that movies of incremental fibre growth can be created.

3.3. Modelling results

Systematic runs of the program have been carried out with different core-object shape, core-object surface morphology, opening direction (object-centre paths) and relative core-object fringe rotation. The results show that face-controlled and displacement-controlled fringes are end-member cases as predicted by Urai et al. (1991). Face-controlled fringes develop around smooth core-objects, but around rough core-objects fringes are not always displacement-controlled since they contain both face- and displacement-controlled fibres (Fig. 3.6). Even single fibres switch from face- to displacement-controlled growth and vice versa, which is often observed close

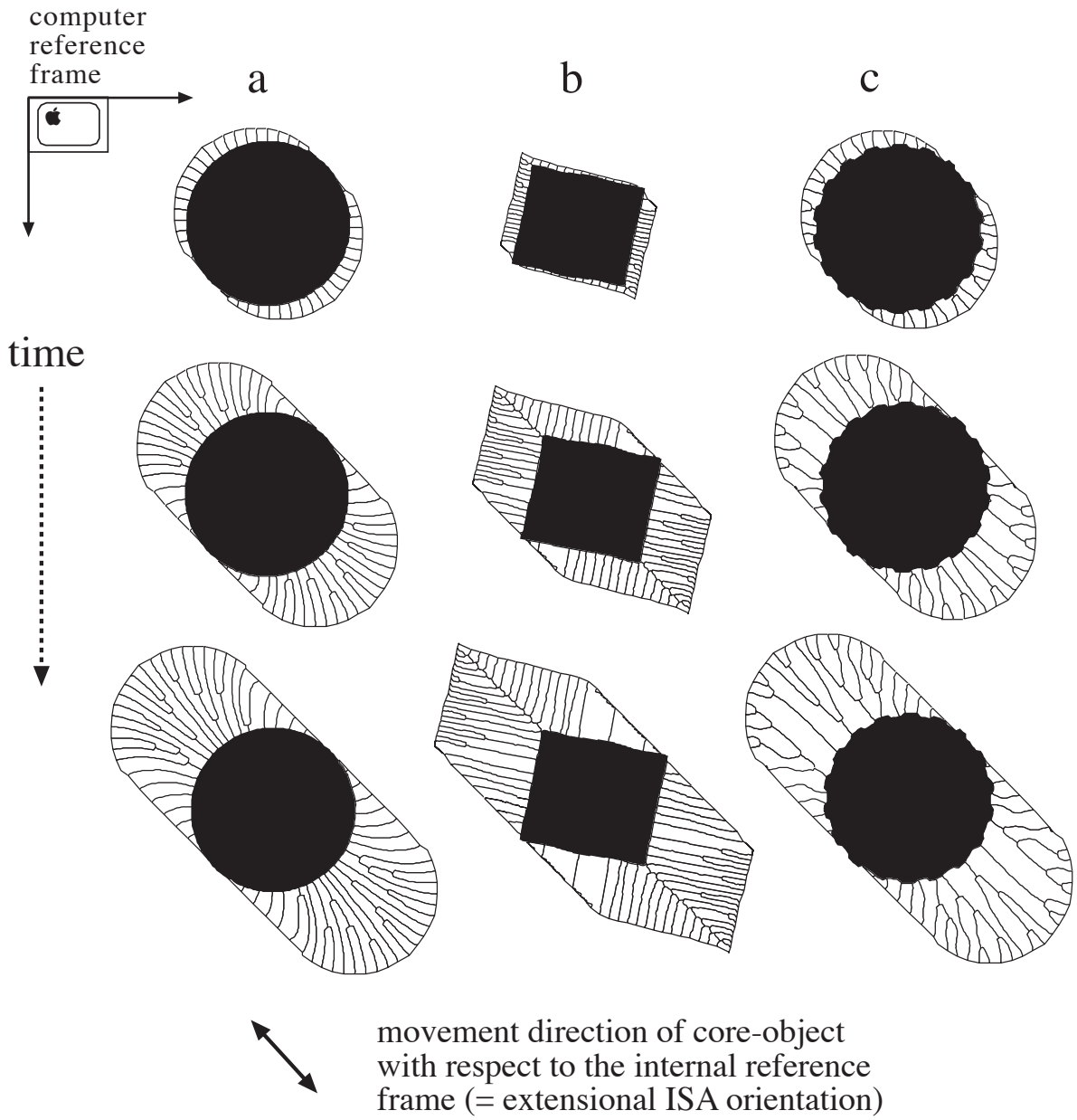

Fig. 3.6 Simulations of "Fringe Growth" mimicking coaxial progressive deformation (straight object-centre paths) with ISA fixed in the internal reference frame and using different core-object shapes. Double fringes are shown to allow comparison with natural objects, although only one is modelled in the computer program. ISA orientation is parallel to movement direction of the core-object. (a) Simulation using a smooth round core-object. All the fibres grow face-controlled. The fibres show a curvature towards the centre of the core-object. (b) Simulation using a smooth square core-object. The fibres grow face-controlled towards the flat faces of the core-object. Displacement-controlled suture lines separate face-controlled fibres that grow in different directions. (c) Simulation with a rough round core-object. Most fibres grow displacement-controlled. Only fibres on the rims of the core-object grow face-controlled. The fibre width is dependent on the distance between the asperities on the core-object surface. (Figure visible as Quicktime movie on CD-ROM attached to the thesis).

to changes of the object-centre path (Figs. 3.7, 3.8). The results of the numerical modelling are discussed in the following sections.

3.3.1. Straight object-centre paths

We us straight object-centre paths to mimick coaxial progressive deformation without fringe rotation with respect to an external reference frame. In this case ISA are fixed in the external reference frame and in the computer reference frame (Fig. 3.6).

Face-controlled fibres around round core-objects with a smooth surface were found to develop in a geometry predicted by Passchier and Trouw (1996). All the fibres grow permanently towards the centre of the core-object (Fig. 3.6a). The fibres tend to get thinner and disappear after they have reached a certain length because fibres grow radially inwards towards the core-object. The fringes are symmetric with respect to a plane through the middle of the fringe and through the centre of the core-object (Fig. 3.6a). The fibres in the fringe develop a curved shape because the orientation of their growth surface changes as they grow from the rim of the fringe towards its centre (Fig. 3.6a).

If the core-objects are square and have a smooth morphology, the fibres grow face-controlled perpendicular to the sides of the square (Fig. 3.6b). A suture line (Ramsay and Huber, 1983) which separates differently oriented face-controlled fibres develops from the corners of the square core-object. The corners have the same effect on suture lines as small asperities on the surface of a rough core-object have on individual displacement-controlled fibre boundaries (Fig. 3.6c). This is valid for all core-objects: as soon as the core-object has corners, suture lines get trapped on these corners and become displacement-controlled.

If the core-object has a rough surface, outward-pointing asperities on the core-object tend to capture grain boundaries and create displacement-controlled fibres as predicted by Urai et al. (1991) (Figs. 3.1c, 3.6c). Whether or not fibre boundaries get locked on these asperities depends on the form of the asperities (amplitude and wavelength/amplitude ratio), on the orientation of the enveloping surface on which the asperities are located with respect to the opening vector, and also on the opening velocity of the fringe with respect to the growth velocity of the crystals (Urai et al., 1991). The tracking capability of asperities is described in detail in section 3.3.3. Not all fibres in the fringes grow displacement-controlled since face-controlled fibres develop at the rims of the fringes where asperities are unable to lock fibre boundaries (Fig. 3.6c).

The width of the growing fibres is directly influenced by the distance between outward-pointing asperities on the core-object surface (Figs. 3.1c, 3.6c). If the asperities are close together, the fibres are thin. If they are further apart, fibres are thicker and fewer

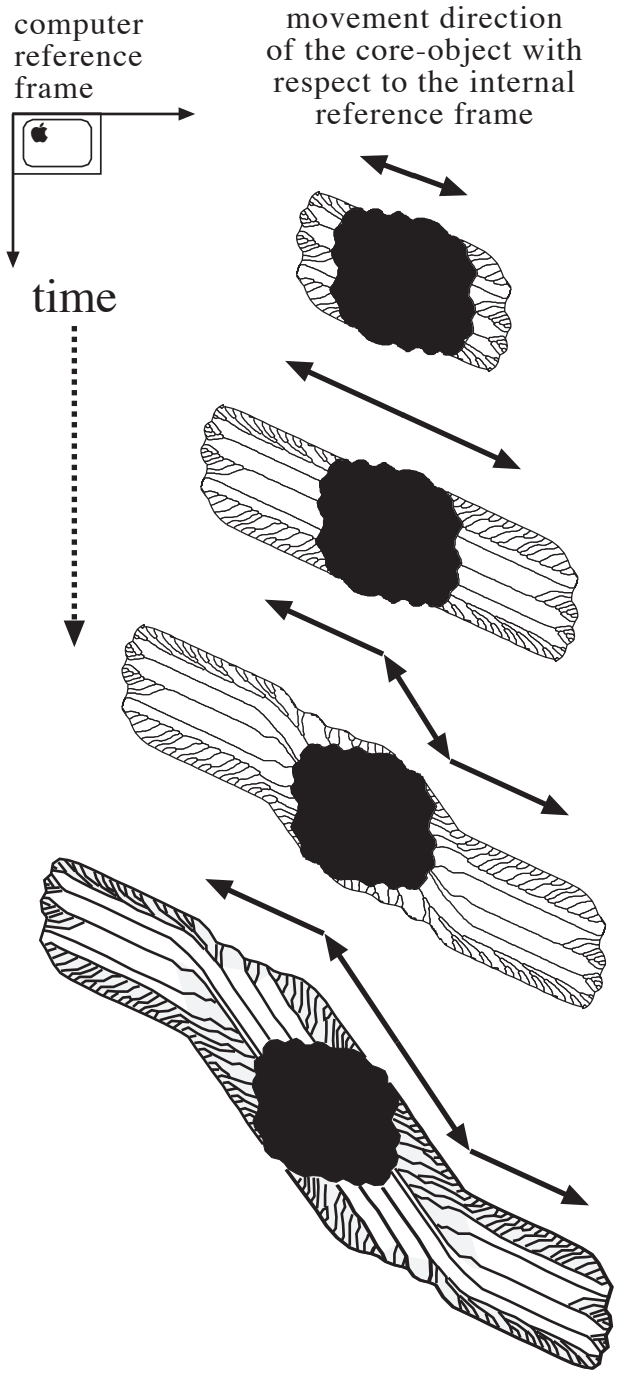

Fig. 3.7 Fringe growth in pure shear flow around a rough core-object. The movement direction of the core-object is suddenly changed with respect to the fixed fringe in the internal reference frame. In nature, this could correspond with a change in the orientation of ISA in the external reference frame. During a change of the opening trajectory some displacement-controlled fibres start to grow face-controlled and vice versa. In the final fringes, face-controlled fibre parts are marked grey and displacement-controlled fibre parts are white. Double fringes are shown to allow comparison with natural objects, although only one is modelled in the computer program. (Figure visible as Quicktime movie on CD-ROM attached to the thesis).

fibres develop. The size of the original nuclei only influences the width and number of the fibres if the nuclei are larger than the distance between the asperities (Hilgers et

al., in press).

3.3.2. Object-centre paths with changing directions

Fibre patterns in strain fringes are most complex if the object-centre path is not straight and progressive deformation is non-coaxial. We tried to investigate two different scenarios: (1) The object-centre path is straight but changes suddenly during deformation by about 30° (Fig. 3.7). This either mimicks a rigid body rotation where the strain fringes rotate suddenly with respect to ISA or a sudden rotation of ISA with respect to the strain fringes fixed in the external reference frame (e.g. polyphase deformation). (2) The object-centre path is curved. This mimicks a progressive non-coaxial deformation, for example simple shear, where strain fringes are progressively rotating with respect to ISA fixed in the external reference frame (Figs. 3.8, 3.9). In nature, this rotation of the fringes is due to the fact that they are rigid objects, and therefore subject to a torque associated with the vortical flow in the matrix. We also try to investigate displacement-controlled fibre patterns that are produced by relative core-object fringe rotation (Fig. 3.9).

Complex fibre geometries develop where we mimick changes in orientation of ISA with respect to the computer screen (internal reference frame) during a simulation. Displacement-controlled fibres may change to grow face-controlled and vice versa (ornamentation in Fig. 3.7). Such fibres containing face- and displacement-controlled parts are named "intermediate fibres". It is therefore dangerous to use single fibres for a kinematic analysis, since fibres are not necessarily displacement-controlled along their whole length. The two different fibre types can be distinguished in Fig. 3.7 because the change in the direction of the object-centre path is sudden and pronounced (30°) and the core-object is not rotating with respect to the fringe. If the change in the direction of the object-centre path is more gradual and the core-object is rotating with respect to the fringe it can be very difficult to distinguish between displacement- and face-controlled fibres (Fig. 3.8).

If object-centre paths are curved, complex face- and displacement-controlled fibre-patterns develop. This is shown in Fig. 3.8 in three steps. Face-controlled fibres are common on the rims of the fringes. Displacement-controlled fibres develop from face-controlled fibres and are locked to outward-pointing asperities on the core-object surface (Fig. 3.8a). These displacement-controlled fibres change to grow face-controlled again during Fig. 3.8b. New displacement-controlled fibres develop towards asperities on another face of the core-object during Fig. 3.8c. It is difficult to distinguish face-controlled parts of fibres from displacement-controlled parts even in the experiments. In nature, where progressive fringe development is not known but only the final geometry of the fibres can be studied, it is in many cases impossible.

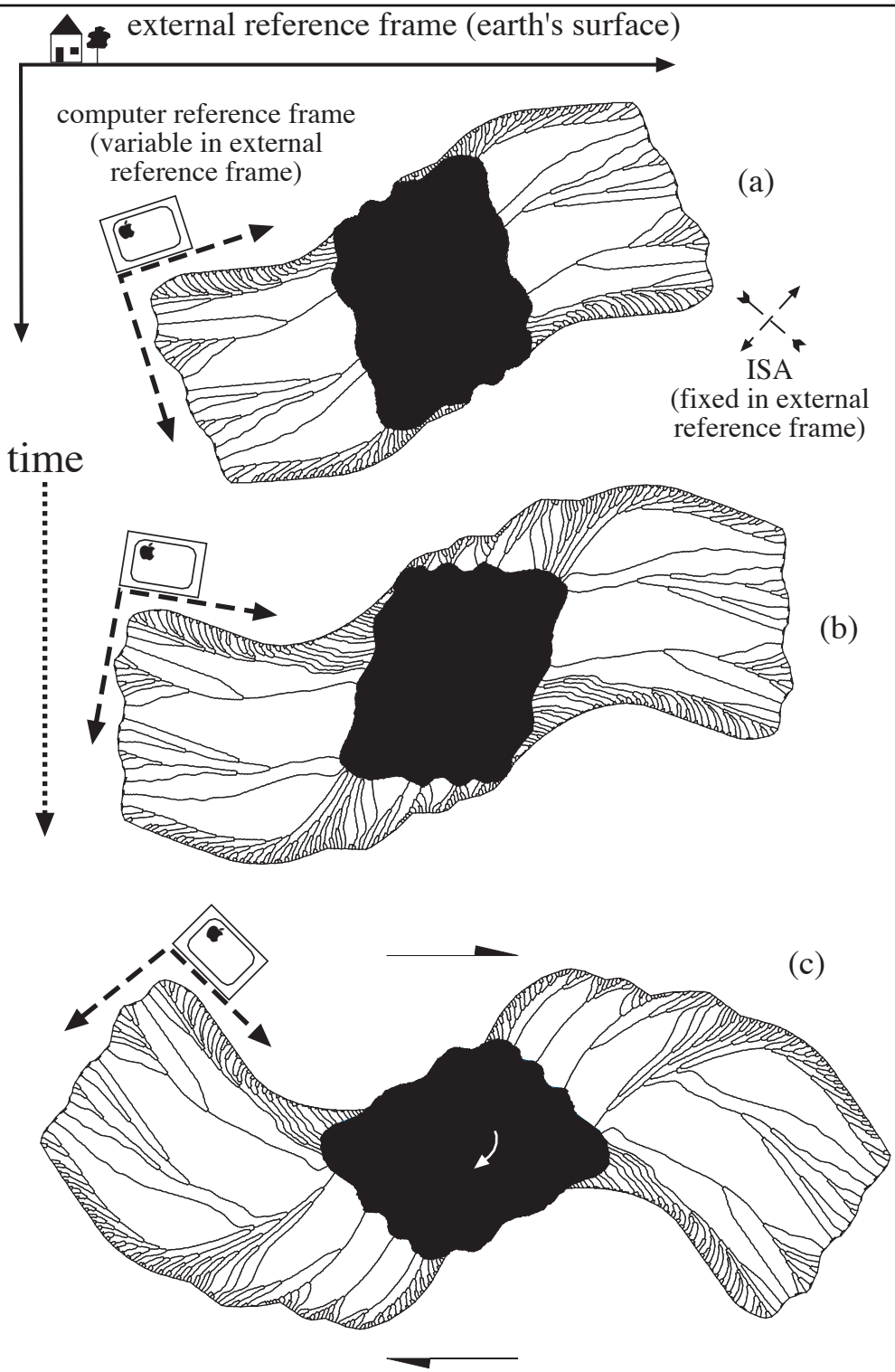

Fig. 3.8 Model of fringe growth with constant rotation rate of the core-object in the internal reference frame. In nature, this could correspond to rotation of both fringes and core-object in the external reference frame (Earth's surface) with fixed ISA (curved object-centre path). This model serves to simulate non-coaxial progressive deformation. Rotation of fringes and core-object with respect to ISA result in complex fibre patterns and fringe forms. None of the fibres grows parallel to the opening trajectory of the fringe. If a pronounced corner of the core-object rotates into the fringe the fibre patterns change completely and a suture develops. The fringe looks as if it experienced two different opening events. Note that the reference frame of the computer is rotating with respect to the external reference frame (Earth's surface) because the fringes are fixed in the computer reference frame. Double fringes are shown to allow comparison with natural objects, although only one is modelled in the computer program. (Figure visible as Quicktime movie on CD-ROM attached to the thesis).

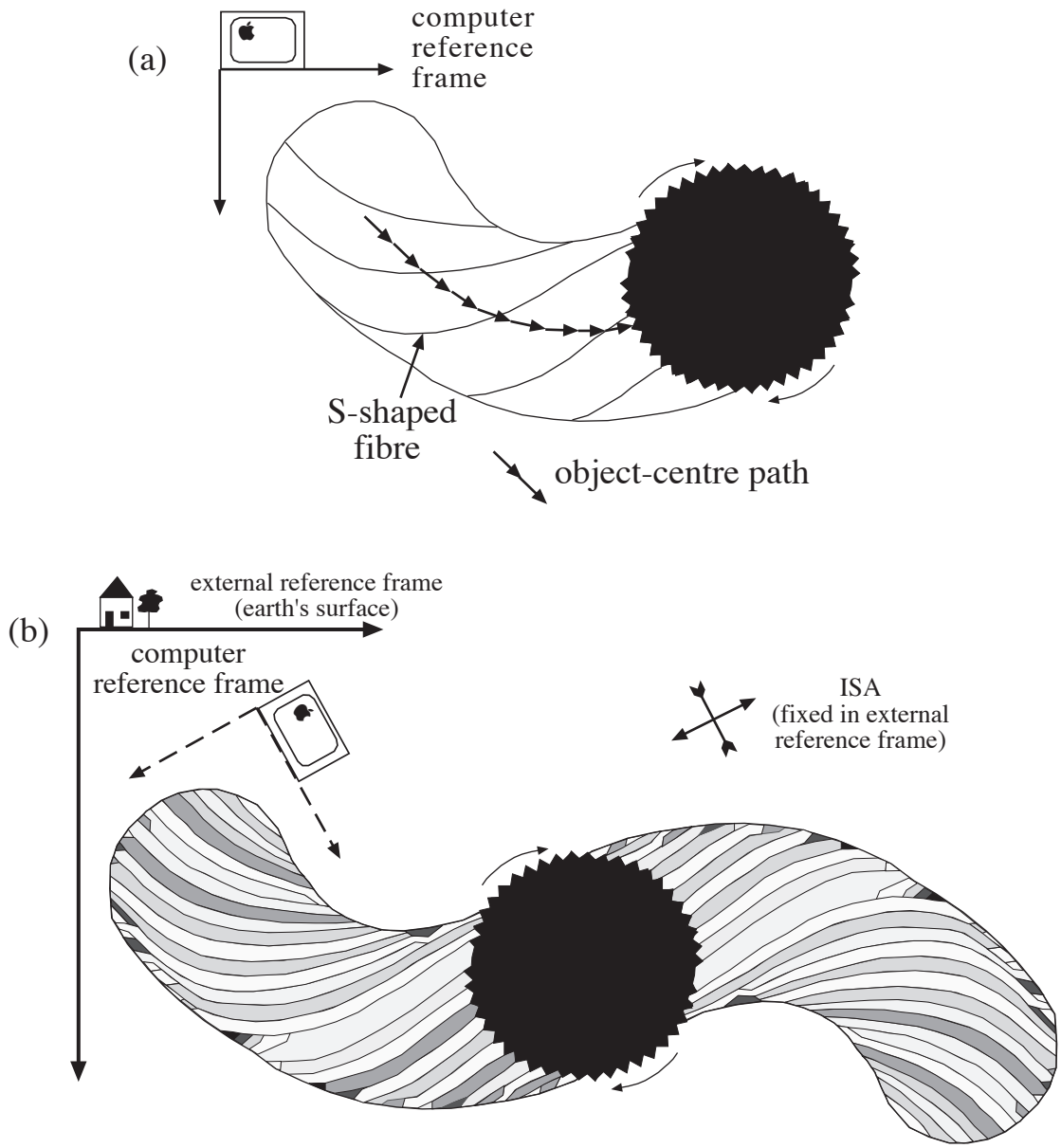

Fig. 3.9 Simulation of a fringe around a rough round core-object during non-coaxial progressive deformation. (a) In the computer model, the core-object rotates 90° with respect to the fixed fringe and the opening path is curved. Relative core-object fringe rotation produces a changing fibre curvature so that the fibres develop an S-form. Displacement controlled fibres are truncated by the rim of the fringe. (b) Double fringes are shown to allow comparison with natural objects, although only one is modelled in the computer program. In nature, the fringes and the core-object are inferred to rotate at different velocities with respect to the external reference frame (Earth's surface), so that core-object and fringes rotate relative to each other. The simulated fibre patterns are similar to the fibre patterns in Fig. 3.1a. This suggests that in nature round core-objects do rotate with respect to their fringes.

Another variable which may be important in fringe development is rotation of the core-object with respect to the internal reference frame, i.e. the fringe. Figure 3.9 shows simulation of a strain fringe around a rough round core-object. The object-centre path

is curved and the core-object is rotated clockwise with respect to the growing fringe. In this experiment, we tried to reproduce the fibre patterns of Fig. 3.1a. If the core-object is rotating with respect to the fringes, the curvature of displacement-controlled fibres will change progressively from one side of the fringe to the other and will have a geometry showing an S-shape during dextral progressive simple shear deformation (Fig. 3.9). This geometry cannot be generated using curved object-centre paths without core-object rotation: it only forms if the core-object has rotated with respect to the fringe, in the case of Fig. 3.9 by about 90°. The fibres are truncated by the rim of the fringe because of the curved object-centre path and the relative rotation of core-object and fringe. Displacement-controlled fibres in the fringe do not grow parallel to the extensional ISA (Fig. 3.9). As can be seen from comparison of Figs. 3.1a and 3.9, the geometry of the natural object closely resembles the modelled one, which suggests that the fringe in Fig. 3.1a formed during progressive non-coaxial deformation.

3.3.3. Tracking capability of outward-pointing asperities

The tracking capability of outward-pointing asperities as postulated by Urai et al. (1991) has been defined for isotropically growing crystals. During isotropic growth all the fibres in a fringe will grow with the same growth speed so that grain boundaries will always be perpendicular to the growth surface of the fibres. Figure 3.3 illustrates how fibre boundaries of isotropically growing fibres can get captured by outward-pointing asperities according to Urai et al. (1991). In our simulations we use anisotropic growth kinetics which are more realistic to model natural crystal growth. The opening velocity of the fringe with respect to the growth velocity of the crystals influences the shape of the crystals and their ability to track displacement. If we consider opening to occur by periodic steps, four different cases can be distinguished (Fig. 3.10) (Mügge, 1928); (a) a single opening step of the fringe is smaller than the incremental growth step of the slowest growing crystal; (b) a single opening step of the fringe lies between the incremental growth step of the slowest and fastest growing crystal; (c) a single opening step of the fringe is larger than the incremental growth step of the fastest growing crystal, but the crystals are growing faster than the average opening velocity; (d) a single opening step of the fringe is larger than the incremental growth step of the fastest growing crystal, and the crystals are growing slower than the average opening velocity of the fringe. In case (a) the crystals have no space to develop crystal facets: they will grow mostly isotropically so that their growth velocity is the same in every direction and will have excellent tracking capabilities as grain boundaries are mostly oriented perpendicular to the growth surface (Figs. 3.3, 3.10a). In this way, the fringe develops continuously in a thin gap along the core-object if we

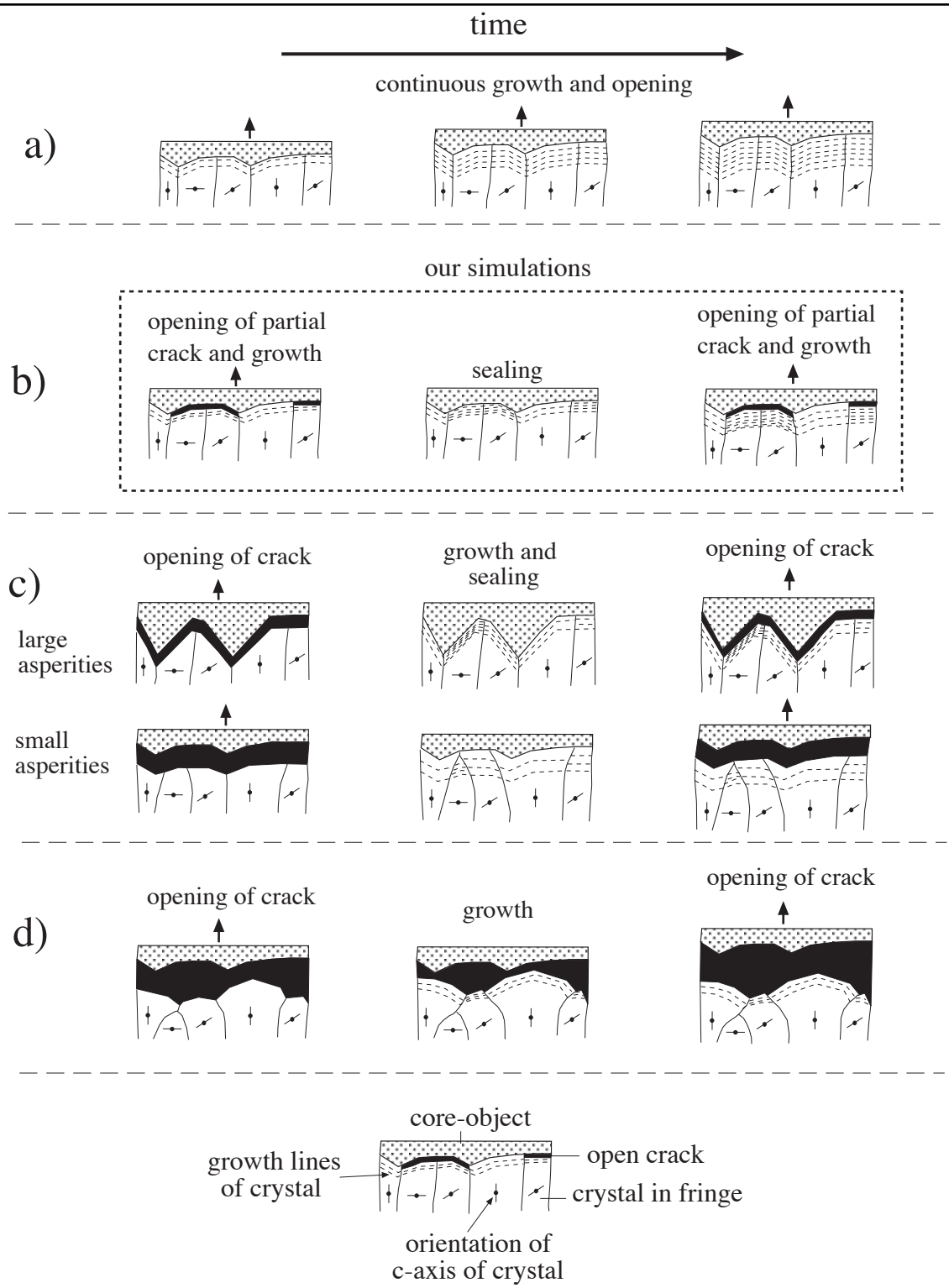

Fig. 3.10 Diagram showing the effect of four different opening rates of the fringe with respect to the growth rate of the growing crystals. (a) A single opening step of the fringe is smaller than the growth step of the slowest growing crystals. Growth and opening process is continuous. (b) A single opening step of the fringe is between the growth step of the slowest and fastest growing crystal. Crystals that are oriented with their slowest growth direction perpendicular to the growth surface are detached from the core-object and grow into small cracks. (c) A single opening step of the fringe is larger than the growth step of the fastest growing crystal, but the crystals seal the open space before the next opening event. The crystals grow in a crack-seal manner and start to form crystal facets as they grow into open space (fluid filled crack). A crack develops between the fringe and the core-object. Crystals may loose their tracking capability depending on the width of the crack compared to the size of the asperities on the surface of the core-object. The crystals will loose their fibrous habit and grow elongate or blocky if the crack width is too large. (d) The core-object is permanently completely detached from the fringe as the crystals do not grow fast enough to seal the open space. The crystals develop facets and have an elongated or blocky form.

consider that periodic opening steps are infinitesimal small. In case (b) the crystals tend to grow anisotropically because they grow partly into larger open cracks, and start to develop crystal facets because their growth velocity depends on the orientation of the growth surface with respect to the crystallographic orientation of the crystal (Fig. 3.10b). This reduces their tracking capability as the growth of grain boundaries is not necessarily perpendicular to the growth surface and the fibres may not be locked on the asperities anymore if these are small with respect to the growth steps of the crystals (Fig. 3.10b). We have tried to simulate case (b) by using an opening vector for incremental fringe opening that is smaller than an incremental growth step of the fastest growing crystal. In case (c) a crack develops between the core-object and the fringe (Fig. 3.10c,d). If the crystals grow fast enough, they seal this crack before the next opening event. This "crack-seal" process (Ramsay, 1980) reduces the tracking capability of crystals since they grow anisotropically. Fibres in the fringe will only follow asperities on the core-object if the crystals do not outgrow each other too quickly (Fig. 3.10c) and then loose their fibrous habit to grow elongate or blocky (Fisher and Brantley, 1992; Bons and Jessell, 1997). Once the crystals are not growing fast enough to seal the crack (case d) they grow anisotropically, loose all abilities to track displacement and develop elongate or blocky crystals instead of fibres (Fig. 3.10d). From case (a) to (d) crystals in fringes show a decreasing ability to track displacement, even if the core-object is rough. Cases (a), (b) and partly (c) may produce very similar structures depending on the anisotropy of the crystals and the roughness of the crack/growth surface.

If the opening of the fringe is a continuous process (case a) a simple diagram illustrates which asperities will lock fibre boundaries (Fig. 3.11) (Urai et al., 1991). The two important parameters are the angle β of the asperity (pointedness) and the angle α of the enveloping core-object surface on which the asperity is located with respect to the opening direction of the fringe (Fig. 3.11). The angle β is defined in Urai et al. (1991) as 2 arctan (λ/2 y), where λ is the wavelength of the asperities on the core-object surface and y the amplitude. The angle α is defined in this paper in a different way from Urai et al. (1991) who define α for veins as the angle between the local orientation of the crack surface and the opening vector so that α is dependent on β. In our case the two angles are independent which simplifies an α-β diagram showing the tracking capability for fibres in strain fringes around core-objects. Using our definition, the asperities will be able to lock the fibre boundaries as long as $\alpha > \beta/2$. If $\alpha = \beta/2$, one side of the asperity will be at 90° to the growing fibre boundary (Fig. 3.11). If $\alpha > \beta/2$, the fibre boundary is locked to the asperity and if $\alpha < \beta/2$ the fibre boundary will grow away from the asperity (Fig. 3.11). This explains why face-controlled fibres can be expected at the rims of fringes where α is low, even on rough core-objects.

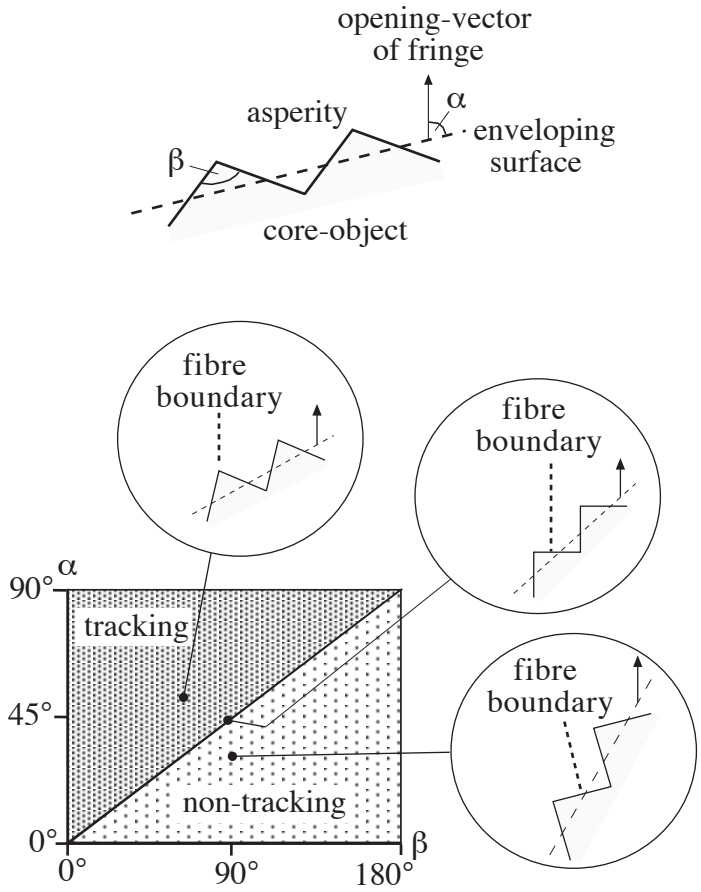

Fig. 3.11 Asperities can lock fibre boundaries depending on the shape (pointedness) of the asperities and the orientation of the enveloping core-object surface with respect to the opening direction. The pointedness of the asperities is described by the angle β of the asperity. The angle α describes the orientation of the core-object surface with respect to the opening-vector of the fringe. Asperities are able to lock fibre boundaries if $\alpha > \beta / 2$. Asperities with an angle β of 180° are flat surfaces so that fibre boundaries cannot be locked. Very pointed asperities with an angle β approaching 0° will be able to lock fibres irrespective of α.

Asperities with an angle β of 180° are flat surfaces so that fibre boundaries cannot be locked. Very pointed asperities with an angle β approaching 0° will be able to lock fibres irrespective of α.

3.4. Discussion

Modelling of fibre growth in strain fringes with the program "Fringe Growth" shows that a strain analysis based on the assumption that the long axis of displacement-controlled fibres is parallel to the extensional ISA (Durney and Ramsay, 1973; Ramsay and Huber, 1983; Ellis, 1986) is only applicable in some very special cases. Our modelling supports the assumption of Urai et al. (1991) and Aerden (1996) that displacement-controlled fibres follow points on the core-object surface. Rotation of core-object and fringe with respect to each other influences fibre patterns (Figs. 3.1a, 3.9). This influence must be taken into account before fringes can be used in

kinematic analysis. The method of Aerden (1996) to interpret object-centre paths and relative object-fringe rotation for strain fringes is supported by our simulations, even though he interpreted only displacement-controlled fibres. Simulations with the model "Fringe Growth" can explain the occurence of both face- and displacement-controlled fibres in one fringe and can reproduce most, if not all, fibre and fringe geometries observed in nature.

Our model confirms the statement of Aerden (1996) that round core-objects do rotate during simple shear deformation with respect to the fringes, since the geometries described in the study presented here correspond to models with a rotating core-object. In nature, its is possible that both fringes and the core-object rotate with respect to ISA and to an external reference frame. This can be expected in non-coaxial flow, e.g. simple shear. Fringes will act as rigid objects, and both fringes and core-object will rotate in the shear sense direction, and with respect to each other. This will create fibre geometries similar to those of a rotating core-object with respect to a stationary fringe in the numerical experiments. An extra complication in nature develops because fringes change their shape by growth at the contact with the core-object. Equidimensional fringes will therefore develop towards an elongate shape, and will gradually decrease their rotation rate with respect to ISA; elongate objects rotate more slowly than equidimensional ones if their long axis makes an angle of less than 45° with the flow plane (Ghosh and Ramberg, 1976). The core-object will rotate at constant velocity if equidimensional, or at pulsating rate if elongate. The fibre geometry can store information on such gradients in relative rotation velocity of fringes and core-object (Figs. 3.1a, 3.9), and such information may be retrieved from the microstructure.

It is also worth noting that fibre geometries that develop in response to a relative rotation of ISA with respect to the internal reference frame (a line in the rigid fringe or, in our modelling, the computer screen) cannot be easily translated to rotation in an external reference frame. If the internal reference frame (i.e. the fringe) is fixed with respect to the external reference frame (e.g. Earth's surface), the ISA orientation is changing with respect to both reference frames. This could correspond to a change in direction of the stress field. Alternatively the orientation of the fringe is changed with respect to the external reference frame and ISA are fixed in the external reference frame. This could occur by rigid body rotation of the fringes, e.g. in non-coaxial flow. These two cases cannot be easily distinguished by the computer simulations or in nature, since fibre geometries may be identical. However, further modelling may lead to recognition of specific relative rotation histories of ISA and fringe that are typical for one case or the other.

A single fibre may have displacement-controlled and face-controlled oriented

segments along its length which will be difficult to distinguish in natural examples. In fact, the terms "displacement-controlled" and "face-controlled" are end-member models, and fibres or sections of fibres can have orientations that fit neither of the two. It is therefore unrealistic to speak of "face-controlled fringes" or "displacement-controlled fringes" except in some special situations. In particular core-objects with pronounced corners produce very complex fibre patterns during non-coaxial progressive deformation. In these cases not even the shape of the fringe itself reflects the opening path, but is strongly influenced by the geometry of the core-object (Figs. 3.1b, 3.8).

For most natural examples, trial and error simulations can be carried out with "Fringe Growth" to produce the observed fibre and fringe geometry and to evaluate the object-centre path and relative core-object fringe rotation. Because of the large number of possible geometries, this is a major project that is now in progress. A new program is also being developed to calculate the core-object paths and relative core-object fringe rotation directly from images of natural examples of strain fringes.

3.5. Limits of the computer program

The "Fringe Growth" program can model fibre growth in fringes, but obviously not all factors governing fibre growth in nature can be included. The following limitations of the program may be important.

(1) The model incorporates the nucleation of new crystals next to the core-object at the rims of the fringe. No nucleation takes place further inside the fringe. A new nucleus is inserted if the growing grain next to the core-object has reached a certain width or if the distance from the fringe to the core-object is larger than half this width. This width can be set by the user and changed during a simulation. In nature the initiation of new nuclei is a function of oversaturation, seeds, opening velocity of the fringe and growth velocity of the crystals. Only the last two parameters are included in "Fringe Growth" so far.

(2) If a core-object has very pronounced corners and is rotating, these corners will tend to move over newly grown grains in the fringe. In nature this will either stop the rotation of the core-object or the fringe, or parts of the fringe will be fractured or dissolved. In the present version of "Fringe Growth" the rotation of the core-object or the fringes can be stopped if the core-object corners move into the fringe but the grains cannot be dissolved.

(3) The present version of "Fringe Growth" is purely kinematic. It models growth of grains into an open space and is based on the crack-seal process. Growth of fibres in strain fringes might also take place by a growth process accompanying pressure

solution. If the fringe is opening more slowly than growth of crystals in the fringe, and if an incremental opening step of the fringe is smaller than the growth step of the slowest growing crystal in the fringe, no "crack" may develop between the core-object and the fringe (Mügge, 1928). The material for the growth of the fibres will be transported by diffusion along the grain boundaries and will precipitate at the interface of core-object and fringe. This interface can support a differential stress, in contrast to the fluid in an open crack. Fibre geometries probably will not change dramatically by this process, since the present version of "Fringe Growth" can already produce natural looking fringes. The tracking capability of the fibres might be enhanced however, and this has to be tested with a version of "Fringe Growth" that includes differential stress effects.

(4) The rotation and opening rates are treated as independent. In a real, dynamic system they are probably not independent. A future version may include this dependence and thus reduce the number of possible fringe and fibre geometries.

3.6. Conclusions

The computer model "Fringe Growth" can simulate progressive growth of fibrous strain fringes. Core-object morphology, the roughness of its surface and the growth rate of crystals compared to the opening velocity of the fringes control the growth of displacement-controlled, face-controlled or intermediate fibres. Displacement-controlled fibres develop because the fibre boundaries are locked to outward-pointing asperities on the surface of the core-object. This supports the assumption that these fibres follow points on the core-object surface. Fringes with only displacement- and face-controlled fibres are rare end-members: most of the simulated fringes contain both face- and displacement-controlled fibres and intermediate fibres that change from displacement- to face-controlled growth. The long axis of displacement-controlled fibres does not follow the orientation of the extensional ISA in most cases. Displacement-controlled fibres follow asperities on the surface of the core-object and thus record the opening direction as well as rotation of the core-object and the fringes with respect to ISA and with respect to each other.

The computer program "Fringe Growth" provides a powerful tool for research and teaching to analyse fibre patterns in antitaxial strain fringes. The program is shareware for Macintosh computers and can be downloaded from the Journal of Structural Geology WWW-page together with Quicktime movies showing progressive fibre growth around different core-objects (on CD-ROM attached to thesis).

Acknowledgments

We thank Paul Williams and Kyuichi Kanagawa for thoughtful reviews that helped to improve this paper. This project was made possible by a visit of DK to the Epsilon Earth Processes Simulation Laboratory, Dept. of Earth Sciences, Monash University, Clayton (Melbourne), Australia. Marlina Elburg is thanked for the hospitality during the visit. The project was funded by DFG Grant Pa 578/3. We thank Mark Jessell, Janos Urai and Domingo Aerden for their comments and suggestions.

References

Aerden, D.G.A.M., 1996. The pyrite-type strain fringes from Lourdes (France): indicators of Alpine thrust kinematics in the Pyrenees. Journal of Structural Geology 18, 75-91.

Bons, P.D., Jessell, M.W., 1997. Experimental simulation of the formation of fibrous veins by localised dissolution-precipitation creep. Mineralogical Magazine 61, 53-63.

Beutner, E.C., Diegel, F.A., 1985. Determination of fold kinematics from syntectonic fibers in pressure shadows, Martinsburg Slate, New Jersey. American Journal of Science 285, 16-50.

Cox, S.F., Etheridge, M.A., 1983. Crack-seal fibre growth mechanisms and their significance in the development of oriented layer silicate microstructures. Tectonophysics 92, 147-170.

Durney, D.W., Ramsay, J.G., 1973. Incremental strains measured by syntectonic crystal growths. In: DeJong, K.A., Scholten, R. (Eds), Gravity and Tectonics, Wiley, New York, 67-95.

Ellis, M.A., 1986. The determination of progressive deformation histories from antitaxial syntectonic crystal fibres. Journal of Structural Geology 8, 701-709.

Etchecopar, A., Malavielle, J., 1987. Computer models of pressure shadows: a method for strain measurement and shear sense determination. Journal of Structural Geology 9,667-677.

Fisher, D.M., Brantley, S.L., 1992. Models of Quartz Overgrowth and Vein Formation: Deformation and Episodic Fluid Flow in an Ancient Subduction Zone. Journal of Geophysical Research 97, 20043- 20061.

Ghosh, S.K., Ramberg, H., 1976. Reorientation of inclusions by combination of pure shear and simple shear. Tectonophysics 34, 1-70.

Kanagawa, K., 1996. Simulated Pressure Fringes, Vorticity, and Progressive Deformation. In: De Paor, D. G. (Ed.), Structural Geology and Personal Computers. Computer Methods in the Geosciences 15, 259-283.

Mügge, O., 1928. Ueber die Entstehung faseriger Minerale und ihrer Aggregationsformen. Neues Jahrbuch für Mineralogie, Geologie und Paläontologie 58A, 303-438.

Pabst, A., 1931. 'Pressure shadows' and the measurement of the orientation in rocks. Journal of the Mineralogical Society of America 16, 55-70.

Passchier, C.W., Trouw, R.A.J., 1996. Microtectonics. Springer, Heidelberg, 289 pp.

Ramsay, J., 1980. The crack-seal mechanism of rock deformation. Nature 284,135-139.

Ramsay, J.G., Huber, M.I., 1983. The techniques of modern structural geology, 1: Stain analysis. Academic Press, London.

Urai, J.L., Williams, P.F., Van Roermund, H.L.M., 1991. Kinematics of crystal growth in syntectonic fibrous veins. Journal of Structural Geology 13, 823-836.

4. Computer experiments to investigate complex fibre patterns in natural antitaxial strain fringes

submitted, Journal of Metamorphic Geology

KOEHN*, Daniel, AERDEN°, Domingo G.A.M., BONS*, Paul D., PASSCHIER*, Cees W.

*Institut fuer Geowissenschaften,Johannes Gutenberg Universitaet,55099 Mainz, Germany, koehn@mail.uni-mainz.de;
°Universidad de Salamanca Departamento de Geologia, Area de Geodinamica, Plaza de la Merced s/n 37008 Salamanca, Spain; now at: Departamento de Geodinamica, Universidad de Granada, Campus de Fuentenueva s/n, 18071 GRANADA, Spain

Abstract

Antitaxial non-deforming strain fringes from Lourdes, France show complex quartz, calcite and chlorite fibre patterns that grew around pyrites in a shale during non-coaxial deformation. These fringes were modelled using a computer program "Fringe Growth 2.0" which can simulate incremental growth of crystal fibres around core-objects of variable shape. It uses object-centre paths as input, which are obtained from fibre patterns in thin-section. The numerical experiments produced fibre patterns that showed complex intergrowth of displacement-controlled-, face-controlled- and intermediate fibres similar to those in the natural examples. The direction of displacement-controlled growth is only dependent on the relative movement between core-object and fringe, so that core-object rotation with respect to the fringe influences the fibre patterns and produces characteristic asymmetric fibre curvatures. Object-centre paths should be used for kinematic analysis of strain fringes instead of single fibres since the paths represent one fringe as a whole. The lenght along the path can be interpreted in terms of finite strain and the curvature in terms of rigid body rotation of fringes with respect to an external reference frame.

4.1. Introduction

Strain fringes are crystalline domains that occur alongside rigid objects such as porphyroblasts or clasts and which differ from the deformed fine grained matrix (Fig. 4.1). Fringes develop on the side of the extensional instantaneous stretching axes (ISA) of bulk flow and crystals that normally develop euhedral faces, like quartz and calcite tend to grow in a fibrous habit in these fringes (Mügge, 1928; Papst, 1931). A core-object and its two strain fringes are termed fringe structure. Fibrous crystals are of special interest to geologists since they can record not only finite strain, but actual deformation paths because they grow progressively while the host-rock is being deformed, so that they have been used to evaluate the deformation history of the host-rock (Mügge, 1928; Pabst, 1931; Zwart and Oele, 1966; Elliot, 1972; Durney and Ramsay, 1973; Wickham, 1973; Wickham and Anthony, 1977; Cox and Etheridge, 1983; Beutner and Diegel, 1985; Ellis, 1986; Sample and Fisher, 1986; Etchecopar and Malavielle, 1987; Beutner et al., 1988; Fisher, 1990; Spencer, 1991; Clark et al., 1993; Fisher and Anastasio, 1994; Hedlund et al., 1994; Aerden, 1996; Kanagawa, 1996).

Strain fringes have been classified into antitaxial-, syntaxial-, deforming- or non-deforming fringes (reviews in Ramsay and Huber, 1983; Passchier and Trouw, 1996) depending on the direction of crystal growth and on strength compared with the matrix. In this paper, we concentrate on the common antitaxial non-deforming type, where crystal growth takes place at the object-fringe interface and the fringes remain rigid and undeformed in the matrix. Antitaxial strain fringes are normally further divided into face-controlled or displacement-controlled fringes according to the geometry of fibre arrangement in the fringes (Ramsay and Huber, 1983; Passchier and Trouw, 1996). "Face-controlled" means that fibres grow normal to the core-object face; "displacement-controlled" that they grow somehow parallel to the relative displacement of fringes and core-object during progressive deformation (Fig. 4.1a). Koehn et al. (submitted, Chapter 3) suggested that these two groups are only end-member cases and that most fringes contain fibres of both groups (Fig. 4.1).

Main problems in fibre analysis are why displacement-controlled fibres develop, what they actually trace and how they can be used to determine the deformation history of the host-rock. Models have been put forward to suggest that fibres grow in the direction of the least principal stress (Durney and Ramsay, 1973), that they grow parallel to the incremental maximum extensional strain axis (Ellis, 1986; Kanagawa, 1996), that their growth is controlled by the orientation of the incremental maximum finite strain axis (Beutner and Diegel, 1985) or that they follow points on the core-object and are not directly dependent on the orientation of either a strain or stress axis (Urai et al., 1991; Aerden, 1996; Koehn et al., submitted, Chapter 3). Koehn et al.

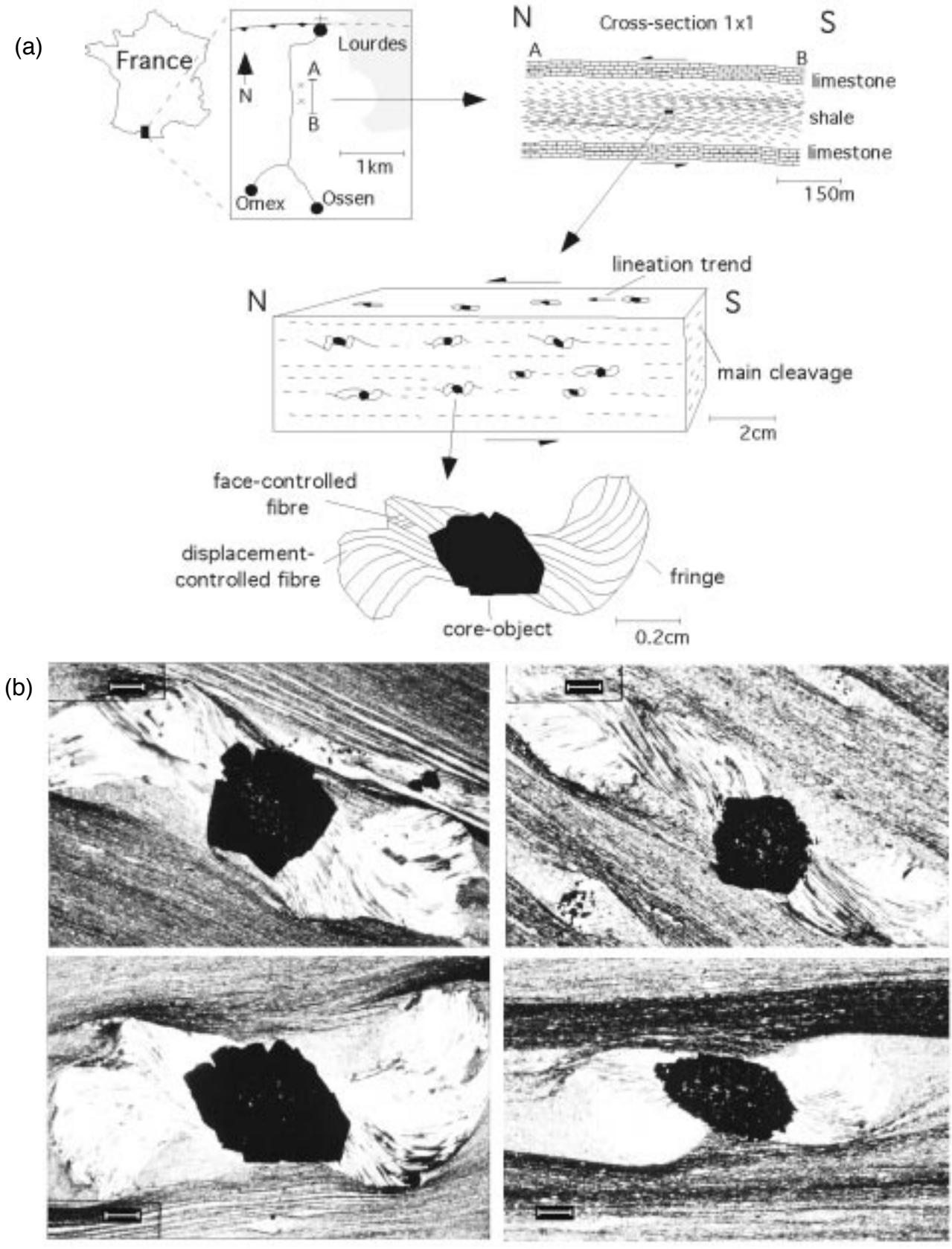

Fig. 4.1 (a) Map indicating the location of the studied samples. A cross-section shows the shale unit containing the strain fringes between two massive limestone units. The cleavage is almost horizontal in the shale unit and is refracted by the limestone indicating strong deformation partitioning. Line drawing of a hand-specimen containing strain fringes from Lourdes, France shows a consistent Z-shape of the strain fringes that indicates sinistral shear sense. Enlargement of one strain fringe shows curved displacement-controlled fibres, and face-controlled fibres which grow perpendicular to the core-object surface. (b) Thin-section micrographs of the four strain fringes used for this study. Scale-bar is 0.8mm.

(submitted, Chapter 3) suggested that the occurence of displacement-controlled and face-controlled fibres next to each other suggests that fibre growth direction is not directly dependent on either stress or strain and support the models of Urai et al. (1991) and Aerden (1996). Apparently, fringes can only be used for conventional strain analysis in a few restricted cases where the core-object does not rotate with respect to the fringes, since core-object rotation influences the fibre patterns (Casey et al., 1983; Aerden, 1996; Koehn et al., submitted, Chapter 3).

Aerden (1996) and Koehn et al. (submitted, Chapter 3) introduced "object-centre paths" that can separate the actual opening paths of fringes from the effect of rotation of the core-object with respect to fringes. A scanned thin-section image of a strain fringe is needed to determine an object-centre path. A simple computer graphics program is used to move the core-object over the fringe and rotate it around its centre with respect to the fringe in a way such that single points on the core-object follow displacement-controlled fibres (Fig. 4.2). The line connecting the core-object centre position during this procedure is termed the object-centre path. It is thought to represent the relative movements between fringes and core-object. The relative rotation of a core-object with respect to its fringes can be indicated along the path as a variable angle of absolute rotation with respect to the initial orientation of the core-object (Fig. 4.2). If one fringe contains at least two displacement controlled fibres the object-centre path can be determined. The orientation of the opening vector of the fringe and the angle of the rotation of the core-object with respect to the fringe must have the same value for all displacement-controlled fibres in one fringe for one incremental opening step. The advantage of the object-centre path method is that the path represents one fringe as a whole and it distinguishes between the relative displacement of fringe and core-object, and their relative rotation (Koehn et al., submitted, Chapter 3).

To model fibre growth in veins and strain fringes the computer models "Vein Growth" (Bons, in press) and "Fringe Growth" (Koehn et al., submitted, Chapter 3) were developed. Using these models Hilgers et al. (1997), Koehn et al. (submitted, Chapter 3) and Hilgers et al. (in press) demonstrated that the fibre growth theory of Urai et al. (1991) is able to explain simple fibre patterns in antitaxial strain fringes and veins. According to this growth theory, displacement-controlled or tracking fibres develop because they will get locked to outward-pointing asperities on the core-object or on the vein wall-rock. The shape of the core-object surface or the vein wall-rock determines whether fibres track or not. If this growth theory is valid for all veins and fringe-structures, then conventional strain analysis using single fibres should not be applied because it is prone to produce large errors since not all fibres in a fringe may track displacement and core-object rotation relative to its fringes influences fibre

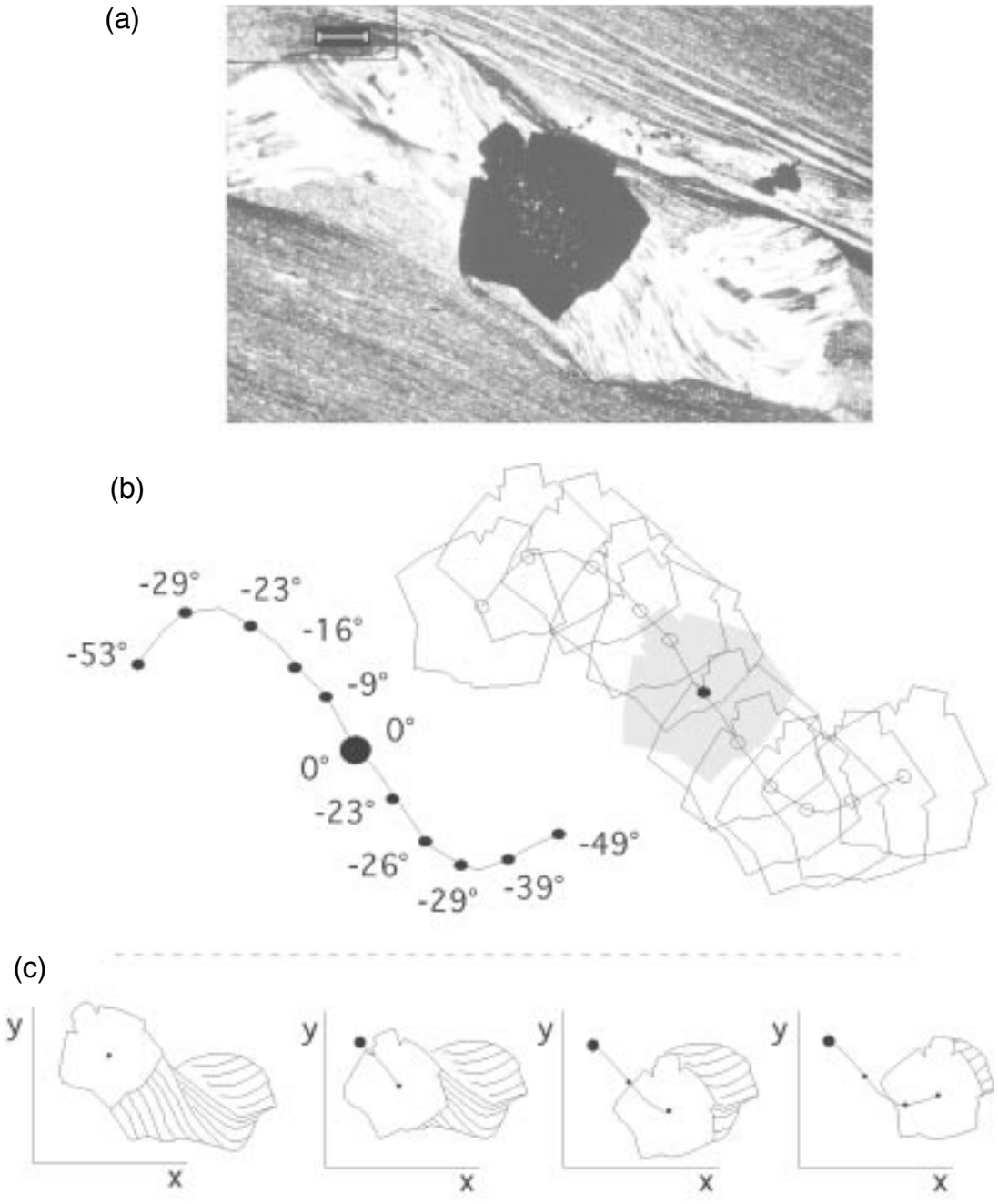

Fig. 4.2 (a) Thin-section micrograph of a strain fringe from Lourdes, France (scale-bar is 0.8mm). (b) Interpretation of (a) using the object-centre path method (Aerden, 1996; Koehn et al., submitted, Chapter 3). The core-object is progressively moved over a fringe and rotated around its centre so that displacement-controlled fibres follow points on the core-object surface. Relative finite rotation of the fringe and the core-object with respect to each other is indicated in numbers next to the path. Anticlockwise rotation of the core-object around its centre with respect to a fixed fringe is positive. (c) Evaluation of the object-centre path for the right fringe of (a) in four steps.

patterns (Koehn et al., submitted, Chapter 3). Instead, object-centre paths should be determined from natural strain fringes and these can be used to determine finite and incremental strain.

In this study we used an advanced version of the computer program "Fringe Growth 1.3" (Koehn et al., submitted, Chapter 3) to simulate fibre growth in strain fringes from a locality in the northern Pyrenees near Lourdes, France. "Fringe Growth" models fibre growth on a rigid core-object of any shape by varying fringe displacement rate, rotation and several other parameters, as described in section 4.3. The strain fringes from Lourdes formed during non-coaxial deformation around pyrites of variable shape and show very complex fibre patterns (Fig. 4.1). They are ideal to test if "Fringe Growth" can reproduce these patterns and if the fibre growth theory of Urai et al. (1991) is realistic for fringes. To do this, we determined the object-centre paths of the four strain fringes shown in Fig. 4.1b and used these paths in "Fringe Growth 2.0" to simulate the fibre patterns. We then compared the simulated strain fringes with the natural examples. In order to improve the understanding of the development of displacement-controlled, face-controlled and other fibres we investigated incremental fibre growth in detail and were able to present an enhanced classification for different fibre types. Finally we developed a method to interpret object-centre paths in terms of finite and incremental strain and in terms of fringe rotation with respect to ISA and applied this method to the strain fringes from Lourdes.

4.2. Geological setting and microstructural description of the strain fringes

The study area lies in the Pyrenees, north of the North Pyrenean fault (for details see Aerden, 1996 and further references therein) in the south of France (Fig. 4.1). The strain fringes occur in a 150m thick layer of cretaceous shale between two 50 to 100m thick cretaceous limestone layers (Fig. 4.1). The whole sequence is folded into km-scale north verging folds and cut by north directed thrusts (Aerden, 1996). The main sample location for the strain fringes used in this study lies about 1 km south of a major thrust at Lourdes where the sequence dips gently to the south (Fig. 4.1). In this area, the shale unit experienced strong internal deformation between the limestone units with a strong flat-lying cleavage and isoclinal folds. The two limestone units above and below the shale are only little deformed. The cleavage shows a strong refraction towards the limestone units: it dips about 0° to 20° towards the south in the shale and about 50° to 75° towards the south in the limestone (Fig. 4.1a).

The strain fringes show a strong linear elongation trending north-south on cleavage planes without any evidence for extension perpendicular to the lineation (Fig. 4.1a). On west-facing outcrop surfaces oriented perpendicular to the cleavage the strain fringes show a consistent Z-shape indicating a top to the north sense of shear (Fig. 4.1a). This geometry infers that the strain fringes and the core-objects have all rotated sinistrally in this outcrop with respect to the limestone layers. Because of this rotation and the strong deformation partitioning in the shale and the weak deformation of the

limestone layers, we concluded that flow in the shear-zone must have been close to simple shear.

In thin-section, strain fringes with a length of 0,5 to 2cm show antitaxial growth of quartz, calcite and chlorite fibres around pyrites of variable shapes (Fig. 4.1b). The mineralogy of the fibres seems to have no significant influence on their shape. The fibres in the fringes show no signs of deformation or recrystallisation so that they represent growth features. Single fibres can be curved up to 100° and are often truncated by suture lines. The fringes show complex intergrowth of displacement-controlled, face-controlled and other fibres (Fig. 4.1).

4.3. The program "Fringe Growth"

4.3.1 General description

Numerical experiments presented in this study were carried out with the computer model "Fringe Growth 2.0". The algorithm of this computer program is based on the program "Vein Growth" by Bons (in press). "Fringe Growth" is described in detail in Koehn et al. (submitted, Chapter 3) and is written in "C" for the Macintosh computer.

"Fringe Growth 2.0" models the growth of fibres in antitaxial non-deforming strain fringes. The user can define the growth velocity of the fibres, the anisotropy of the crystal lattice in the fibres, the opening direction and opening velocity of the fringe and the relative rotation of the core-object with respect to the fringe. Only one fringe is simulated during a run of the program with the fringe fixed in the xy-frame of the computer screen, while the core-object can move in x-y space on the computer screen and can rotate with respect to the fringe. The boundary of the model lies between the matrix and the strain fringe, so that matrix deformation is not included in the simulation (Fig. 4.3a). "Fringe Growth 2.0" is a front-tracking model: the grains in the fringe and the core-object are defined by a number of nodes that connect straight segments defining the grain boundaries (details described in Koehn et al., submitted, Chapter 3, Appendix). Triple nodes lie on the vertices between three neighbouring grains and double nodes between two neighbouring grains. Growth takes place by incremental movement of the nodes. For a detailed description of the growth routine see Bons (in press; Appendix).

Two new features have been added to the version of "Fringe Growth" presented in Koehn et al. (submitted, Chapter 3): the nucleation of new crystals inside the fringe (Fig. 4.3b) and dissolution of crystals (Fig. 4.3c).

4.3.2 Nucleation inside the fringe

Observations of thin-sections of strain fringes from Lourdes have shown that

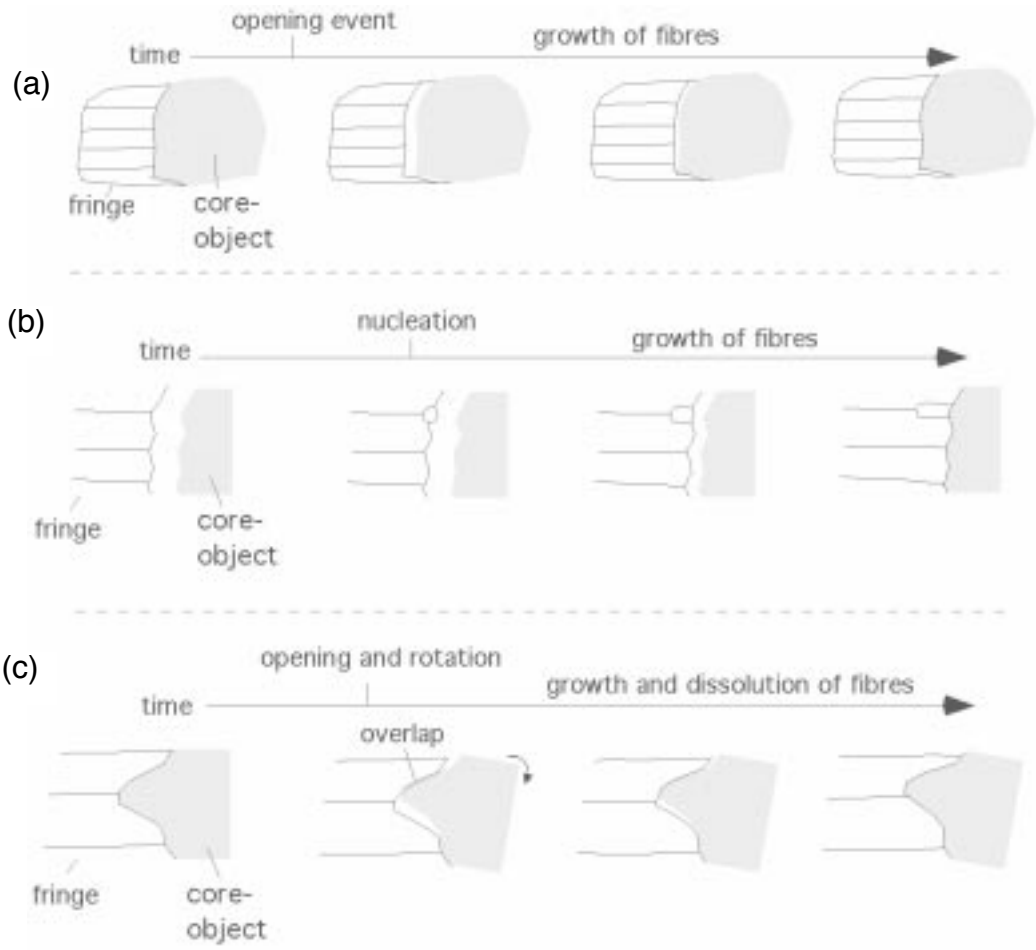

Fig. 4.3 Three versions of a single growth cycle in the program "Fringe Growth". (a) An opening event of the fringe is followed by progressive growth of fibres in the open fringe towards the core-object. (b) A new nucleus is inserted at the growth interface of the fringe between two fibres. (c) Rotation of a core-object with pronounced corners leads to an overlap of core-object and fringe. Fibres that are overlapped by the core-object dissolve.

displacement-controlled fibres can contain face-controlled fibres on the fringe rims (Koehn et al., 1999) as well as inside the fringes. These bands can only develop if new grains nucleate on the fringe rims and inside the fringe between the core-object and the growing fibres. The program randomly nucleates new grains at triple points on the growth interface of the fringe between two fibres that have a minimum width (Fig. 4.3b). The minimum width is defined as a grain that has at least two double nodes on its growing surface.

4.3.3 Dissolution of crystals

Because of the rotation and of the changing movement path of the core-object with respect to the fringes, parts of the core-object tend to overlap with parts of the fringe (Koehn et al., submitted, Chapter 3). In nature, this must either influence the path and rotation of the core-object, or parts of the fringe are dissolved. To model fibre growth against core-objects with pronounced asperities and corners that are rotating with

respect to the fringes, crystals have to be able to grow and be dissolved. The crystals in "Fringe Growth" are dissolving by "growing" backwards into themselves once parts of the core-object move over them (Fig. 4.3c). Single grains are removed from the fringes once they reach a critical minimum size as a result of the dissolution process. The critical minimum size of a grain that is removed from the fringe is defined as a grain that consists only of triple nodes without any double nodes.

4.4. Experiments

We tried to reproduce the fibre patterns in the four samples from Lourdes that are shown in Figs. 4.1b and 4.4a. The core-objects have axial ratios that range from 1.0 (object I and object II) to 1.4 (object III) and 2.0 (object IV). We determined the object-centre paths of the four samples (Fig. 4.4b) and used these and the core-object shape as input for the simulations.

4.4.1 General results of the experiments

The fibre patterns in the simulated strain fringes (Fig. 4.4c) are not exactly identical to the natural fringes but show the following similarities to the natural examples: (1) single fibres curve up to 100°, (2) fringes show complex intergrowth of different fibre types, (3) curvature of fibres changes along single fibres, (4) fibres growing next to each other do not necessarily have the same curvature, (5) none of the fibres is parallel to an object-centre path along its whole length and (6) fringes develop multiple suture lines (Ramsay and Huber, 1983) that separate sets of differently oriented fibres.

Main differences between the simulated and natural strain fringes are (Fig. 4.4): (1) simulated fibres are not as thin as fibres in the natural examples and (2) the outline of the fringes is not always the same. The difference in fibre width depends on the roughness of the core-object. The roughness of the core-object surface used for the simulations is not as fine as that of the natural examples because the computer program is restricted to a maximum number of nodes (20000 to 40000) due to memory and time constraints. This results in a lower resolution of the simulated fringes (wider fibres) compared to the natural examples. The outline of the fringes cannot be modelled as the outline is the boundary of the computer model. To model the outline of the fringes deformation of the matrix has to be included in the simulations, since we do not know how wide a fringe will be with respect to its core-object. Fringes next to a core-object will not open along the core-object's whole width (Fig. 4.4a) (Selkman, 1983) in nature.

The fibre patterns produced by the numerical experiments are very similar to the patterns observed in the natural examples (Fig. 4.4) which indicates that the fibre

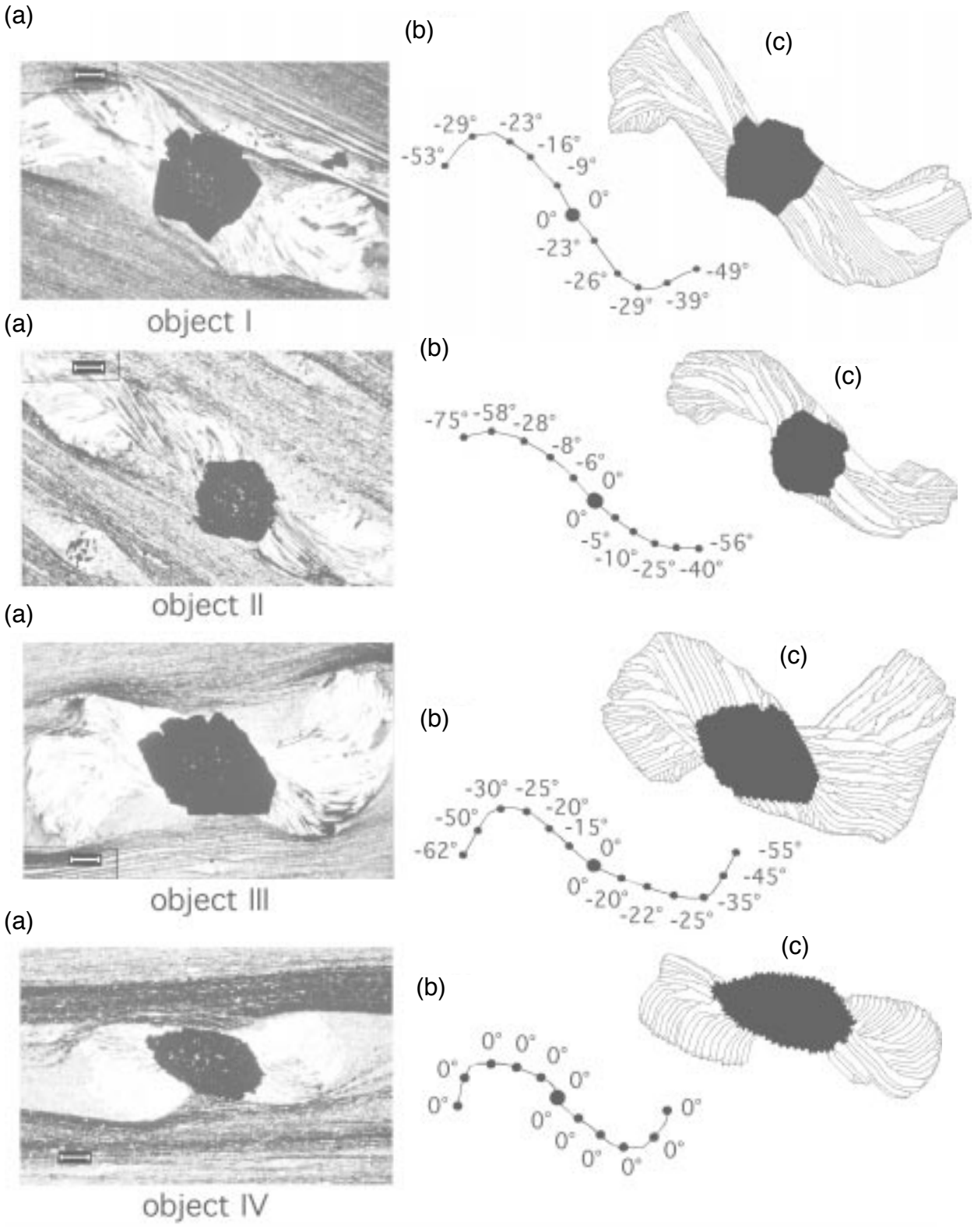

Fig. 4.4 (a) Thin-section micrographs of the studied strain fringes. Scale-bar is 0.8mm. (b) Object-centre paths for the four strain fringes. (c) Simulated fringes around core-objects shown in (a). None of the fibres in the fringes is parallel to the object-centre path along its whole length. For a detailed discussion of the fibre patterns see the main text.

growth model of Urai et al. (1991) is realistic.

The simulated and natural fringes differ in the following aspects from each other (Fig. 4.4b): (1) the number of suture lines per fringe varies depending on how many pronounced corners the core-objects have, (2) the width of fibres differs depending on the roughness of the core-object surface, (3) sites of dominantly face-controlled or displacement-controlled fibre growth vary depending on the orientation of the core-object and on the roughness of its surface and 4) the outline of the fringes differs depending on the geometry of the object-centre path and on the axial ratio, shape, orientation and size of the core-object.

Because the experiments were able to mimick the internal geometry of the fringes quite well (Fig. 4.4) a detailed analysis of the evolution of specific fibre types can be undertaken. In the following paragraphs, fibre types are defined and treated separately to show which factors lead to the development of individual types and shapes.

4.4.2. Classification of fibre patterns

The numerical experiments show that fibre patterns in the fringes develop by complex intergrowth of face-controlled, displacement-controlled and intermediate fibre segments (Fig. 4.5). The shape of the fibre growth front determines which fibre type develops because fibre boundaries either get "locked" to outward-pointing asperities on the core-object surface or grow perpendicular to this surface if it is flat (Urai et al., 1991; Koehn et al., submitted, Chapter 3). We suggest an enhanced classification for fibres and fibre boundaries based on our numerical experiments (Fig. 4.5). Fibre boundaries can be either displacement-controlled (tracking), face-controlled (non-tracking) or intermediate (partial-tracking). Intermediate fibre boundaries contain face-controlled and displacement-controlled segments along their length. Displacement-controlled fibres have two displacement-controlled fibre boundaries. Face-controlled fibres have two face-controlled fibre boundaries. Intermediate fibres are either made up of one displacement-controlled fibre boundary and one face-controlled fibre boundary or they are made up of intermediate fibre boundaries (Fig. 4.5). It is difficult to detect intermediate fibre boundaries in natural strain fringes and to identify their displacement-controlled and face-controlled parts. Fibre bands are sets of face-controlled fibres within a displacement-controlled fibre (Fig. 4.5). Suture lines (Ramsay and Huber, 1983) represent a special kind of fibre boundary. They separate sets of differently oriented fibres in a fringe.

4.4.2.1. Displacement-controlled (tracking) fibre boundaries

Displacement-controlled fibre boundaries in the fringes track asperities on the surface

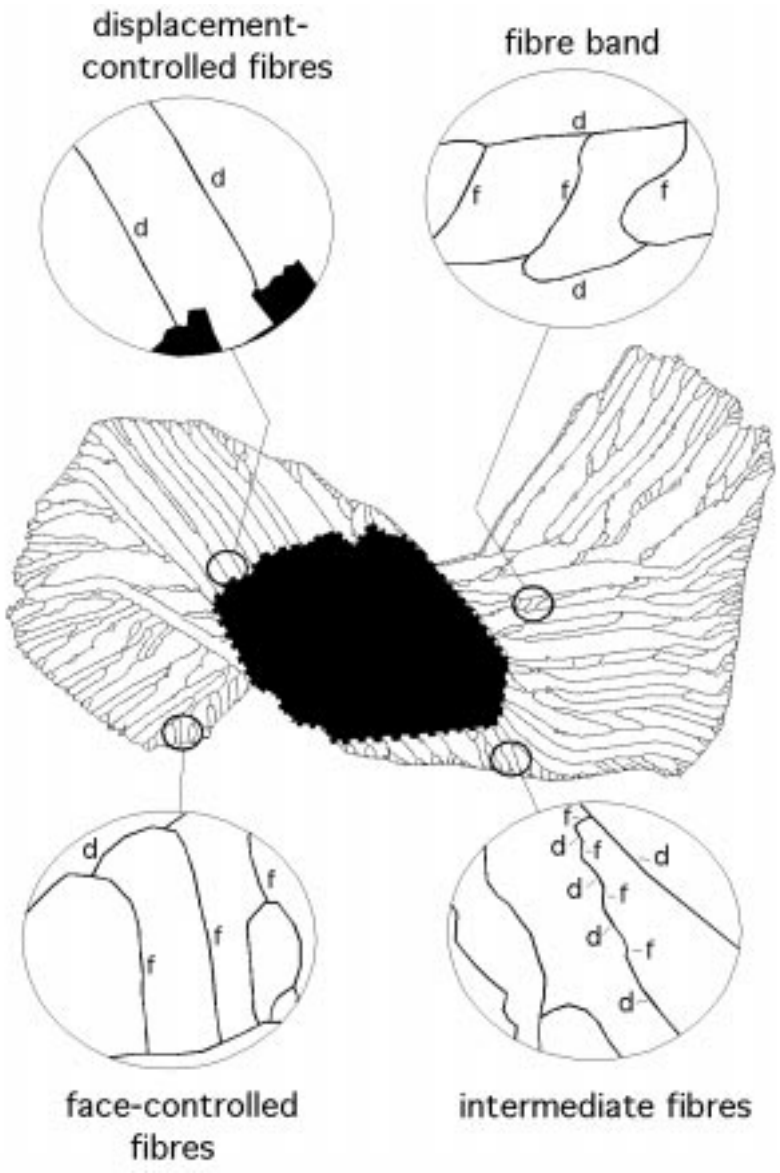

Fig. 4.5 Classification suggested for fibres and fibre boundaries illustrated by the simulated fibre patterns of object III. f=face-controlled fibre boundary, d=displacement-controlled fibre boundary.

of the core-object. The width of displacement controlled fibres depends mainly on the distance between adjacent asperities of sufficient pointedness to capture fibre boundaries (Hilgers et al., in press). The growth direction of displacement-controlled fibres is a function of (1) the orientation of the object-centre path and (2) the rotation of the core-object with respect to the fringe. Displacement-controlled fibres in a fringe only grow all parallel to each other and parallel to the object-centre path if the core-object is not rotating with respect to the fringe (Fig. 4.6). A rotation of the core-object with respect to its fringe produces complex fibre patterns where single fibres change their curvature along the fibre's length even if the core-object rotation with respect to the fringe is constant (Fig. 4.6). In this case fibres grow in different directions depending on the growth site of the fibre with respect to the centre of rotation (centre

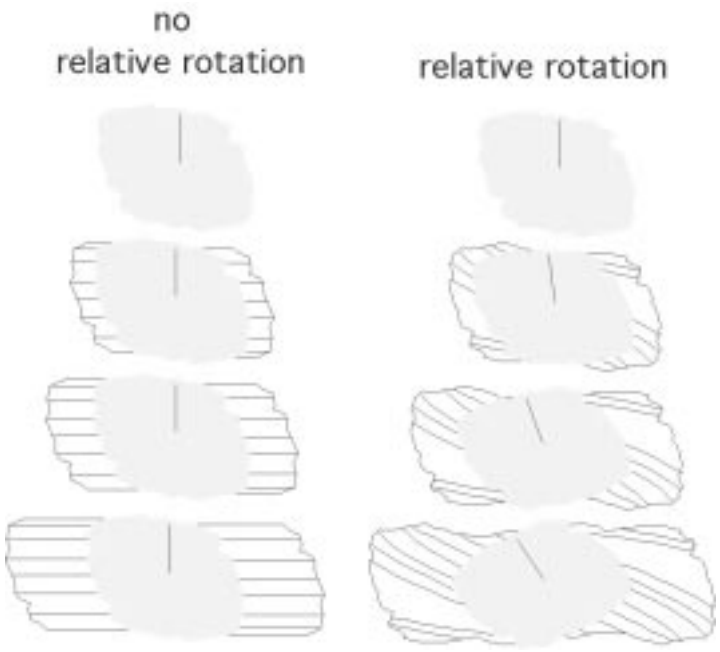

Fig. 4.6 Schematic drawing of displacement-controlled fibers after two simulations with the program "Fringe Growth 2.0" with a constant opening vector parallel to the horizontal. Left simulation shows growth of all displacement-controlled fibres parallel to each other, the core-object is not rotating relative to its fringes. Right simulation shows different growth direction of fibres due to an anticlockwise rotation of the core-object relative to its fringes.

of the core-object) (Fig. 4.6). The more elongate the core-object is and the more it rotates with respect to the fringes the more complex the fibre patterns will be. Our results show that rotation of the core-object tends to produce an asymmetric fibre curvature that opposes the fibre curvature resulting from curved object-centre paths on one side of the fringe but might enhance the curvature on the other side. This will produce fibre patterns that have an S or Z shape depending on the shear sense.

Figure 4.6 shows two series of line drawings of displacement-controlled fibres in a fringe simulated with "Fringe Growth 2.0". The object-centre path is straight and parallel to the horizontal during the simulations. At left, the core-object is not rotating with respect to its fringes so that all fibres grow parallel to each other and parallel to the object-centre path (Fig. 4.6). At right, an anticlockwise rotation of the core-object with respect to the fringe is induced and the fibres have different growth direction depending on their position with respect to the core-object. This will result in fibres with varying curvature along their length if fibres grow from one side of the fringe to the other. Figure 4.7 shows a natural example of a strain fringe from Lourdes that shows single fibres that change their curvature from one side of the fringe to the other resulting in a Z-shape. This Z-shape indicates that the core-object did rotate anticlockwise with respect to its fringes.

For an infinitesimally small growth step of displacement-controlled fibres in one fringe

(a) (b)

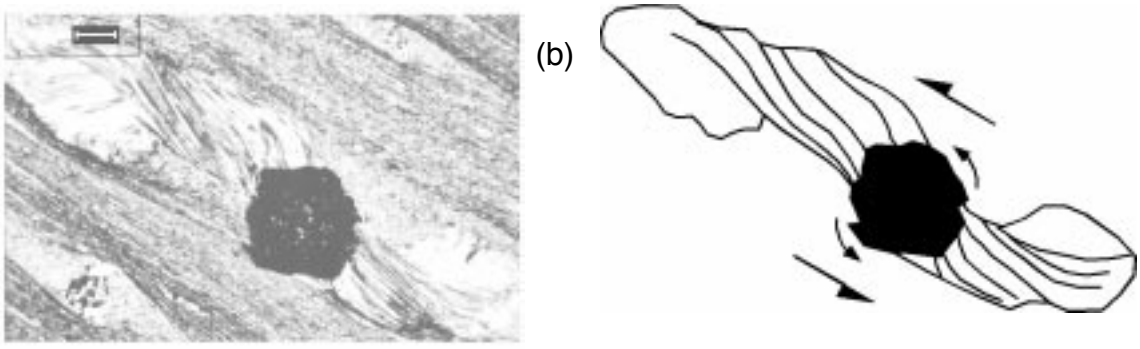

Fig. 4.7 (a) Micrograph of a natural strain fringe around a circular core-object (object II). Scale-bar is 0.8mm. (b) Line drawing of some displacement-controlled fibres of (a) that have a typical asymmetric fibre curvature due to relative core-object fringe rotation. The Z-shaped fibres indicate that the core-object rotated anticlockwise relative to its fringes.

there is only one combination of opening and core-object rotation with respect to the fringe. Thus object-centre paths are unique for each fringe.

4.4.2.2. Suture lines

Suture lines in strain fringes (Ramsay and Huber, 1983) separate sets of differently oriented fibres. Suture lines are similar to displacement-controlled fibre boundaries since they are also locked to asperities on the core-object surface but to first order asperities (corners) rather than second order ones described above. They can form because (1) the core-object has pronounced corners, (2) the opening direction of the fringe changes suddenly, (3) parts of the fringe are dissolved and (4) face-controlled fibre growth on the rims of fringes and in fibre bands. Figure 4.8a illustrates four common types of suture lines: (1) suture lines between sets of differently oriented face-controlled fibres, (2) suture lines between face-controlled and displacement-controlled fibres, (3) suture lines between displacement-controlled and intermediate fibres and (4) suture lines between displacement-controlled fibres of different age. Figure 4.8b shows a simulation with "Fringe Growth 2.0" where suture lines are locked to corners on the core-object.

4.4.2.3. Face-controlled (non-tracking) fibre boundaries

Face-controlled fibre boundaries grow on smooth core-object surfaces that have no asperities or that have low amplitude asperities that are unable to track or lock fibres (Koehn et al., submitted, Chapter 3). They are commonly found in strain fringes around smooth square or rectangular core-objects (Ramsay and Huber, 1983), but they can also occur inside fringes around rough core-objects (Koehn et al., submitted, Chapter 3) (Fig. 4.9). In some cases, only one displacement controlled fibre band contains face-controlled fibres in contrast to the neighbouring fibres (Fig. 4.9b).

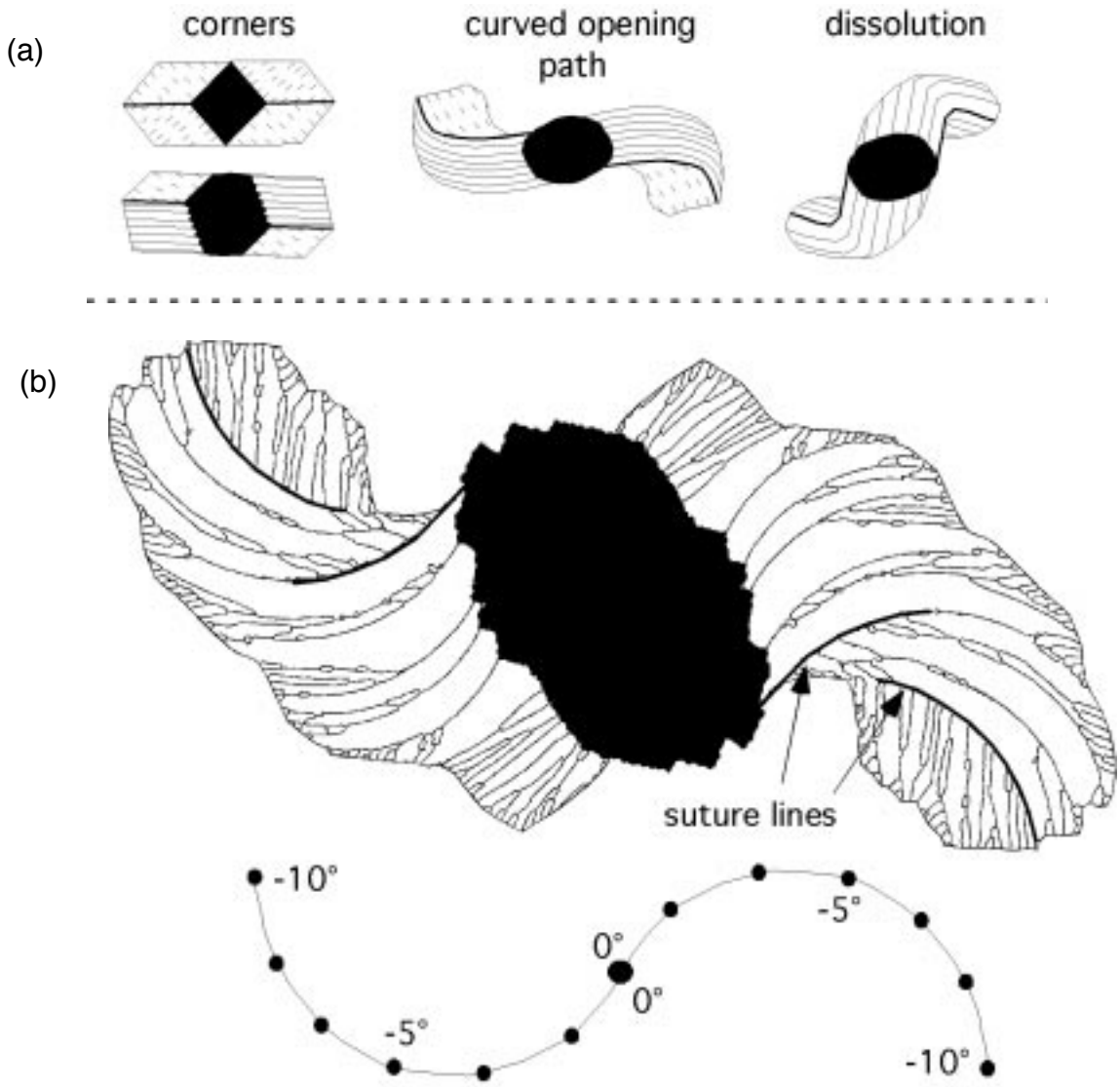

Fig. 4.8 (a) Sketch of different suture lines that are common in strain fringes. Face-controlled and intermediate fibre boundaries are strippled. (b) Simulation of a strain fringe with "Fringe Growth 2.0" where suture lines develop towards pronounced corners on the core-object surface.

Displacement-controlled fibre bands can develop when a core-object has two distinct asperities that are separated by a smooth surface. The two asperities lock the outside boundaries of the fibre band which are therefore displacement-controlled. Nuclei inside the fibre band can grow face-controlled against the smooth surface and therefore grow oblique to the fibre band boundaries (Fig. 4.9c).

4.4.2.4. Intermediate (partial-tracking) fibres

Purely face-controlled and purely displacement-controlled fibres are end-members because some single fibres, termed intermediate fibres can have segments where (1) one grain boundary is displacement-controlled and the other face-controlled or (2) single grain boundaries switch between face- and displacement-controlled growth

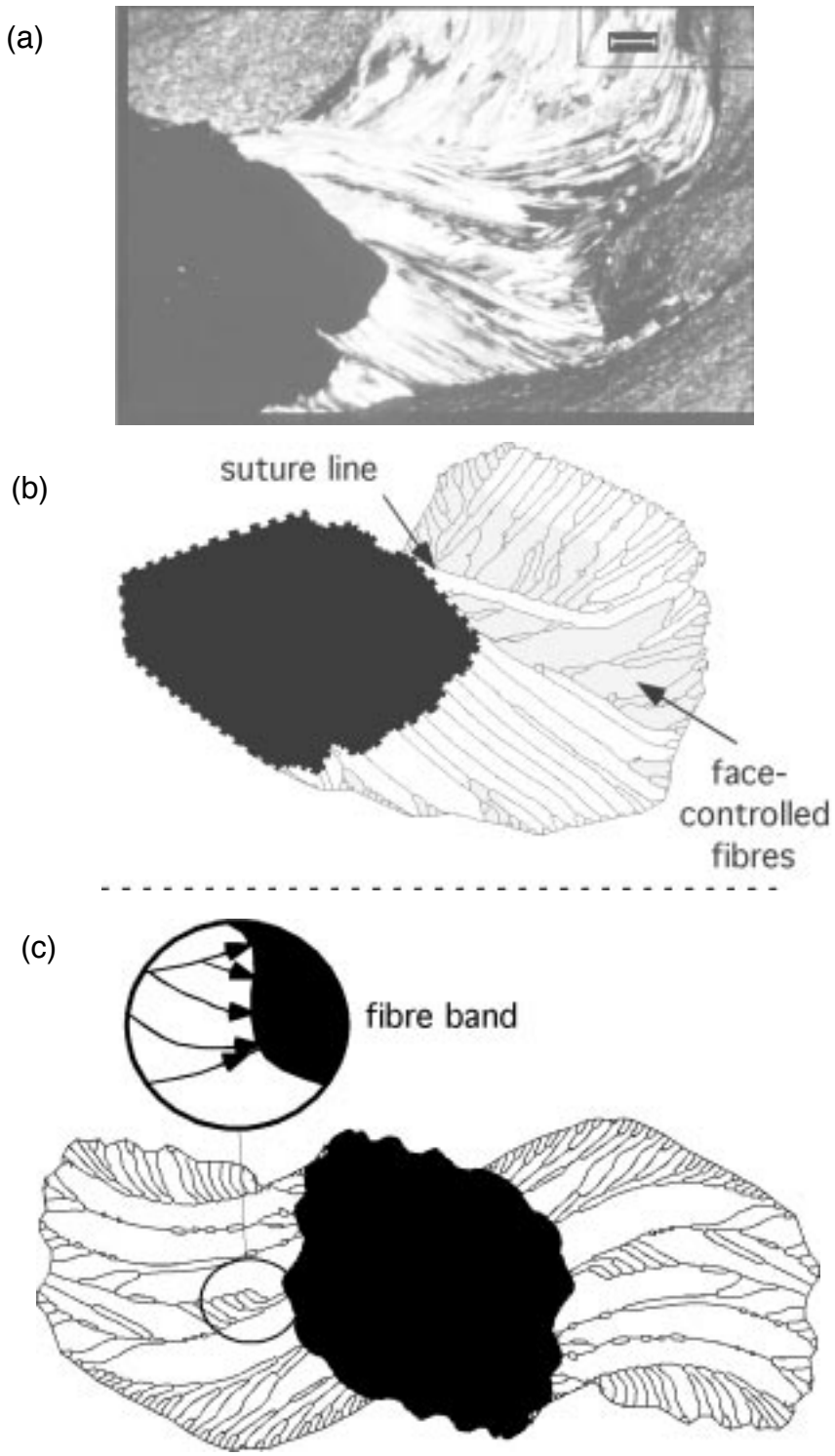

Fig. 4.9 (a) Micrograph of a natural strain fringe that shows face-controlled fibres next to a pronounced suture line and in displacement-controlled fibre bands. Scale-bar is 0.8mm. (b) Simulation of the natural example with "Fringe Growth 2.0". The fibre patterns of the natural and the simulated fringe are similar. Face-controlled and intermediate growing fibres are ornamented. A pronounced suture line separates displacement-controlled fibres from intermediate fibres. Fibre curvatures of neighbouring displacement-controlled fibres are not equal. (c) Simulation with "Fringe Growth 2.0" that produced a displacement-controlled fibre band containing smaller face-controlled fibres. The arrows in the closeup show the direction of fibre growth.

(intermediate fibre boundaries) (Fig. 4.10). This is commonly observed next to suture lines. Fibres that end on suture lines have to be treated with care as they may be intermediate and rarely contain information on the opening path of the fringes. Figure 4.10 shows a computer simulation of a Lourdes fringe in two steps. A close-up shows intermediate fibres next to a suture line. They switch progressively from face-controlled to displacement-controlled growth so that they develop a zig-zag form (Fig. 4.10). Figure 4.10 illustrates that it is difficult to determine the exact age relationship

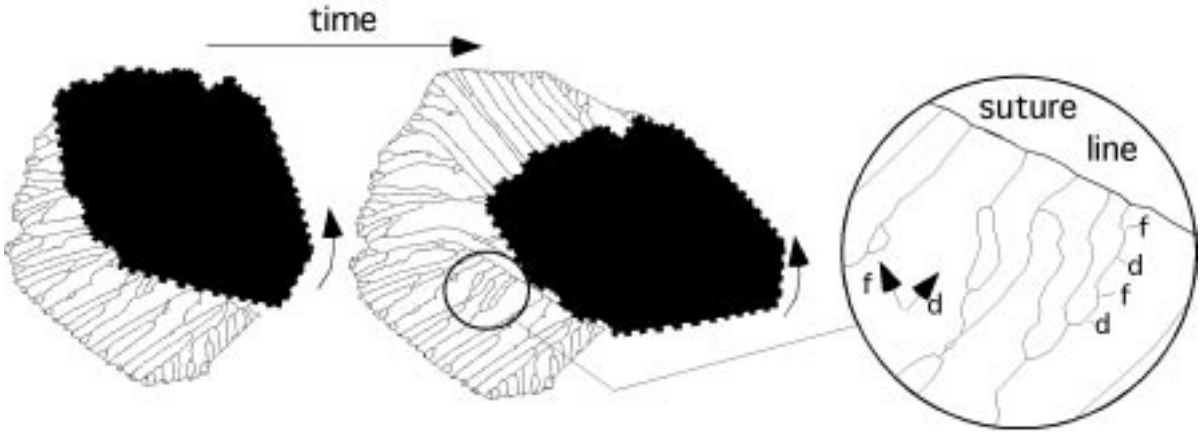

Fig. 4.10 Simulation with "Fringe Growth 2.0" that produced intermediate fibres next to a suture line. The first time step shows the position of the core-object during the growth of the intermediate fibres and the second time step shows the development of the suture line. A closeup of the intermediate fibres shows their typical "zig-zag" patterns with f=face-controlled (non-tracking) parts and d=displacement-controlled (tracking) parts.

of the intermediate fibres next to a suture line since the orientation of the growth surface is not known and it can be expected that parts of the fringe have been dissolved.

4.5. Interpretation of object-centre paths

Object-centre paths contain three values: (1) length of the path, (2) curvature of the path and (3) core-object rotation relative to the fringes. The length along the path can be interpreted in terms of incremental and finite strain and the curvature gives estimates on absolute rotation of fringes with respect to an external reference frame. We tried to interpret the object-centre paths of the four objects used for this study. Before interpreting the length along the paths in terms of strain and the curvature in terms of absolute rotation we had to make the assumption that the four objects developed during simple shear deformation as illustrated in section 4.2 of this study. We also assumed that the deformation is plane strain and that the fringes opened parallel to the extensional ISA. We can then plot the absolute rotation of the fringes against bulk shear strain in the shale as illustrated in Fig. 4.11. The following sections describe the analysis of object-centre paths in detail.

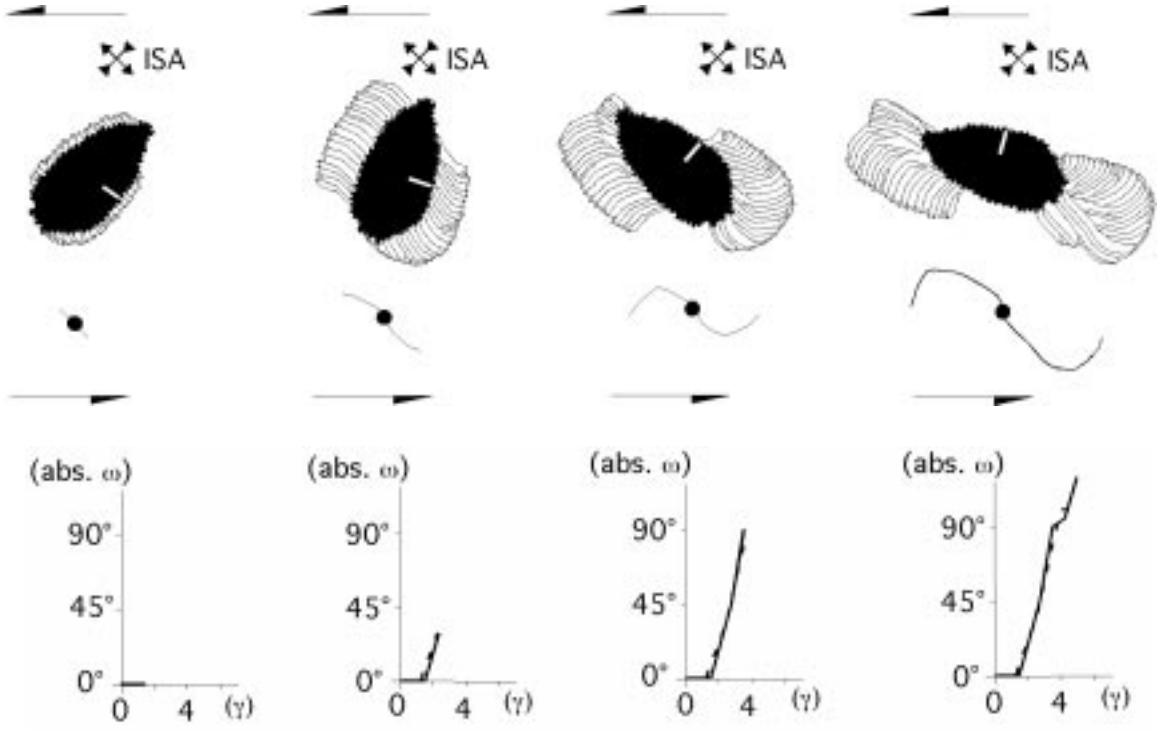

Fig. 4.11 Interpretation of an object-centre path as progressive rotation of the fringes and core-object with respect to ISA. The curvature of the object-centre path results from progressive rotation of the older parts of the fringe. The outer parts of the object-centre path contain always the oldest growth increments, since object-centre paths grow from the centre (antitaxial growth in strain fringes). The absolute rotation of the fringes with respect to ISA can also be visualized in plots of absolute rotation versus shear strain where zero rotation is the orientation of the oldest part of the object-centre path. The orientation of younger parts of the path is plotted with respect to the oldest part. Strippled line represents right fringe and solid line left fringe.

4.5.1. Incremental and finite strain

If the fringes open parallel to the extensional ISA infinitesimally small object-centre path segments represent segments of infinitesimally small strain. To determine finite strain one has to integrate along the object-centre path, since the finite length along the path does not represent finite strain but an accumulation of segments of "incremental strain". These segments of "incremental strain" are only equal to the finite strain for the very first infinitesimally small fringe-opening step. The following section illustrates how finite strain can be calculated from object-centre paths. The Mohr circle for infinitesimal strain in the plane perpendicular to the cleavage and parallel to the lineation assuming that the normal strain e_2 remains 0 (plane strain) (Means, 1976) shows that

$$\gamma_{max} = e_1 - e_3 \qquad \text{(after Means, 1976)}$$

where γ is the shear strain and e_1 and e_3 are the normal strains with

$$e = \frac{\Delta l}{l_0}$$

If the shear strain is infinitesimally small and the area remains constant, then

$$de_3 = -de_1$$

for

$$d\gamma \Rightarrow 0$$

so that

$$d\gamma_{max} = 2de_1$$

(for inifinitesimally small strain)

To calculate the finite shear strain we have to integrate along the length of the object-centre path:

$$d\gamma = 2de_1 = \frac{2dl}{l_0}$$

where dl is the incremental length of the object-centre path and l_0 is the diameter of the core-object. Integration gives:

$$\gamma_{finite} = \frac{2}{l_0}\int_0^L dl \Leftrightarrow \gamma_{finite} = \frac{2}{l_0}L$$

where L is the finite length measured along the object-centre path. Thus we can determine the shear strain using the object-centre paths and can also determine the displacement along the shear-zone using its width. Note that l_0 varies if the core-object is elongate.

Results for the four strain fringes studied are shown in Fig. 4.12b. Calculated shear strains have finite values of 5.0, 6.3, 7.6 and 9.8 so that the finite displacement along the 150m thick shear-zone studied would be between 750m and 1420m. The shear strain values coincide with a small angle of the cleavage in the shale to the shear-zone boundary of 5° to 10°. Etchecopar and Malavielle (1987) determined a shear strain of 6.0 for a fringe structure from the same shear-zone using a computer program which includes matrix deformation. They also assumed that the flow in the shear zone is close to simple shear.

4.5.2. Finite rotation of fringes with respect to an external reference frame

The curvature of the object-centre path can be used to estimate the progressive rotation of fringes with respect to the shear-zone boundary or ISA if fringes open parallel to the extensional ISA. The method is illustrated in Fig. 4.11 in four steps. The first step shows the oldest part of the object-centre path parallel to the extensional ISA. During the next time steps the object-centre path is progressively becoming curved while the fringes rotate with respect to ISA since older parts of the path rotate

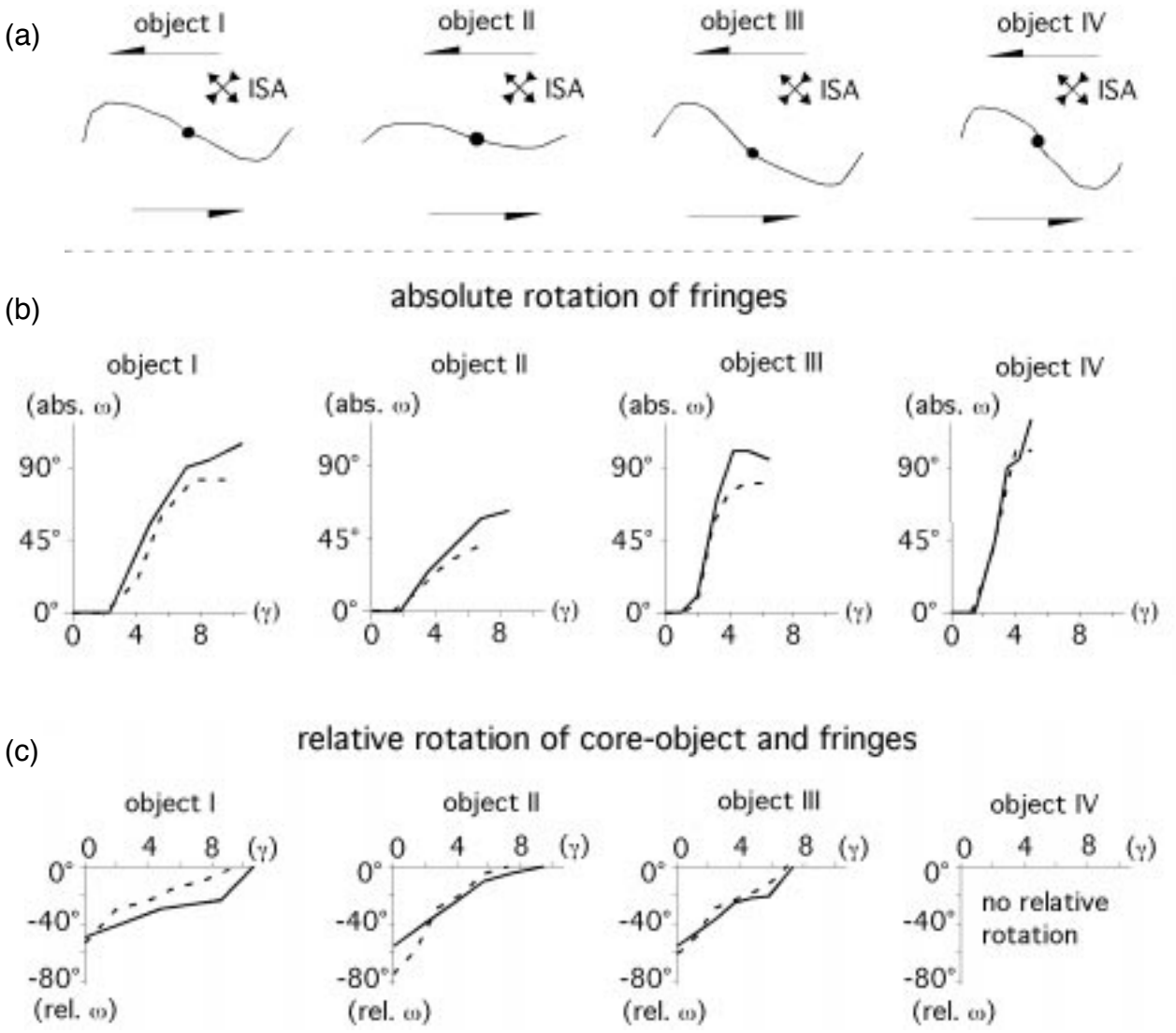

Fig. 4.12 (a) Orientation of object-centre paths of the four objects studied with respect to ISA. (b) Plots showing estimates on absolute rotation of fringes with respect to ISA versus shear strain obtained from object-centre paths (see Fig. 4.11). Objects I-III show first increasing and then decreasing rotation rates. Objects III and IV rotate faster than objects I and II. Strippled line represents right fringe and solid line left fringe. (c) Plots of core-object rotation relative to their fringes versus shear strain. Object IV shows no core-object rotation relative to its fringes. Objects I to III show finite values of object rotation with respect to their fringes of 49° to 75°. Strippled line represents right fringe and solid line left fringe.

with the fringes. This can be illustrated in plots showing progressive fringe rotation versus shear strain. Angles of incremental fringe rotation in the plots represent the angle between the orientation of the oldest part of the object-centre path and the incremental orientation of its younger parts. The finite rotation of the fringes with respect to an external reference frame (ISA) is the angle between the orientation of the oldest and the youngest part of the path.

Figure 4.12b shows these plots for the four objects studied. The plots indicate that all

four strain fringes examined have a slow rotation rate during the first stages of their development. The rotation rate increases rapidly after a shear strain of 1 to 2. Rotation rates of fringes of objects I to III decrease during late stages of fringe growth. This could be due to the fact that the strain fringes behave in a similar way as a rigid object that increases its axial ratio progressively while it grows. According to Ghosh and Ramberg (1976) rigid objects with high axial ratios will have decreasing rotation rates once they rotate with their long axis towards parallelism with the flow plane during simple shear deformation. Finite rotation of the studied strain fringes varies from 55° to 110°. Core-objects with an axial ratio of 1.0 (objects I and II) show slower rotation rates of fringes with respect to ISA than core-objects with axial ratio of 1.4 and 2.0 (objects III and IV) indicating that fringes around elongate core-objects rotate faster.
One has to note that the assumption that the fringes open parallel to the extensional ISA is NOT always valid. This can be seen in Fig. 4.12a where the finite orientation of the object-centre paths is not always parallel to indicated ISA (see object I and II). This has two implications for the structural analysis of object-centre paths: (1) strain analysis is not always correct and (2) the curvature of the object-centre path does not necessarily represent the rotation of fringes with respect to ISA. However, the curvature of the object-centre path does at least give an estimate on fringe rotation with respect to ISA, since in the early stages of fringe development it can be expected that fringes open parallel to the extensional ISA. This is discussed in detail in section 4.6.

4.5.3. Relative rotation of core-object and fringes

The relative rotation of core-object and fringes can be directly obtained from displacement-controlled fibres and is indicated on the object-centre path (Fig. 4.4b). Figure 4.12c shows plots of the rotation of core-objects with respect to their fringes versus shear strain. Relative rotation rates of core-object and fringes show that elongate core-objects with an axial ratio of 2.0 (Fig. 4.12c, object IV) tend to rotate at the same rate as their fringes whereas core-objects approaching a circular shape with axial ratios of 1.0 to 1.4 (Fig. 4.12c, object I-III) tend to have faster rotation rates than their fringes with respect to an external reference frame. This has to do with (1) the shape of core-objects and (2) the interaction of fringes and core-object. Round core-object will rotate faster than elongate ones (with an orientation of their long axis of less than 45° to the flow plane) and core-objects with corners and elongate core-objects cannot easily rotate with respect to their fringes because the corners hinder the rotation. Finite rotation angles of the studied core-objects with axial ratios of 1.0 to 1.4 are 49° to 75° anticlockwise with respect to their fringes.

4.6. Discussion

Conventional strain analysis is difficult to apply on fibres in strain fringes from Lourdes because (1) single fibres do not continue along the whole fringe; (2) not all fibres grow displacement-controlled and (3) displacement-controlled fibres are not parallel if the core-object rotates with respect to its fringes. These problems probably do exist for most natural strain fringes especially if the deformation is non-coaxial. Therefore we suggest that object-centre paths should be used by geologists for a structural analysis of strain fringes instead of single fibres or even instead of sets of fibres.

Object-centre paths can be used to estimate finite bulk strain and vorticity of fringes and core-object. However, care has to be taken because object-centre paths reflect movement of fringes and core-object with respect to each other and not necessarily indicate their movement with respect to ISA or an external reference frame. The opening vector of fringes does not have to be exactly parallel to the extensional ISA during each incremental move (Fig. 4.12). Therefore, hook shaped object-centre paths do not necessarily record a sudden rotation of strain fringes with respect to ISA. They only record a sudden change of the pull apart direction of strain fringes and core-object; these can be just the effect of rotation of the corner of a rectangular core-object in a strain fringe towards the extensional ISA, so that fibres suddenly start to grow at another side of the core-object. The curvature of an object-centre path records the rotation of the oldest part of a fringe with respect to the orientation of the youngest part of the object-centre path. In order to transfer this rotation to the rotation of fringes with respect to an external reference frame (e.g. ISA) the orientation of the incremental opening of the fringes has to be constant with respect to this reference frame over time. If this is not the case the curvature of an object-centre path will only give estimates on absolute rotation depending on how much the opening path varies with respect to an external reference frame. One can assume that the fringes in our examples opened parallel to the extensional ISA during early stages of growth. From Fig. 4.12a one can see that they did NOT all open parallel to the extensional ISA during late stages of growth. Therefore one knows that the curvature of the object-centre path only gives estimates and no absolute values. It is worth noting that this might also apply for displacement-controlled (tracking) fibres in extension veins and shear veins which presumably also record only the relative movement of the walls of veins and not necessarily the orientation of the extensional ISA in all cases.

The two fringes and the core-object of a strain fringe behave like three rigid objects in a weaker matrix that influence each other. The curvature of the object-centre path does reflect a rigid body rotation (or a more complex movement) of fringes with respect to the shear-zone boundary and not rotation of the bulk finite strain ellipsoid. A finite strain ellipse cannot rotate over more than 45° during progressive deformation

with irrotational ISA and invariable flow parameters. Fibres can curve more than 45° during one non-coaxial deformation event and a curvature of fibres of more than 45° does not necessarily imply polyphase deformation history. The curvature of fibres should not be included in strain analysis as the curvature is a function of a rigid body rotation (Ellis, 1986). Instead, only the length of the object-centre path should be taken since it represents an accumulation of infinitesimally small strain that can be transferred into finite strain.

The "Fringe Growth" computer model has still a number of shortcomings. The model is only two dimensional and it can be expected that there are three dimensional effects in the fibre patterns, since especially face-controlled and intermediate fibres might grow out of section. However, most of the fibre patterns in the natural examples are reproduced by the computer growth experiments and in thin-section most fibres appear to remain in section so that we suggest that three dimensional effects are of minor importance at least in the examples presented in this study.

4.7. Conclusions

The program "Fringe Growth 2.0" is able to reproduce complex fibre patterns that are found in natural strain fringes from Lourdes, France. Even though most of the fibres in the fringes show displacement-controlled growth, there are face-controlled and intermediate fibres in the rims of fringes, within displacement-controlled large fibre bands, and next to suture lines. Intermediate fibres contain both face-controlled and displacement-controlled fibre boundaries or intermediate fibre boundaries that have face-controlled and displacement-controlled segments along their length. Care has to be taken not to interpret displacement-controlled fibres in strain fringes as fibres that grow parallel to the extensional ISA since the fibres only record relative movement between core-object and fringe.

Object-centre paths should be used by geologists for strain analysis instead of single fibres, because object-centre paths separate core-object rotation with respect to its fringes from translation of fringes away from the core-object and represent all fibres in one fringe. The length along an object-centre path can be interpreted in terms of bulk finite strain and its curvature as estimates on rigid body rotation of fringes with respect to an external reference frame. The rotation component cannot be reconstructed with the same reliability as the fringes do not always open parallel to the extensional ISA.

Acknowledgements

This project was made possible by a visit of DK to the Epsilon Earth Processes Simulation Laboratory, Department of Earth Sciences, Monash University, Clayton (Melbourne), Australia and by a visit of DK to the University of Salamanca, Salamanca, Spain. Marlina Elburg, Beatriz and Tensing are thanked for their hospitality during the visits. The project was funded by the DFG Grant Pa 578/3. We thank Mark Jessell, Janos Urai, Chris Hilgers for their comments and suggestions.

References

Aerden, D.G.A.M., 1996. The pyrite-type strain fringes from Lourdes (France): indicators of Alpine thrust kinematics in the Pyrenees. Journal of Structural Geology 18, 75-91.

Beutner, E.C., Diegel, F.A., 1985. Determination of fold kinematics from syntectonic fibers in pressure shadows, Martinsburg Slate, New Jersey. American Journal of Science 285, 16-50.

Beutner, E.C., Fischer, D.M., Kirkpatrick, J.L., 1988. Kinematics of deformation at a thrust fault ramp (?) from syntectonic fibers in pressure shadows. In: Geometries and Mechanisms of Thrusting, With Special Reference to the Appalachians (edited by Mitra, G. & Wojtal, S.). Special Paper of the Geological Society of America 222, 77-88.

Casey, M., Dietrich, D., Ramsay, J.G., 1983. Methods for determining deformation history for chocolate tablet boudinage with fibrous crystals. Tectonophysics 92, 211-239.

Clark, M.B., Fisher, D.M., Chia-Yu, L., 1993. Kinematic analysis of the Hfuehshan Range: A large-scale pop-up structure. Tectonics 12, 205-217.

Cox, S.F., Etheridge, M.A., 1983. Crack-seal fibre growth mechanisms and their significance in the development of oriented layer silicate microstructures. Tectonophysics 92, 147-170.

Durney, D.W., Ramsay, J.G., 1973. Incremental strains measured by syntectonic crystal growths. In: DeJong, K.A., Scholten, R. (Eds), Gravity and Tectonics, Wiley, New York, 67-95.

Elliot, D., 1972. Deformation paths in structural geology. Bull. geol. Soc. Am. 83, 2621-2638.

Ellis, M.A., 1986. The determination of progressive deformation histories from antitaxial syntectonic crystal fibres. Journal of Structural Geology 8, 701-709.

Etchecopar, A., Malavielle, J., 1987. Computer models of pressure shadows: a method for strain measurement and shear sense determination. Journal of Structural Geology 9,667-677.

Fisher, D.M., 1990. Orientation history and rheology in slates, Kodiak and Afognak Islands, Alaska, Journal of Structural Geology 12, 483-498.

Fisher, D. & Anastasio, D. J., 1994. Kinematic analysis of a large-scale leading edge fold, Lost River Range, Idaho. Journal of Structural Geology 16, 337-354.

Ghosh, S.K., Ramberg, H., 1976. Reorientation of inclusions by combination of pure shear and simple shear. Tectonophysics 34, 1-70.

Hedlund, C.A., Anastasio, D.J., Fisher, D.M. 1994. Kinematics of fault-related folding in a duplex, Lost River Range, Idaho, U.S.A.. Journal of Structural Geology 16, 571-584.

Hilgers, C., Urai, J.L., Post, A.D., Bons, P.D., 1997. Fibrous vein microstructure: Experimental and numerical simulation. Aardkundige Mededelingen 8, 107-109.

Kanagawa, K., 1996. Simulated Pressure Fringes, Vorticity, and Progressive Deformation. In: De Paor, D. G. (Ed.), Structural Geology and Personal Computers. Computer Methods in the Geosciences 15, 259-283.

Koehn, D., Passchier, C.W., & Bons, P.D., 1999. Kinematic analysis of strain fringes. Journal of Conference Abstracts 4 (EUG 10), 830.

Means, W.D., 1976. Stress and Strain, Springer, Heidelberg.

Mügge, O., 1928. Ueber die Entstehung faseriger Minerale und ihrer Aggregationsformen. Neues Jahrbuch für Mineralogie, Geologie und Paläontologie 58A, 303-438.

Pabst, A., 1931. 'Pressure shadows' and the measurement of the orientation in rocks. Journal of the Mineralogical Society of America 16, 55-70.

Passchier, C.W., Trouw, R.A.J., 1996. Microtectonics. Springer, Heidelberg, 289 pp.

Ramsay, J.G., Huber, M.I., 1983. The techniques of modern structural geology, 1: Stain analysis. Academic Press, London.

Sample, J.C., Fisher, D.M., 1986. Duplex accretion and underplating in an ancient accretionary complex, Kodiak Islands, Alaska.. Geology 14, 160-163.

Selkman, S. O., 1983. Stress and displacement distributions around pyrite grains. Journal of Structural Geology 5 (1), 47-52.

Spencer, S., 1991. The use of syntectonic fibres to determine strain estimates and deformation paths: an appraisal. Tectonophysics 194, 13-34.

Urai, J.L., Williams, P.F., Van Roermund, H.L.M., 1991. Kinematics of crystal growth in syntectonic fibrous veins. Journal of Structural Geology 13, 823-836.

Wickham, J.S., 1973. An estimate of strain increments in a naturally deformed carbonate rock. American Journal of Science 237, 23-47.

Wickham, J.S., Anthony, M., 1977. Strain paths and folding of carbonate rocks near Blue Ridge, central Appalachians. Bulletin of the geological Society of America 88, 920-924.

Zwart, H.J. & Oele, J.A., 1966. Rotated magnetite crystals from the Rocroi Massif (Ardennes). Geol. Mijnb. 45, 70-74.

5. General conclusions and suggestions for future research

In this Chapter the conclusions of Chapters 2-4 are summarized and their implications for structural analysis are discussed. Suggestions for future research on fibrous aggregates are presented.

5.1. General conclusions

In order to develop a full theory and understanding of fibrous crystal growth in strain fringes and veins the following steps have to be undertaken: (1) development of a physical/chemical theory, (2) field observations, (3) numerical modelling and (4) physical modelling. This thesis focused on field observations (step 2) and numerical modelling (step 3) based on a fibre growth theory (step 1) of Urai et al. (1991). Step 4 was not undertaken because it is beyond the scope of this thesis. However, work is now in progress to investigate rotation of fringes in non-coaxial flow and to investigate fibre growth with physical experiments. In this thesis, natural examples of fibrous aggregates in veins and strain fringes were investigated in detail. The computer program "Fringe Growth" was developed and used to reproduce fibre patterns in antitaxial strain fringes. The validity of conventional analysis of fibrous aggregates was discussed and a new method to interpret antitaxial strain fringes was presented based on the theory of Urai et al. (1991) and the method of Aerden (1996).

5.1.1. Investigation of natural fibrous aggregates to understand the fibre growth process

The study of striped bedding-veins from the Orobic Alps (Italy) has shown that elongate quartz crystals in these veins do not track the displacement but grow face-controlled. These elongate crystals outgrow each other, grow into open cracks and develop a crystallographic preferred orientation (CPO). Contrary to the elongate

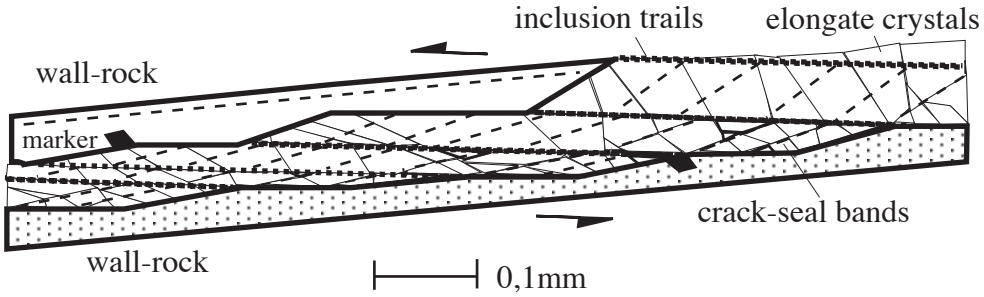

Fig. 5.1 A striped bedding-vein from the Orobic Alps (Bedding-type). Elongate crystals grow face-controlled and do not track the opening trajectory of the vein. Vein opening is parallel to inclusion trails.

crystals, inclusion bands and inclusion trails in the veins can be used for structural

analysis to determine the opening history of the veins (Fig. 5.1). According to the geometry of their inclusion trails and inclusion bands striped bedding-veins can be classified into Bedding-type, Jog-type and Orthogonal-type veins. The veins from the Orobic Alps classify as Bedding-type veins. Striped bedding-veins are excellent shear sense indicators if they contain inclusion bands and inclusion trails (Fig. 5.1). If no inclusion bands or trails are visible, the stair-stepping symmetry of the wall-rock indicates shear-sense. Striped bedding-veins can be used to estimate strain in a rock-pile since the length of an inclusion trail in the vein is identical to the displacement along a striped bedding-vein (Fig. 5.1).

The study of calcite, quartz and mica fibres in strain fringes from the Yilgarn Craton, (Australia) the Hamersley Ranges (Australia) and Lourdes (France) has shown that

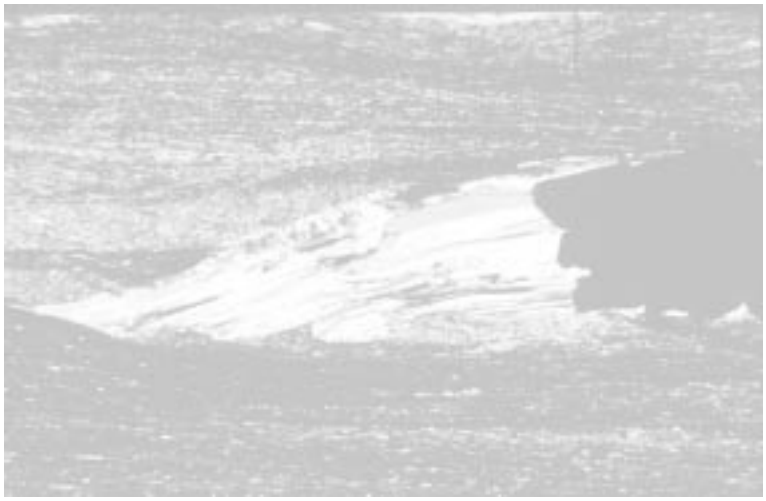

Fig. 5.2 Thin-section micrograph of a strain fringe from Lourdes. Fibres in the fringe grow face- and displacement-controlled. Face-controlled fibres are visible at the upper rim of the fringe. Width of view is 10mm.

strain fringes show complex intergrowth features of fibres that grow in different directions. Contrary to previous studies, this study concludes that fringes with only face-controlled or displacement-controlled fibres are rare end-members since most fringes contain both fibre types. Face-controlled fibres are often found on the rims of fringes (Fig. 5.2) and in displacement-controlled fibre bands within the fringes. Displacement-controlled fibres are locked to outward-pointing asperities on core-objects in accordance with the theory of Urai et al. (1991).

5.1.2. Systematic numerical experiments on fibre growth

Systematic experiments with the program "Fringe Growth" have shown that face-controlled fibres develop around core-objects with a smooth surface and displacement-controlled fibres around core-objects with a rough surface. Figure 5.3 shows six simulations of fibre growth around different core-objects with straight and

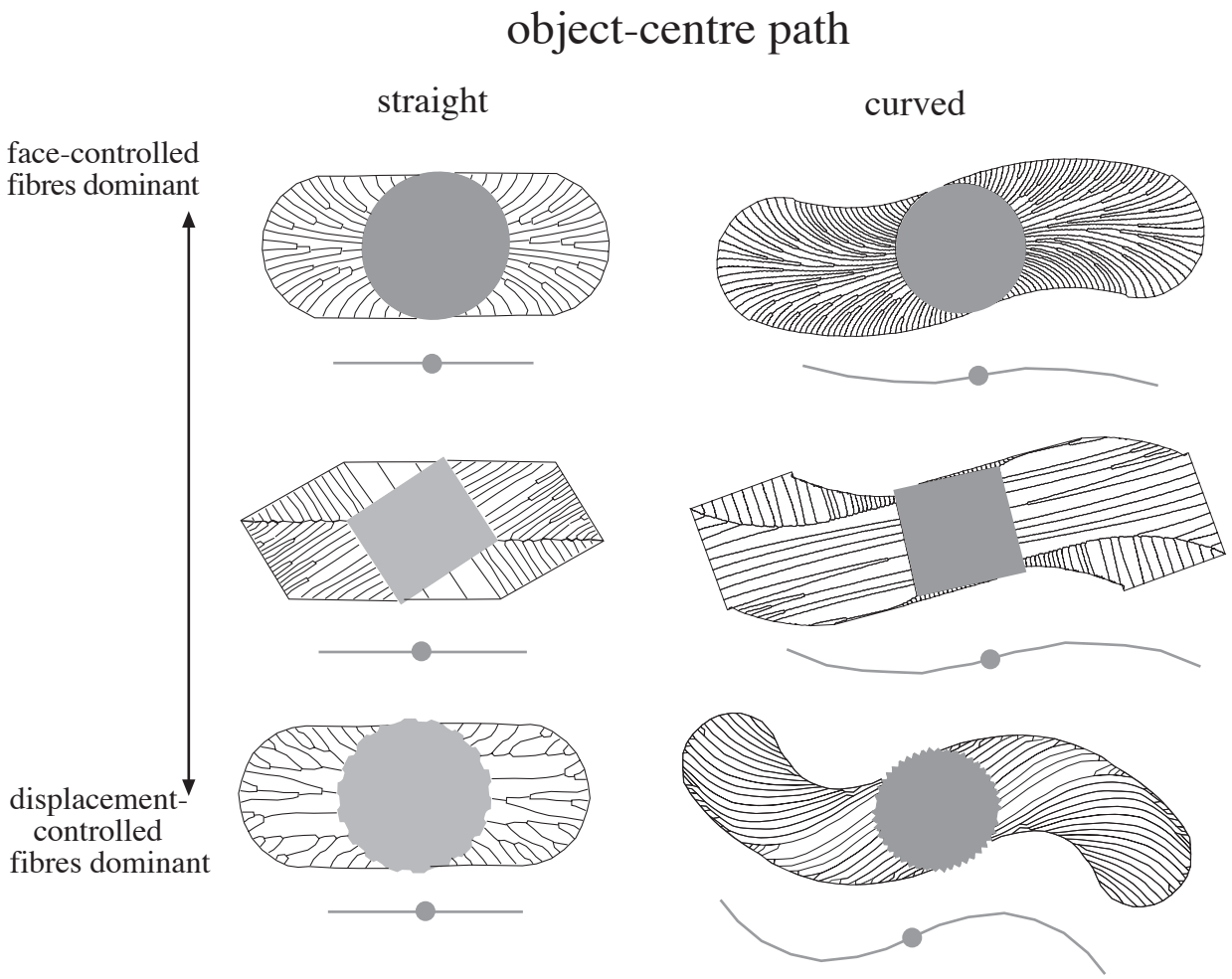

Fig. 5.3 Simulation (with "Fringe Growth") of fibre growth around core-objects of different shape with straight and curved object-centre paths. Displacement-controlled fibres and suture lines develop towards first order (corners) and second order asperities on the core-object surface. Core-objects are rotating clockwise relative to their fringes during the simulations with curved object-centre paths (square core-object 15° and rough round core-object 90°)

curved object-centre paths. Object-centre paths are traces of the centre of the core-object with respect to the fringe. They separate relative rotation of core-object and fringes from their relative translation (Aerden, 1996). Purely face-controlled fringes develop around smooth round core-objects. Fringes around smooth square core-objects develop tracking suture lines towards corners of the core-object (first order asperities). Fringes around rough core-objects contain both displacement-controlled and face-controlled fibres. Displacement-controlled fibres are locked to outward pointing asperities on the core-object surface (second order asperities) and face-controlled fibres are common on the rims of fringes.

A revised classification for fibres is presented (Fig. 5.4): displacement-controlled and face-controlled fibres are end-members of a range of fibre morphologies. Intermediate fibres are fibres that contain face- and displacement-controlled sections (partial-tracking fibres in veins). Fibre bands are defined as sets of face-controlled

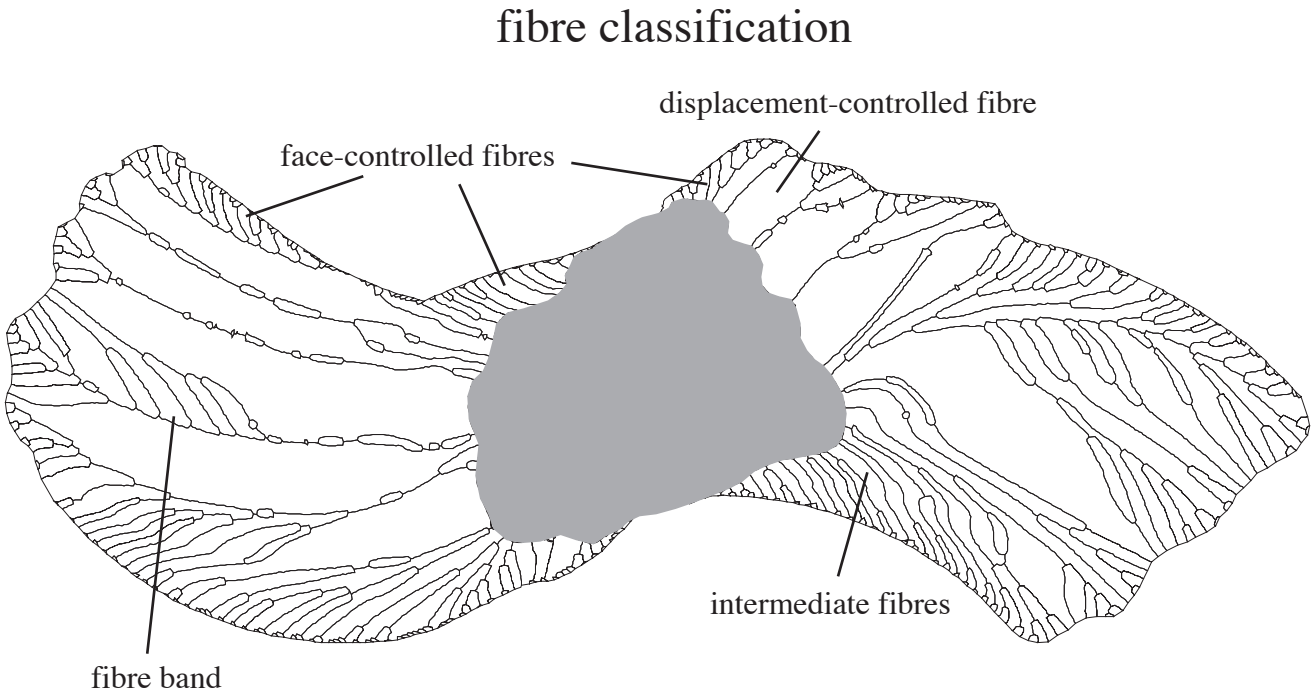

Fig. 5.4 Different fibre types illustrated in a simulated fringe. The simulation was performed with "Fringe Growth 2.0" with a curved object-centre path and clockwise core-object rotation relative to its fringes (about 30°).

fibres that together form a displacement-controlled band. Intermediate fibres commonly develop if the orientation of the opening path of a fringe changes with time (e.g. if the opening path is curved or hook-shaped). Fibre bands develop in the numerical experiments if random nucleation takes place on the growth surface of the fringe and the two grain boundaries of a nucleus grow into different directions, one face-controlled and the other displacement-controlled. The development of different fibre types is controlled by the core-object shape, the roughness of its surface and the growth rate of fibres relative to the opening velocity of the fringe. Displacement-

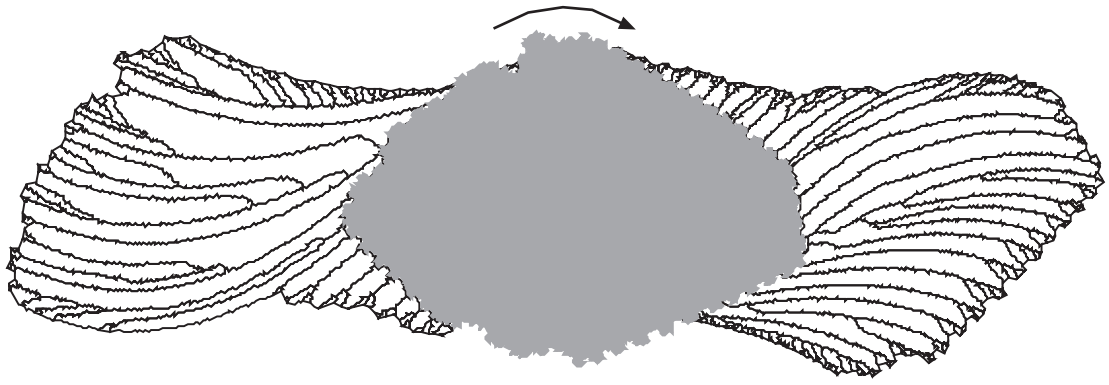

Fig. 5.5 Fibre patterns that develop if the core-object is rotating relative to its fringes (about 24°) (simulation with "Fringe Growth"). Displacement-controlled fibre-segments grow in different directions depending on their orientation with respect to a line connecting growth point and centre of core-object.

controlled fibres follow points on the core-object surface since they are locked to outward pointing asperities. A rotation of the core-object with respect to its fringes produces displacement-controlled fibres with changing curvature along their length so that fibre-segments of the same age will not all grow parallel to each other (Fig. 5.5).

5.1.3. Numerical experiments to reproduce natural fibre patterns

The program "Fringe Growth" is able to reproduce complex fibre patterns that are

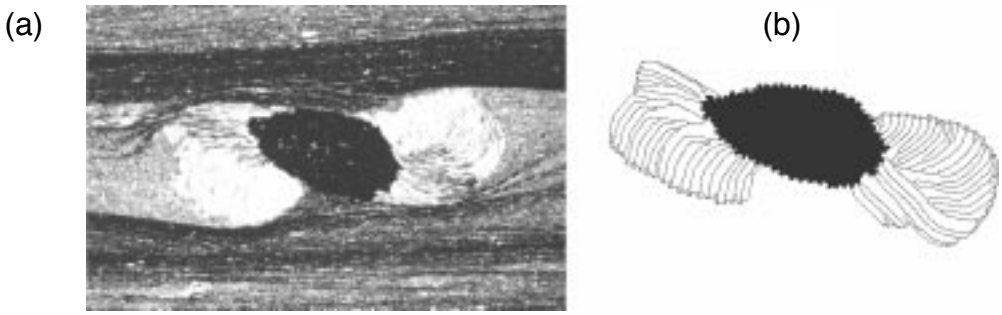

Fig. 5.6 (a) Micrograph of a fringe structure from Lourdes (France) and (b) simulation of the natural example (with ”Fringe Growth”). Width of view is 20 mm.

observed in natural strain fringes from Lourdes (France) and from the Yilgarn Craton (Australia). The similarity between simulated and natural examples (Fig. 5.6) suggests that the assumptions that were used in the computer program are realistic

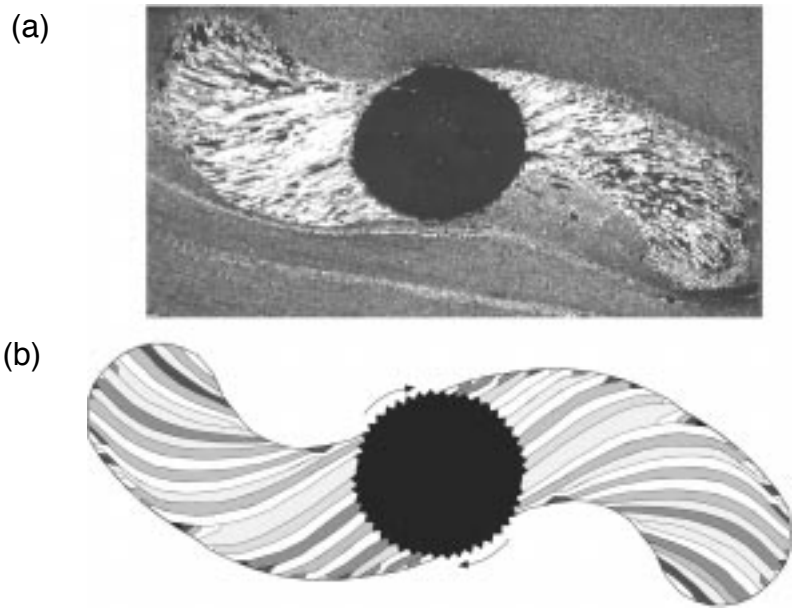

Fig. 5.7 (a) Micrograph of a fringe structure from the Yilgarn Craton (Australia). Width of view is 20 mm. (b) Simulation of the natural example (with ”Fringe Growth”) with a clockwise rotation of the core-object relative to its fringes (90°). Because of the similar geometry of (a) and (b) it is assumed that in the natural example the core-object also rotated relative to its fringes resulting in displacement-controlled fibres that do not all grow parallel to each other or parallel to extensional ISA.

and that displacement-controlled fibres follow points on the core-object surface. Most fibres in the natural and simulated examples grow displacement-controlled but face-controlled and intermediate fibres are commonly found on the rims of fringes, within fibre bands and next to suture lines. Simulations of fringes around core-objects with low aspect ratios suggest that these core-objects can rotate relative to their fringes (Fig. 5.7). This relative rotation produces fibres with an S- or Z-shape in the numerical and natural examples where displacement-controlled fibre-segments of the same age do not grow parallel to each other or parallel to the opening path of a fringe. No single fibre in the modelled or natural fringes represents the whole movement path of the fringes away from the core-object since fibres commonly end on suture lines or on the rims of fringes or they are affected by relative rotation of core-object and fringe. This has major implications for the use of fibres for structural analysis as outlined in the next section.

5.1.4. Structural analysis of fibrous aggregates in antitaxial strain fringes

Observations of natural examples of strain fringes and numerical experiments with the program "Fringe Growth" have supported the assumption that displacement-controlled fibres follow points on the core-object surface in strain fringes (tracking hypothesis of Urai et al. (1991)). Therefore displacement-controlled fibres do NOT necessarily grow parallel to the axis of maximum finite strain or parallel to the extensional ISA. They do grow parallel to the axis of maximum finite strain and parallel to the extensional ISA if progressive deformation is coaxial and if core-objects or fringes do not rotate relative to ISA. During non-coaxial progressive deformation displacement-controlled fibres do NOT grow parallel to the axis of maximum finite strain and they only grow parallel to the extensional ISA if the core-object is rotating at the same rate as its fringes with respect to ISA. In addition, conventional single fibre analysis (e.g. Durney and Ramsay, 1973; Wickham, 1973; Ramsay and Huber, 1983; Ellis, 1986) has two main problems: (1) not all fibres in a fringe grow displacement-controlled and (2) rotation of the core-object with respect to its fringes influences the fibre growth direction so that even displacement-controlled fibre-segments of the same age do NOT grow parallel to each other. Therefore single fibres should not be used for structural analysis but object-centre paths (Aerden, 1996) that (1) represent a whole fringe and (2) separate the opening path of fringes from relative rotation of core-object and fringes (Chapter 4).

It is assumed that fringes open parallel to the extensional ISA since small fringes will be pulled away from the core-object approximately in that direction during progressive deformation. Using this assumption object-centre paths can be interpreted in the following way: (1) the length along the object-centre path gives estimates on

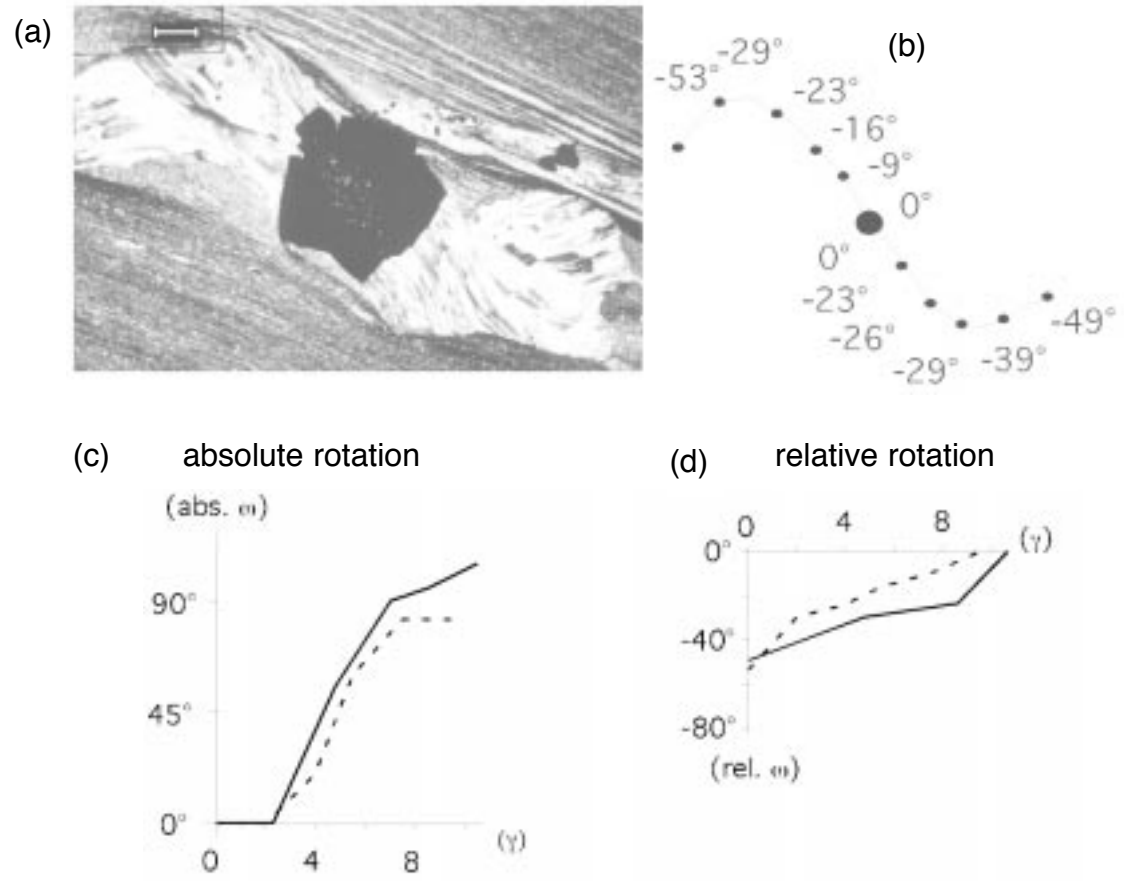

Fig. 5.8 (a) Micrograph of a fringe structure from Lourdes (France). Width of view is 20 mm. (b) Object-centre path of (a) as reconstructed from the photograph (method discussed in Chapter 4). Numbers on the path indicate relative core-object fringe rotation angles. (c) Interpretation of (b) showing absolute rotation of fringes with respect to ISA versus shear strain. Strippled line represents right fringe and solid line left fringe. (d) Plot of fringe rotation relative to the core-object versus shear strain. Strippled line represents right fringe and solid line left fringe. Note that in this plot the final orientation of the core-object is used as reference (0°) as indicated on the object-centre path.

incremental and finite strain and (2) the curvature gives estimates on the rotation and rotation rate of fringes with respect to ISA (Fig. 5.8) (Chapter 4).

However, care has to be taken since observations of fringe structures from Lourdes (France) have shown that fringes do NOT always open parallel to the extensional ISA (Chapter 4) so that vorticity analysis is less reliable than strain analysis. Present available data indicate that the object-centre path method is an improved and reliable method for the interpretation of fibre patterns in antitaxial strain fringes since it is based on a realistic fibre growth hypothesis. It is easy to apply and should be used by geologists for kinematic analysis of fibres in strain fringes in the future. The program "Fringe Growth" provides a tool for research and teaching of progressive fibre growth.

5.2. Suggestions for future research

A number of open questions still exist on the development of fibrous aggregates in

veins and strain fringes. Especially the dynamic problems introduced in Chapter 1 have not been addressed in the present work since this thesis focused on the kinematics of fibrous growth. The following paragraphs state remaining problems and contain suggestions for future research.

Structural analysis: A number of open questions still exist on structural analysis of fibrous aggregates:

(1) Object-centre paths cannot be used for deforming or deformed fringes. Thus a new method should be developed to interpret deforming fringes.

(2) Numerical and/or physical experiments are needed to test the reliability of a structural analysis using strain fringes. Basic questions are:
   (a) can a strain analysis of fringes/veins reflect the bulk strain in the matrix,
   (b) how reliable is a vorticity analysis using fringes/veins and
   (c) how valid is the assumption that fringes open parallel to the extensional ISA.

(3) Numerical and/or physical experiments are needed to study the behaviour of fringe structures and veins in non-coaxial flow. Strain fringes and veins cannot be treated as simple rigid objects since they progressively grow and change their shape and fringe structures are made up of three different rigid objects that influence each other (Ildefonse et al., 1992b). Once the behaviour of fringe structures and veins during non-coaxial progressive deformation with different vorticity numbers is know geologists may be able to use strain fringes and veins to determine the vorticity of the host-rock and to separate single- from polyphase deformation.

(4) Three dimensional analysis of fibres becomes important if the host-rock was subject to volume change or if deformation was non-plane strain (of trigonal symmetry) or polyphase with a change in direction. Three dimensional physical and/or numerical experiments are needed in order to study three dimensional growth of fibres.

(5) Numerical experiments could be conducted on fibre patterns that develop if the centre of rotation of the core-object is not equal to the centre of the core-object itself as assumed in this study or if the core-object rotates in three-dimensional space.

Processes of vein and fringe formation: Processes of vein and fringe formation are still not fully understood. Future research could concentrate on:

(1) a better understanding of the source of material. Microprobe analysis and isotope studies could lead to a better understanding of the source of material. This has

been done in some studies for veins (e.g. Gray et al., 1991; Kirschner et al., 1993; Henderson and McCaig, 1996; Lee et al., 1997; Mapani and Wilson, 1998) but not for fringes.

(2) a better understanding of the transport mechanism of material towards the vein or fringe. The microstructure of a vein/fringe and of the host-rock might indicate whether or not the transport was via fluid flow or diffusion.

(3) a better understanding of the process of fringe and vein opening. The process of vein and fringe opening should be investigated in physical experiments to see if a crystal structure in veins and fringes can be related to a dilatation process. (e.g. Li and Means, 1995; Means and Li, 1995a,b; Bons and Jessell, 1997; Hilgers et al., 1997; Brok et al., 1998).

External conditions of vein and fringe formation: It is important to know under what conditions fibres in veins and fringes form. Once these conditions are known the existence of different veins and fringes in natural rocks might indicate under what external conditions they formed. External conditions that might be important are temperature, differential stress, bulk strain, chemistry of the fluid and chemistry and texture of the host-rock. Different methods could be used to study the effect of these different conditions on fringe and vein development.

(1) Fluid inclusion studies might indicate the pressure of the fluid phase from which material was precipitated in the vein/fringe. This has been done by many authors for veins (e.g. Foreman and Dunne, 1991; Robert et al., 1995) but not for fringes.

(2) Physical experiments could be conducted with known external conditions to investigate exactly when a fringe/vein forms and with what texture based on experiments by Li and Means (1995), Means and Li (1995a,b), Bons and Jessell (1997), Hilgers et al. (1997) and Brok et al. (1998).

(3) Numerical experiments could be conducted based on known physical and chemical theories to test these theories and predict theoretically under what conditions a vein/fringe forms.

References

Aerden, D.G.A.M., 1996. The pyrite-type strain fringes from Lourdes (France): indicators of Alpine thrust kinematics in the Pyrenees. Journal of Structural Geology 18, 75-91.

Bons, P.D., Jessell, M.W., 1997. Experimental simulation of the formation of fibrous veins by localised dissolution-precipitation creep. Mineralogical Magazine 61, 53-63.

Den Brok, B., Passchier, C.W., Sieber, M., 1998. Fibre growth in wet salt aggregates in a temperature gradient field. Mineralogical Magazine 62, 527-532.

Durney, D.W., Ramsay, J.G., 1973. Incremental strains measured by syntectonic crystal growths. In: DeJong, K.A., Scholten, R. (Eds), Gravity and Tectonics, Wiley, New York, 67-95.

Ellis, M.A., 1986. The determination of progressive deformation histories from antitaxial syntectonic crystal fibres. Journal of Structural Geology 8, 701-709.

Foreman, J.L., Dunne, W.M., 1991. Conditions of vein formation in the southern Appalachian foreland: constraints from vein geometries and fluid inclusions. Journal of Structural Geology 10, 1173-1183.

Gray, D.R., Gregory, R.T., Durney, D.W., 1991. Rock-buffered fluid-rock interaction in deformed quartz-rich turbidite sequences, Eastern Australia. Journal of Geophysical research B12, 19,681-19,704.

Henderson, I.H.C., McCaig, A.M., 1996. Fluid pressure and salinity variations in shear zone-related veins, central Pyrenees, France: Implications for the fault-valve model. Tectonophysics 262, 321-348.

Hilgers, C., Urai, J.L., Post, A.D., Bons, P.D., 1997. Fibrous vein microstructure: Experimental and numerical simulation. Aardkundige Mededelingen 8, 107-109.

Kirschner, D. L., Sharp, Z. D. & Teyssier, C., 1993. Vein growth mechanisms and fluid sources revealed by oxygen isotope laser microprobe. Geology 21, 85-88.

Lee, Y., Wiltschko, D.V., Grossman, E.L., Morse, J.W., Lamb, W.M., 1997. Sequential vein growth with fault displacement: An example from the Austin Chalk Formation, Texas. Journal of Geophysical Research B10, 22,611-22,628.

Li, T. & Means, W. D., 1995. Experimental antitaxial growth of fibrous crystals 1: technique, fibre character, and implications. GSA Annual Meeting Conf. Abstr.

Mapani, B.E.S., Wilson, C.J.L., 1998. Evidence for externally derived vein forming and mineralising fluids: An example from the Magdala gold mine, Stawell, Victoria, Australia. Ore Geology Reviews 13, 323-343.

Means, W.D. & Li, T., 1995a. Experimental antitaxial growth of fibrous crystals. II: internal structures. GSA Annual Meeting Conf. Abstr.

Means, W.D. & Li, T., 1995b. Tracking and non-tracking experimental fibrous veins. GSA Annual Meeting Conf. Abstr.

Ramsay, J.G., Huber, M.I., 1983. The techniques of modern structural geology, 1: Stain analysis. Academic Press, London.

Robert, F., Boullier, A, Firdaous, K, 1995. Gold-quartz veins in metamorphic terranes and their bearing on the role of fluids in faulting. Journal of Geophysical Research B7, 12,861-12,879.

Urai, J.L., Williams, P.F., Van Roermund, H.L.M., 1991. Kinematics of crystal growth in syntectonic fibrous veins. Journal of Structural Geology 13, 823-836.

Wickham, J.S., 1973. An estimate of strain increments in a naturally deformed carbonate rock. American Journal of Science 237, 23-47.

6. Appendix

The appendix of this thesis is separated into two sections. Section one describes the program "Fringe Growth" in detail and section two contains the programs "Fringe Growth 1.3" and "Fringe Growth 2.0" together with Quicktime movies of fibre growth in fringes on a CD-ROM.

6.1. The computer program "Fringe Growth"

This section describes the computer program "Fringe Growth", contains a user manual to operate the program and gives the settings that were used in simulations presented in Chapters 3 and 4 of this thesis. Two versions of "Fringe Growth" are available at the moment (CD-ROM): (1) "Fringe Growth 1.3" used for simulations presented in Chapter 3 and (2) "Fringe Growth 2.0" used for simulations presented in Chapter 4. "Fringe Growth 2.0" is a further developed version of "Fringe Growth 1.3" and includes nucleation of crystals in the fringe and dissolution of crystals. For simple simulations the use of "Fringe Growth 1.3" is recommended since "Fringe Growth 2.0" runs slower because of the dissolution routines and is a beta version that still contains a number of problems (see 6.1.4.4.).

6.1.1. General introduction

The computer model "Fringe Growth" is a numerical front-tracking model. It is based on the model "Vein Growth" by Bons (in press). "Fringe Growth" can model two-dimensional growth of crystals in non-deforming antitaxial strain fringes. Only one fringe is modelled during a simulation with the fringe being fixed with respect to the computer screen (Fig. 6.1). The core-object can (a) move with respect to the fringe

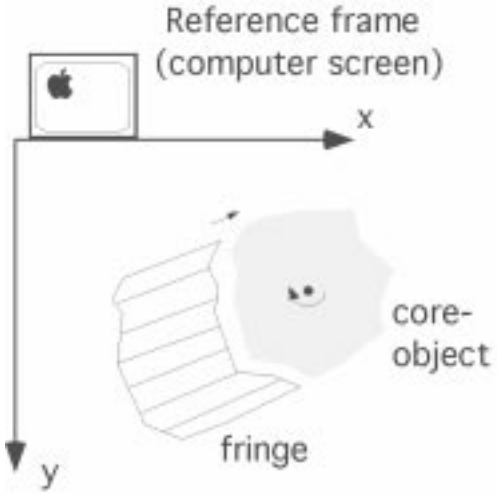

Fig. 6.1 The core-object in "Fringe Growth" can be translated relative to the fringe (fringe is fixed relative to computer screen) and can rotate around its centre.

on the screen and (b) rotate around its centre, both in user defined increments. Grains in the model are defined by nodes that are connected by straight line segments. Growth of grains is simulated by incremental movement of nodes depending on the growth anisotropy of grains and their growth velocity (see 6.1.2. and Bons, in press). The boundary of the model is the contact of the fringe to the matrix so that the matrix (host-rock) is not included in the simulations. Input parameters of "Fringe Growth" are a file describing the core-object plus optional nucleated grains (Node file) and a file discribing the anisotropy of the growing crystals (”mineral type”) (Crystal file). Only one type of crystal anisotropy can be used for all grains during a run of the program. In the program ”pixel” is used as length unit and ”step” as time unit. Parameters that can be changed by the user during a run of the program are:

(1) maximum number of growth stages,
(2) number of growth stages after which the program will draw a picture of the microstructure,
(3) distance between nodes (=resolution of the growing grains),
(4) maximum growth rate of crystals,
(5) a function that can change the effect of the anisotropy of the crystal growth rate defined in the crystal file,
(6) the number of growth stages after which the core-object is moved incrementally,
(7) the amount of core-object movement per opening step,
(8) the opening direction,
(9) a permutation angle that the opening direction will change incrementally,
(10) an angle that the core-object will rotate around its centre,
(11) the size of new nuclei,
(12) boundary conditions that describe the width of the fringe,
(13) whether or not nucleation takes place in the fringe,
(14) the grain boundary growth speed.

These parameters are described in detail in section 6.1.4.2. The program provides default settings of all these parameters that enable reasonable simulations. Pictures of the running simulation can be saved automatically to create movies of incremental fibre growth.

6.1.2. Growth algorithm of grains

This section describes the growth routine used in "Fringe Growth" in detail. Grains in the model are defined by nodes which are connected by straight line segments. Double nodes connect two neighbouring grains and triple nodes lie on the vertices between three neighbouring grains (Fig. 6.2). Nodes can have the following ”activites” or ”states”:

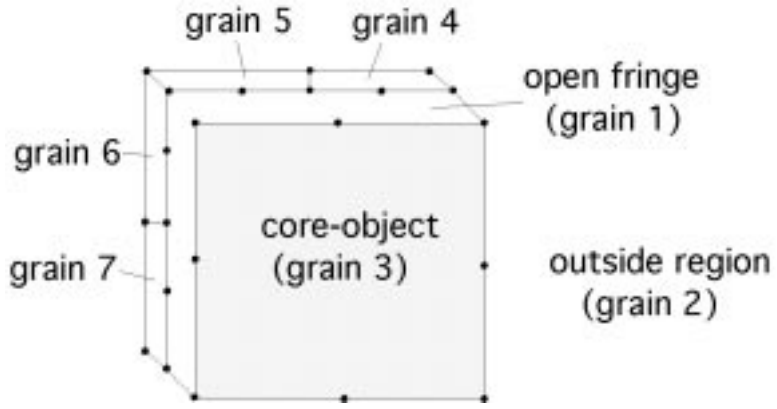

Fig. 6.2 Simple drawing illustrating how grains are defined in "Fringe Growth".

(1) = growing nodes,
(2) = temporarily locked nodes,
(3) = stationary nodes,
(4) = boundary nodes (between fringe and core-object),
(5) = nodes of core-object,
(6) = dissolving nodes and
(7) = special kind of dissolving node.
Only the nodes between the open fringe and growing grains can move (activity 1). Nodes that are still in the core-object directly after the opening event of the fringe will move backwards into their grain until they are not in the core-object anymore (activity 6). This simulates the dissolution of parts of a fringe. Movement of nodes is calculated in incremental growth steps, the magnitude of which is defined by the user. During an incremental crystal growth step the computer runs through the following routines (Bons, in press):

(1) Movement of double nodes: The orientation of the right segment (if the growth is towards the bottom of the computer screen) of each active double node with respect to the crystallographic orientation of the corresponding grain (each grain has a c-axis defined) is checked and the growth vector is calculated (growth vector=vector from crystal file (file containing a magnitude for each degree from 0°-90°) depending on crystal orientation multiplied by the maximum growth rate (defined by user)). This growth vector is added to the midposition between the checked double node and the next node to the right. The new position of the double node is stored in its memory (Bons, in press) (Fig. 6.3b).

(2) Movement of triple nodes: Before the movement of a triple node is calculated the program has to check if the node left of the triple node is a double node that is active.

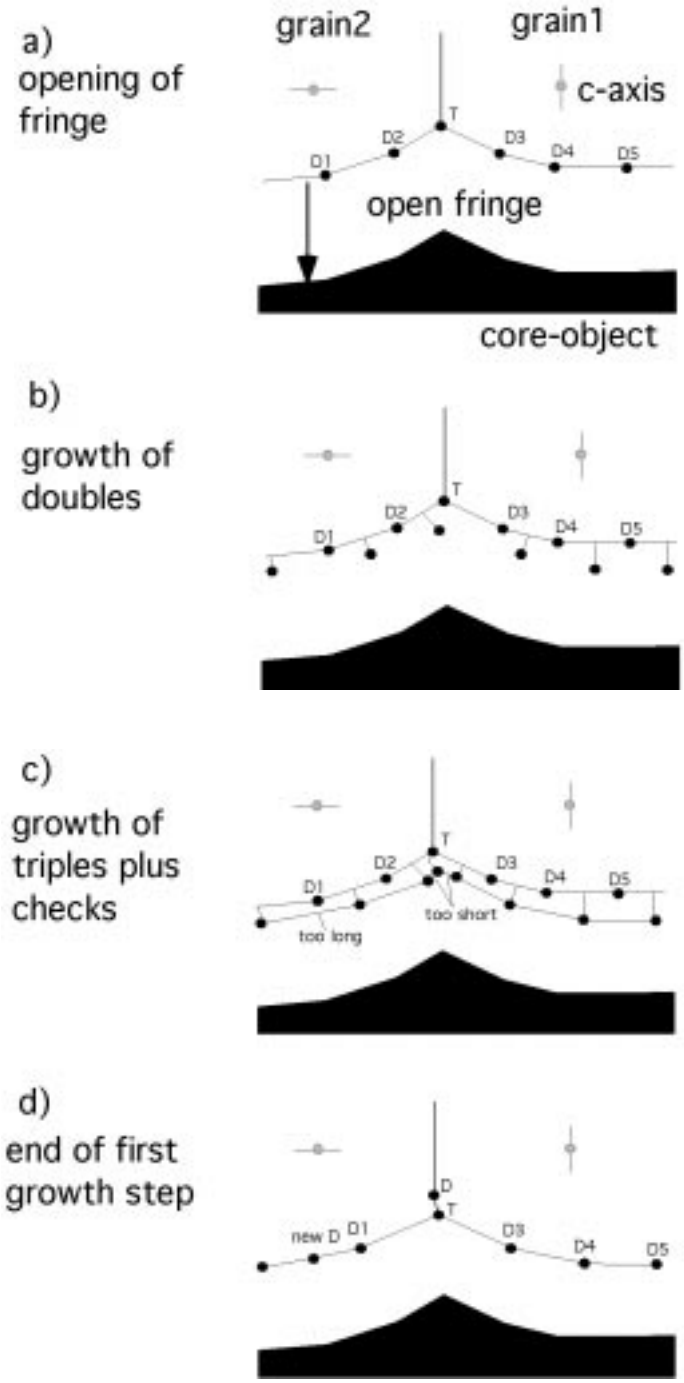

Fig. 6.3 Growth routine for "Fringe Growth" (see also Bons, in press).

In that case a new double node is created and positioned between the two (because double nodes move towards the right a gap would occur otherwise). To move the triple node the growth vectors of the two neighbouring active double nodes are calculated, added and divided by two (Note that this routine is different from the routine used in Bons, in press). The resulting growth vector for the triple node is multiplied by a factor (grain boundary growth speed) that determines how fast triple nodes grow relative to

double nodes (80% in the default settings of the program, can be varied by the user). This is important since triple nodes probably tend to grow slower than double nodes in nature because they tend to have higher energies. The grain boundary growth speed has an influence on the anisotropy of the growing grains, anisotropy has a larger effect if the grain boundary growth speed is low (e.g. 50%) relative to the growth speed of doubles. Triple nodes of dissolving grains "grow" (or dissolve) faster than double nodes (120% in the default settings of the program).

(3) Nodes that connect the core-object with the fringe (activity 4 nodes) need a special routine for movement. They move similar to double nodes but stay on the boundary between the fringe and the outside of the model (matrix or host-rock).

(4) Once all new postions of active nodes are calculated all nodes are moved.

(5) A number of checks have to be performed at the end of each growth routine:
- Two neighbouring active triple nodes are connected with each other (if the distance between them is less than the user defined distance for doubles) so that only one active triple node remains (neighbour switch; Bons, in press).
- Grains that are too small (consisting of only triple nodes) are removed.
- The distance between nodes is checked, if it is larger than a user defined amount additional nodes are added, if it is smaller than half this amount nodes are removed (Bons, in press) (Fig. 6.3c).
- Nodes that reach the core-object are switched off (activity 2) (Bons, in press).
- Nodes that are in the core-object after an opening event are switched to dissolve (activity 6), these nodes are switched off once they are again in the open fringe (activity 2).
- Checks are preformed to avoid nodes growing over other grains.

The user defines how many of these growth routines are performed before the next opening event of the fringe takes place. Note that the program will run through growth routines even if all grains are locked.

6.1.3. Boundary conditions

The boundary of the model is the contact between the fringe/core-object and the matrix. Once grains have nucleated on this boundary it is stable unless it is dissolved again. The fringe is connected to the core-object with activity 4 nodes (Fig. 6.4). These two nodes require a special growth routine. They move similar to double nodes. Every fringe opening event the angle between the boundary of the fringe and the core-

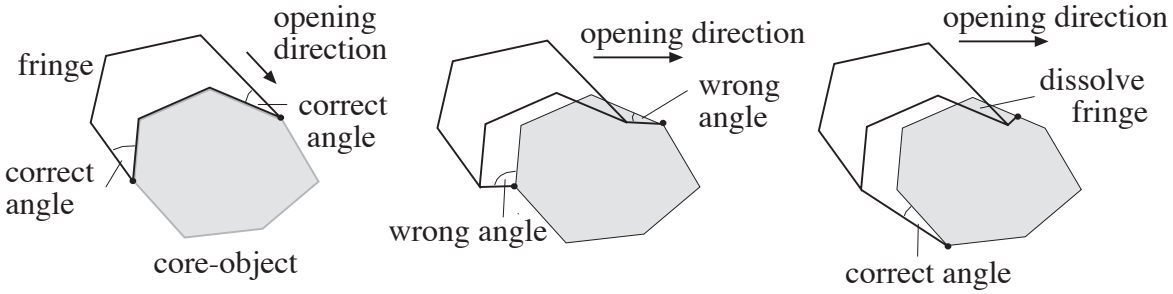

Fig. 6.4 Illustration of a new connection of activity 4 nodes with nodes of the core-object after a change in the opening direction of the fringe. The correct angles in the drawing are larger than three degrees for illustration. For the correct connection of the upper rim of the fringe to the core-object parts of the fringe have to dissolve first in this example (after the opening direction changed).

object surface on the inside of the fringe is checked (should be larger than three degrees). If the angle is less than three degrees the program connects an activity 4 node with a node of the core-object further towards the fringe, if the angle is larger the program connects the activity 4 node with a node further away from the fringe. This process is important once the opening path of the fringe is curved or the core-object

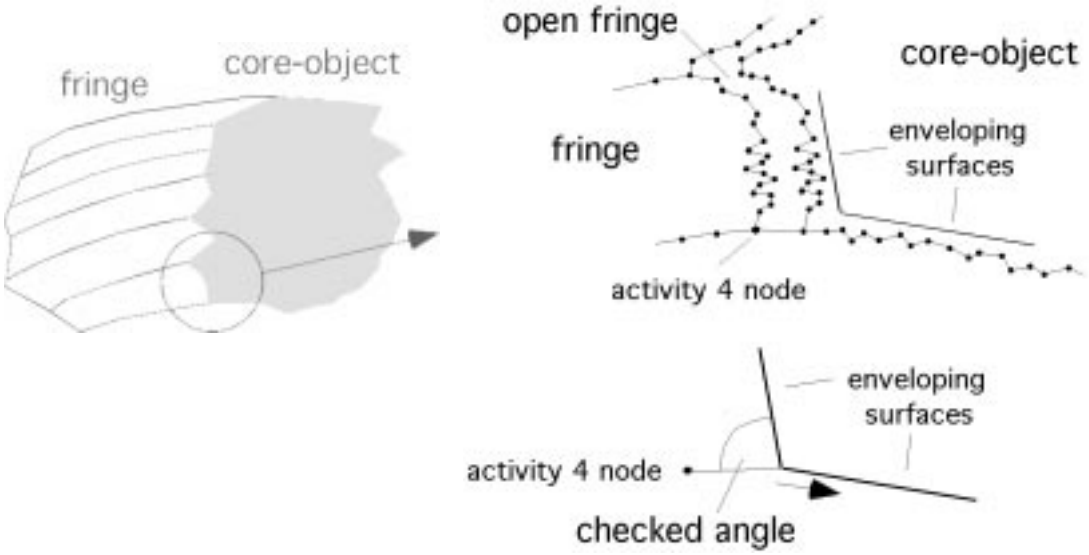

Fig. 6.5 After an opening event of the fringe the angle between the rim of the fringe and the core-object surface is checked. If the surface is rough a number of nodes have to be used to get an average that represents the enveloping surface of the core-object since local roughnesses of the core-object surface should not influence the width of the fringe (roughness exaggerated in example). In this example the angle is larger than 3 degrees so that the activity four node will be connected with a node of the core-object that is further away from the fringe (in the direction of the arrow).

rotates relative to the fringe. To check the angle between the boundary of the fringe and the core-object surface a number of nodes on the core-object are used (Fig. 6.5) and their connections are averaged. This is important if the core-object has pronounced corners since the local morphology of the core-object should not

influence the width of the fringe (the user can define how many nodes on the core-object are used for an average via the settings dialog -> level4activity).

6.1.4. User manual

Before "Fringe Growth" is started all input files have to be in the same folder as the program. All output files will be saved automatically in that same folder as well. The

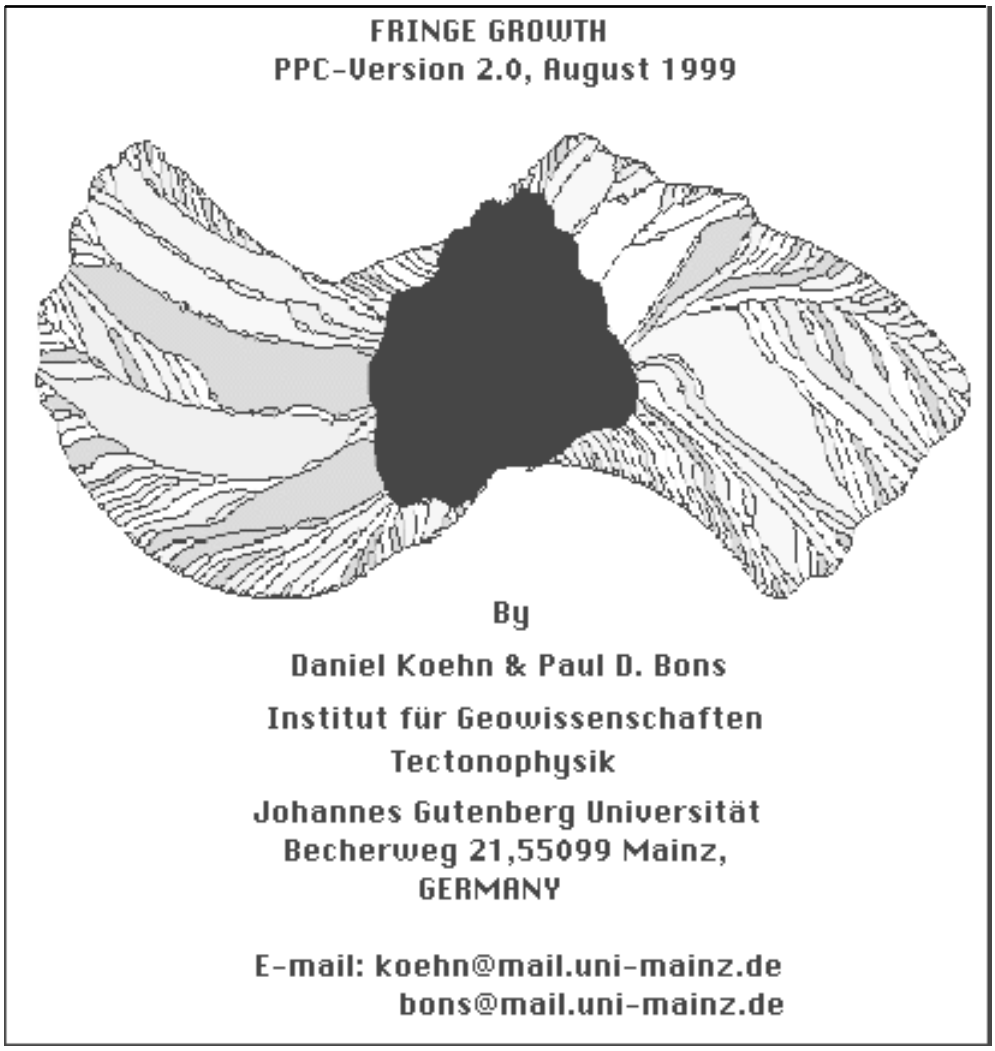

Fig. 6.6 ”Fringe Growth 2.0” welcome window.

memory (RAM) of the program may have to be expanded for large simulations (up to 20-25MB) After opening the program by clicking at the ”Icon” a welcome window (Fig. 6.6) will appear on the screen. It will disappear once the user clicks on the window or on the menu bar. "Fringe Growth" features two main menues:

(1) Fringe Growth to run simulations (Fig. 6.7) and

(2) Make data set to create new core-objects (Fig. 6.8).

Clicking on these activates the menu bars. Items that can be chosen are highlighted. Using the menu Fringe Growth the user can:

(1) start a simulation (Start Growing),

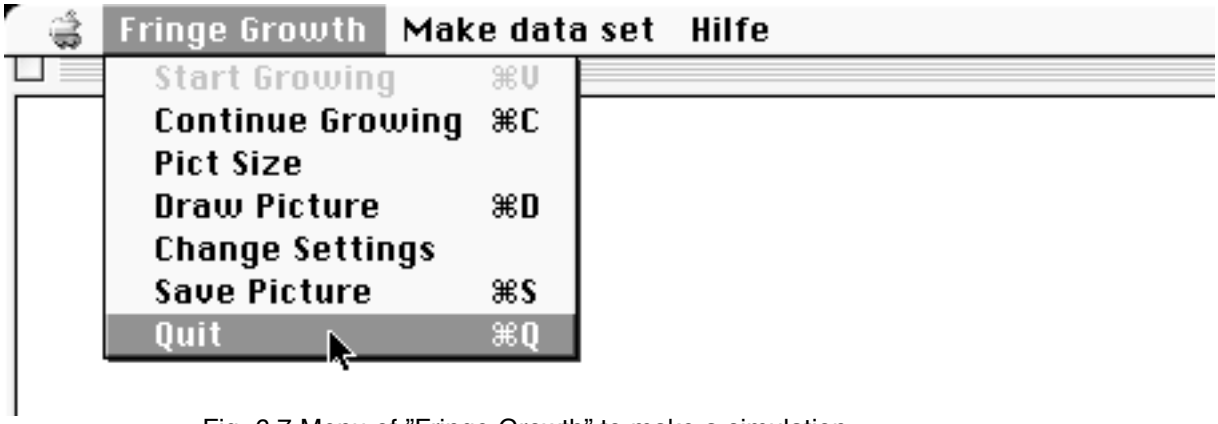

Fig. 6.7 Menu of ”Fringe Growth” to make a simulation.

(2) continue a simulation (Continue growing),
(3) change the picture size (Pict Size),
(4) draw a picture of the current fringe (Draw Picture),
(5) change the currently used settings (Change Settings),
(6) save a picture (Save Picture) or

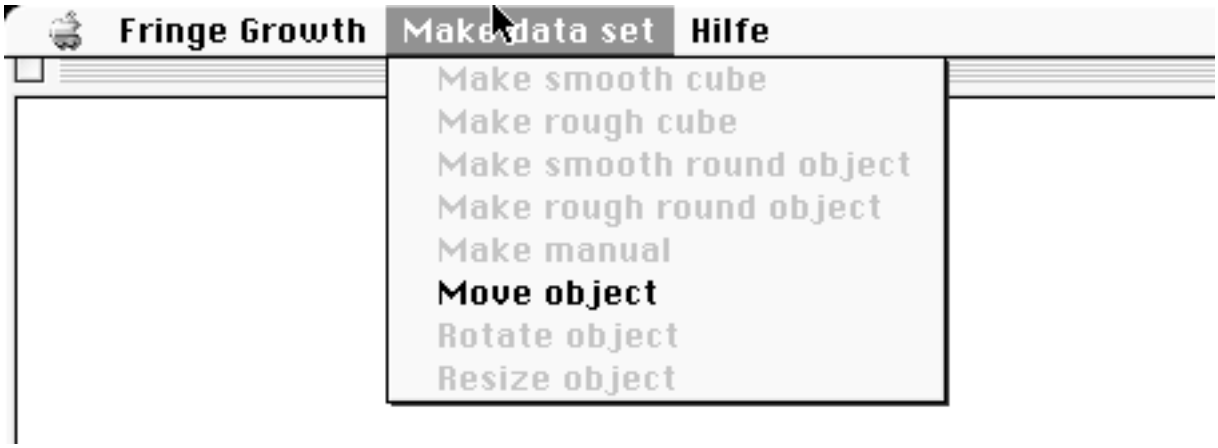

Fig. 6.8 Menu of ”Fringe Growth” to create new core-objects and to change core-objects.

(7) quit the program (Quit).

Using the menu Make data set the user can generate new core-objects (Make smooth cube, Make rough cube, Make smooth round object, Make rough round object, Make manual) or the user can change the size of the core-object, rotate the core-object or move it on the screen (Resize object, Rotate object, Move object). The generation of new core-objects is described in detail in section 6.1.4.3.

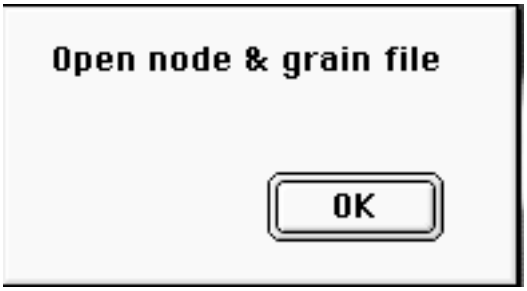

Fig. 6.9 ”Fringe Growth” asking for a .NODE file.

After starting a simulation (Fringe Growth: Start Growing) the program asks for a "node & grain file" (Fig. 6.9). This file describes a core-object and optional first nuclei,

Fig. 6.10 ”Fringe Growth” asks for a .CRYS file

files are marked with ".NODE" at the end. After the user opened a ".NODE"-file the computer asks for a "growth rate file" (Fig. 6.10). This file contains information on the crystal anisotropy of the growing grains in the fringe. It is marked with ".CRYS" at the

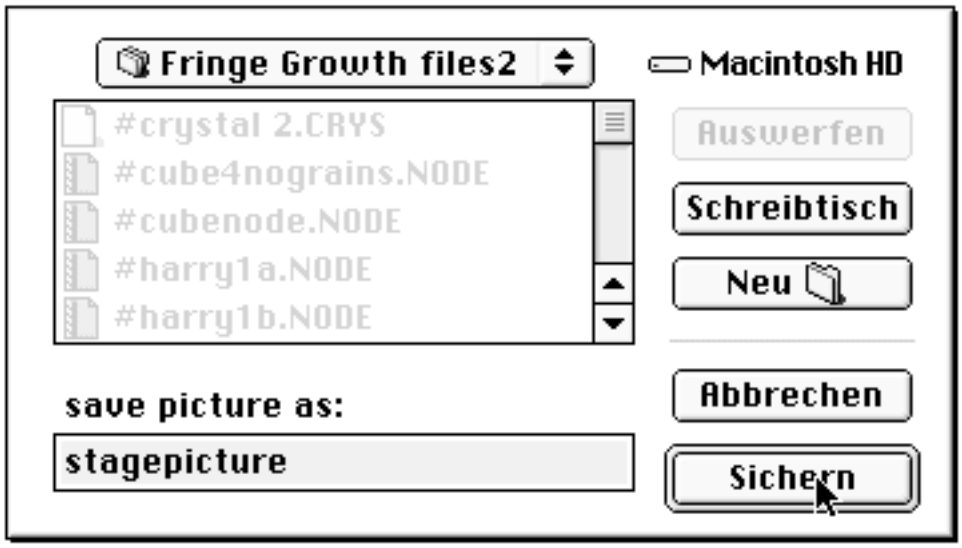

Fig. 6.11 Dialog in ”Fringe Growth” asking for a name for automatically saved pictures. The user has to stay in the same folder as the program. ”Sichern” or ”Save” means save picts automatically and ”Abbrechen” or ”Cancel” means do not save picts automatically.

end. The input files are described in detail in section 6.1.4.1. The program finally asks for a name for the "PICT" files that will be created (Fig. 6.11). The number of steps when the picture is taken will be added at the end of the file name each time a picture is saved automatically. If the "CANCEL" button is pressed the program will not save pictures automatically, if the "OK" button is pressed it will save pictures automatically. After pressing one of these buttons a white window appears with the core-object. The core-object can be rotated around its centre and changed in size as long as no grains have nucleated (Make data set: Rotate object or Resize object). The core-object together with the grains in the fringe can be moved on the computer screen in x- and y-direction (Make data set: Move object). Once the menu bar item Continue Growing

is activated the program will nucleate the first grains on one side of the core-object (opposite of the direction in which the core-object will move). The following settings will appear on the window:
(1) current stage number and final number of stages chosen,
(2) the files used (Node and Crystal file),
(3) the node spacing (resolution),
(4) the growth rate,
(5) the anisotropy,
(6) number of growth stages between fringe opening events,
(7) amount of core-object movement per opening event,
(8) the permutation angle of the opening direction,
(9) the current number of fringe opening events,
(10) direction of core-object movement,
(11) angle of core-object rotation per opening event and
(12) the size of nuclei.
These settings will only be updated once a new picture is drawn. If Continue Growing is activated for the second time the core-object will start to move away from the fringe and the grains in the fringe will start to grow. On top of the window the number of stages will be indicated as well as the number of actively growing grains and the number of currently used nodes. To stop a simulation in order to change the settings

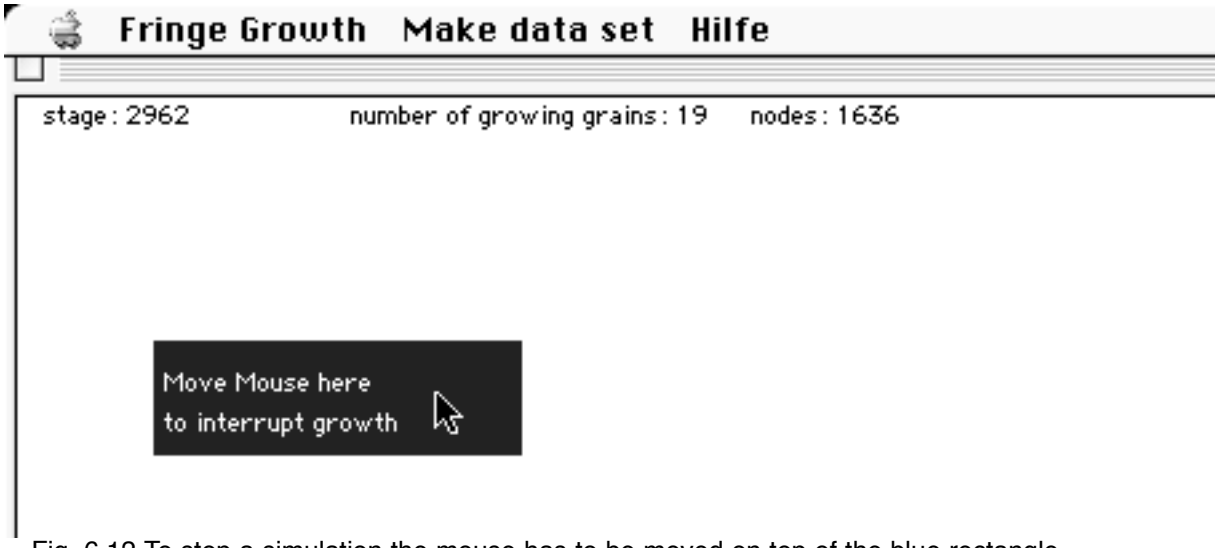

Fig. 6.12 To stop a simulation the mouse has to be moved on top of the blue rectangle.

or save a picture the mouse has to be moved on the blue rectangle ("Move mouse here to interrupt growth") (no mouse click is needed) (Fig. 6.12). Once growth stops, settings can be changed. This is described in detail in section 6.1.4.2. The program stops automatically when it reaches the maximum number of growth steps. The user can exit the program at anytime with Quit once the program is halted.

6.1.4.1. Input files

Two input files are used in "Fringe Growth", a ”Node (.NODE) file” and a ”Crystal (.CRYS) file”.

Node file: The ”Node file” (”Node and Grain file” in Bons, in press) contains data that describes the morphology of the core-object and optional nuclei. It is a text file that contains the parameters described in the following example of a ”Node file”:

20264 (This number is just an index for a .NODE file)
You can write text here and anywhere before the cross-hatch.
Do not add or delete any cross-hatch in this file. #

1 The index for the object #
(important for boundary conditions of core-objects)

0 0 200 500 The outline of the work area; last numbers can be changed #

11 The number of grains in this list #

The grain data (index, mineral type, number of nodes, lattice orientation) #
1 0 28 0.0 (grain 1 is the open fringe)
2 0 30 0.0 (grain 2 is the outside of the fringe)
3 0 36 0.0 (grain 3 is the core-object)
4 2 4 68.0 (grains 4 to 11 are nuclei)
5 2 4 -66.0
6 2 4 -105.0
7 2 4 111.0
8 2 4 35.0
9 2 4 97.0
10 2 4 -164.0
11 2 4 52.0

54 The number of nodes in this list #

The node data (index, location(x and y), number of neighbours, 3 neighbouring nodes, 3 neighbouring grains, activity status) #
(activity status 1=node can grow, 2=node temporarily locked, 3=node static, 4=boundary node between fringe and core-object, 5=node of core-object)
1 81.00 320.00 3 10 19 2 1 4 2 4

2	81.00	310.00	3	11	1	3	1	5	4	1
3	81.00	300.00	3	12	2	4	1	6	5	1
4	81.00	290.00	3	13	3	5	1	7	6	1

etc.

”Node files” can be changed or the user can create ”Node files” manually. However the latter is not recommended since ”Node files” of complex core-objects contain 800 to 2000 nodes which describe only the morphology of the core-object's surface.

Crystal files: Each grain in a fringe contains a number that describes its lattice orientation. The crystal morphology is described in a ”Crystal file” that contains the growth rate of crystals for lattice orientations of 0° to 90°. The growth rate is normalised to 1.0 and will be multiplied by the maximum growth rate during simulations. In the simulations presented in this thesis the following prismatic crystal file was used (Fig. 6.13):
0 = orientation in degrees, 1.0000 = growth rate in pixel

0	1.0000	1	0.9938	2	0.9861	3	0.9772	4	0.9669
5	0.9552	6	0.9422	7	0.9279	8	0.9123	9	0.8955
10	0.8775	11	0.8582	12	0.8378	13	0.8164	14	0.7938
15	0.7702	16	0.7457	17	0.7202	18	0.6939	19	0.6668
20	0.6389	21	0.6103	22	0.5811	23	0.5514	24	0.5212
25	0.4905	26	0.4595	27	0.4282	28	0.3967	29	0.3651
30	0.3333	31	0.3539	32	0.3745	33	0.3949	34	0.4151
35	0.4350	36	0.4545	37	0.4736	38	0.4923	39	0.5103
40	0.5278	41	0.5445	42	0.5606	43	0.5758	44	0.5901
45	0.6036	46	0.6160	47	0.6275	48	0.6378	49	0.6471
50	0.6552	51	0.6622	52	0.6679	53	0.6723	54	0.6755
55	0.6774	56	0.6780	57	0.6772	58	0.6750	59	0.6715
60	0.6667	61	0.6604	62	0.6528	63	0.6438	64	0.6335
65	0.6219	66	0.6089	67	0.5946	68	0.5790	69	0.5622
70	0.5441	71	0.5249	72	0.5045	73	0.4830	74	0.4605
75	0.4369	76	0.4123	77	0.3869	78	0.3606	79	0.3334
80	0.3056	81	0.2770	82	0.2478	83	0.2181	84	0.1878
85	0.1572	86	0.1262	87	0.0949	88	0.0634	89	0.0317
90	0.0157								

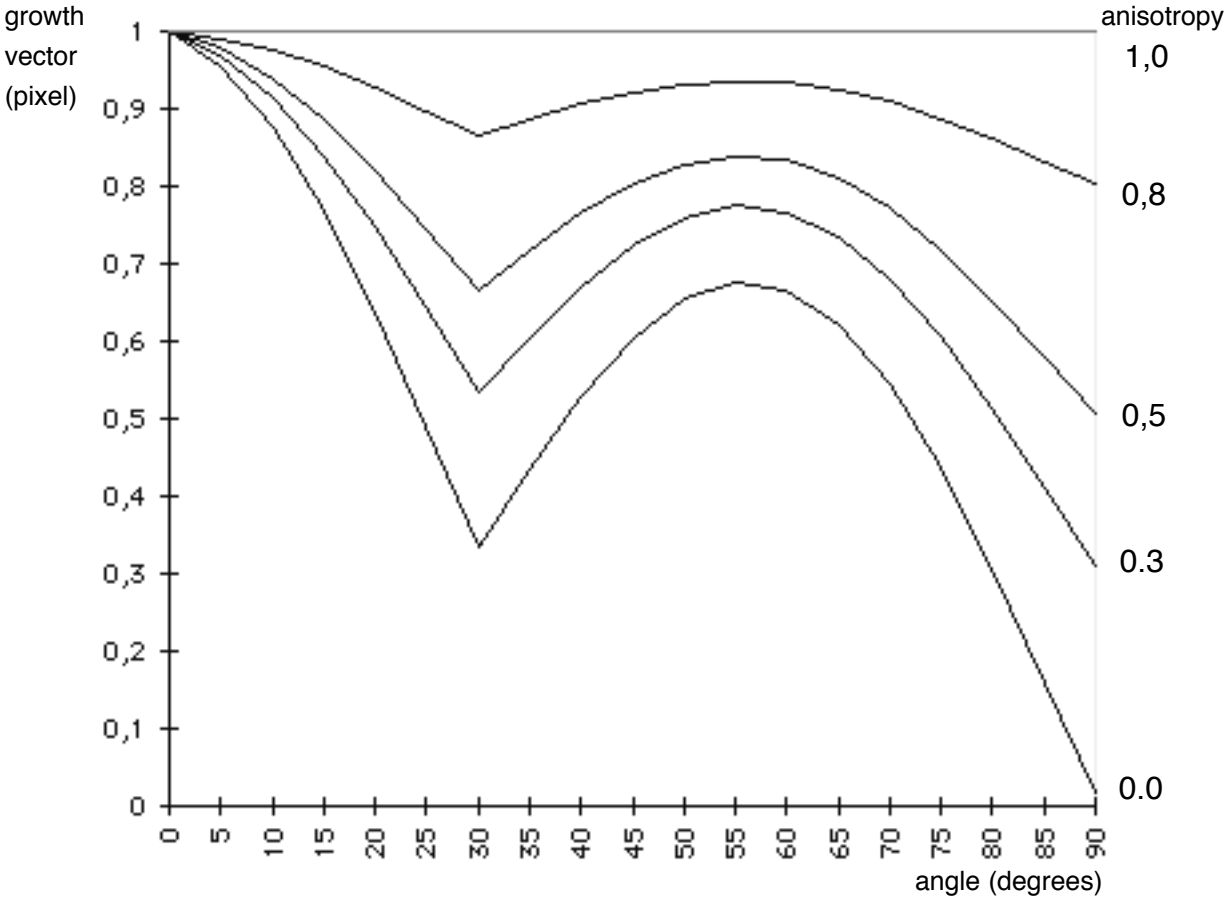

Fig. 6.13 Growth rate functions for a prismatic mineral used in the simulations for different anisotropies in growth rate (1.0 - 0.0). 1.0 is isotropic growth and 0.0 maximum anisotropic growth.

Any two-dimensional crystal shape can be created by the user.

6.1.4.2. "Fringe Growth" settings

The settings of the program "Fringe Growth" can be changed any time during a simulation. This can be done under the menu item "Fringe Growth" -> "Change Settings". A window appears on the screen that contains the current settings of the simulation (Fig. 6.14). These settings are:

(1) Number of stages (integer): This number gives the number of growth stages (of crystals in the fringe) that the program will run through during a simulation. The simulation stops once the program reaches this number, but can be continued by increasing the Number of stages in the settings.

(2) Save picture every N stages (integer): This parameter determines (a) how often a picture of the growing fringe is saved automatically and (b) how often a picture of the growing fringe is drawn on the screen (also if pictures are not saved automatically). For large simulations >8000 growth stages this number should be set to 200-500, otherwise memory problems might occur depending on how much

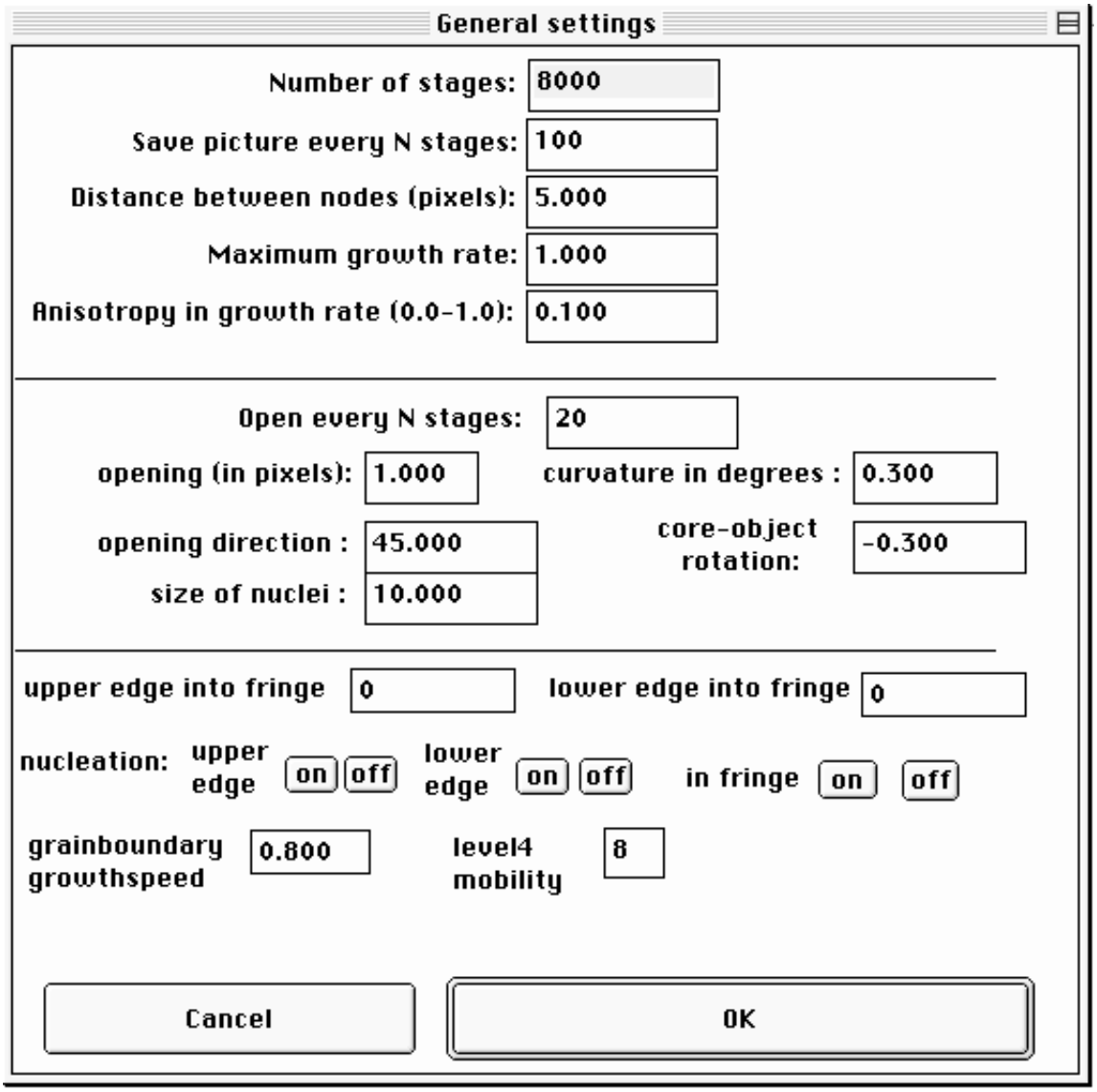

Fig. 6.14 Settings dialog in ”Fringe Growth” with default settings

memory the user allocated to "Fringe Growth" because the program will open a new window everytime it draws a fringe if the pictures are not saved automatically.

(3) Distance between nodes (double): This number is important for the resolution of the picture on the screen. If the distance between two nodes is larger than the given value a node will be added between the two nodes and if the distance is smaller than half the given value one of the nodes will be removed. The Maximum growth rate of crystals (parameter 4) has to be at least one fourth or one fifth of the Distance between nodes to avoid errors. A distance of 5.0 gives a resonable resolution. A distance of 3.0 and a Maximum growth rate of 0.5 result in a better tracking capability and smaller fibres, but the required RAM (number of nodes) increases significantly and simulations take longer.

(4) Maximum growth rate (double): The crystal growth file will be normalized to this

number. It indicates the maximum growth increment of the fastest growing face of a crystal in pixel.
(5) Anisotropy in growth rate (double): The Crystal file function can be smoothened with this function. The value 0.0 does not influence the Crystal file function whereas the value 1.0 results in isotropic growth. Values 0.1 to 0.9 smoothen the Crystal file function progressively (final growth vector=anisotropy + growth vector (from crystal file) multiplied by (1.0 - anisotropy)) (Fig. 6.13). The user can influence the anisotropy of crystals during a run of the program with this number.
(6) Open every N stages (integer): A value that gives the number of crystal growth stages between fringe opening events.
(7) opening (double): This number indicates the magnitude (in pixel) that the fringe will open during a single opening event.
(8) opening direction (double): The direction of fringe opening is given by this value in degrees. 0° is opening parallel to the horizontal of the screen. Clockwise counted angles are positive.
(9) size of nuclei (double): This number indicates how wide the first nuclei will be and how wide a grain on the rim of the fringe can grow before a new nucleus is inserted.
(10) curvature in degrees (double): This value gives a permutation angle (in degrees) that the fringe opening direction will change each opening event.
(11) core-object rotation (double): This number indicates the angle (in degrees) that the core-object will rotate around its centre each opening event. Clockwise core-object rotation is negative.
(12) upper edge into fringe/lower edge into fringe (integer): The width of the fringe relative to the width of the core-object can be influenced with this number. Normally the fringe in "Fringe Growth" will tend to be as wide as the core-object. This may not be realistic in nature (Fig. 6.15). The value indicates how many nodes of the core-

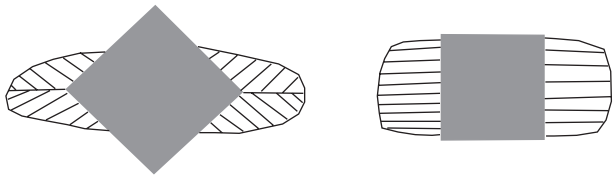

Fig. 6.15 Drawing of fringes around differently oriented cubic pyrites (example from the Eifel, Germany). The fringes are not as wide as the core-object.

object the boundary of the fringe will move inwards (smaller fringe) along the core-object. The value is dependent on the number of nodes that define the core-object. Problems can occur with very complex core-objects with pronounced corners so that the boundary conditions of the program will create errors.

(13) nucleation upper edge/lower edge: This value is switched off in the default settings. If it is switched on nucleation on the fringe rim is partly turned off and the connection of the fringe to the core-object is stationary.
(14) nucleation in fringe: This value is only available in "Fringe Growth 2.0". It is switched off in the default settings. Once it is switched on grains are nucleated in the fringe on triple points on the growth surface of grains.
(15) grain boundary growth speed (double): Grain boundaries (triple nodes) are growing slower and dissolving faster in the default settings of "Fringe Growth". In nature this effect is probably due to a higher energy of grain boundaries. The growth speed of triple nodes relative to double nodes is expressed in percent in "Fringe Growth" (80% in the default settings).
(16) level 4 mobility (integer): Level (or activity) 4 nodes are nodes that connect the fringe with the core-object. To determine if the fringe is still connected with the right node on the core-object the program checks the angle between the rim of the fringe and the core-object surface (see section 6.1.3.). Since different core-objects are made up of different numbers of nodes and have different roughnesses the number of nodes that describe an enveloping core-object surface change. This can be influenced with the level4mobility since this number gives the number of nodes on the core-object surface that will be used to do an angle check. Higher numbers result in better averages if core-objects are complex. This number should not exceed 50.
Note that the program does not check whether or not the input values are reasonable! Thus the program might crash if the user enters unreasonable or contradictory settings.

6.1.4.3. Generating core-objects

The user can generate four core-objects with predefined shapes, smooth round, rough round, smooth square and rough square objects. The user can also create core-objects of any shape from scanned drawings of objects. Core-objects are generated under the menu item Make data set. If the user creates predefined core-objects the program will always include first nuclei assuming that the fringe opens at 45°. Manually created objects can be loaded without nulcei so that the sites of nucleation can be influenced before a simulation is started.
Make smooth cube: If the user activates this menu item the program opens a window ”give settings for new object” (Fig. 6.16). The user can enter the number of grains (first nuclei) and the width of these nuclei. These values also determine the size of the core-object (number of grains multiplied by width of grains = length of one side of square). The number of grains should be an even number. Nucleation takes place on two faces of the core-object so that the final number of grains is number of grains

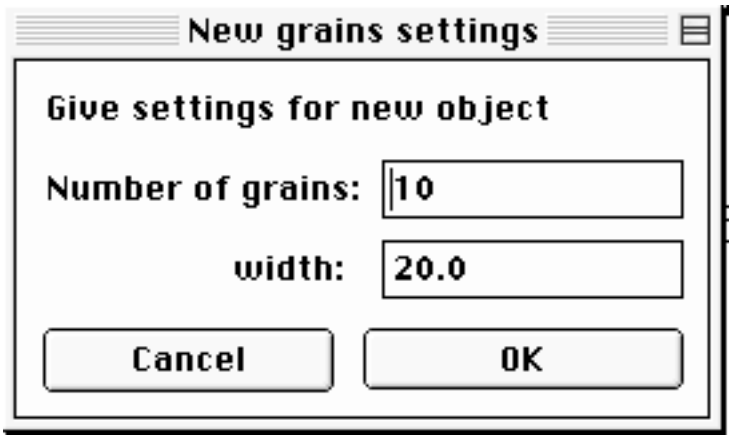

Fig. 6.16 Settings dialog in ”Fringe Growth” for new core-objects.

times two.

Make rough cube: The first window that will appear is the same as that for smooth objects. Then a second window will appear: ”give roughness of object”. The object roughness gives the number of asperities on one object face divided by two and the amplitude is given in pixel (Fig. 6.17).

Make smooth round object: If the user activates this menu item the program opens a

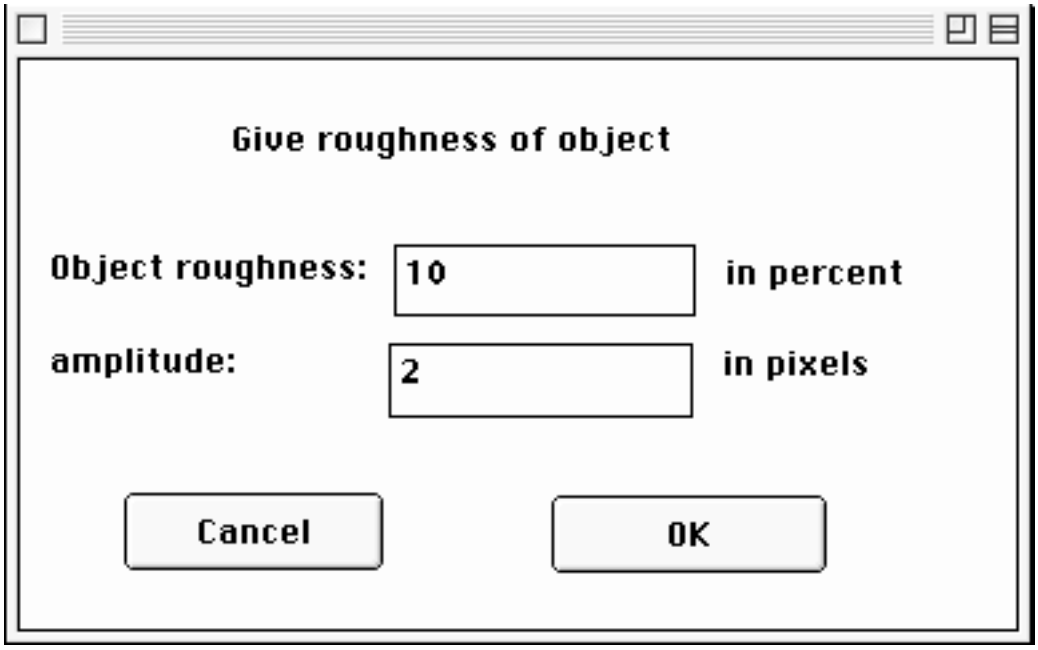

Fig. 6.17 Settings dialog in ”Fringe Growth” for the roughness of new core-objects.

window ”give settings for new object”. In the case of round objects only the item number of grains is important (number of final grains is number of grains times two). Now the program asks for the radius of the core-object in pixel. This radius will influence the size of the first grains.

Make rough round object: The first part of this process is the same as that for smooth

round objects. After the radius and the number of nuclei are entered the program will ask for the roughness of the core-object. Amplitude is ampltiude of asperities in pixel. Number of asperities per core-object is 100 divided by the roughness.

Make manual: To load self created objects into "Fringe Growth" a text file of the object has to be created that can be read by "Fringe Growth". The picture saved as text file should have a width of 400 pixel and a height of 300 pixel. The core-object can be drawn using a simple graphics program (e.g. Canvas, NIH-image, Freehand or Illustrator). Only the outline of the object is needed. The roughness of the core-object has to be adjusted so that fibres track displacement (natural core-objects have relatively "small" roughnesses, normally too small for the resolution of the program). The pen size of the outline should be very small (hairline, black). Now a file can be opened in NIH-image with the size: width = 400, height = 300 and the object can be transferred to NIH-image with copy and paste. The core-object should just fit the window (adjust size before copying it into NIH-image). Now the file can be saved into the same folder as "Fringe Growth" as ”text only” format. To read the file with "Fringe Growth" the program has to convert the ”text file” into a ”node file”. This is done under the menu Make data set -> Make manual. The program first asks if the user wants to include first nuclei or not. If the user wants to include first nuclei the size and number of nuclei have to be given and the text file has to be opened. The "duck" walks while the core-object is drawn (Fig. 6.18). It can now be saved in the Fringe Growth folder. If the user does not want the object to have nuclei from the beginning, the ”text file” is

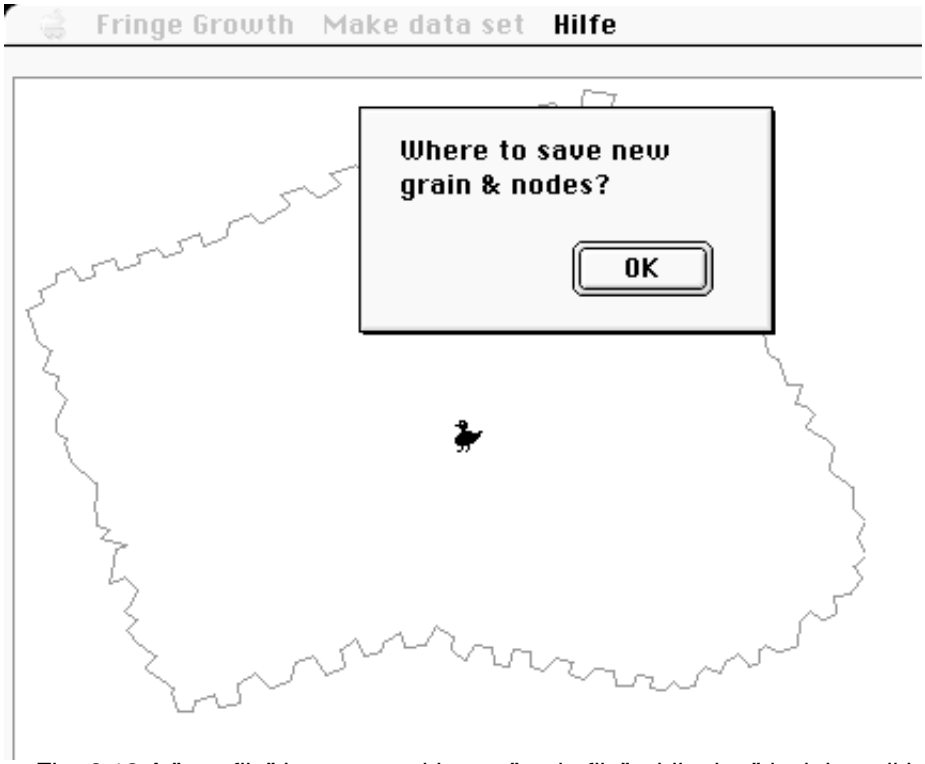

Fig. 6.18 A ”text file” is converted into a ”node file” while the ”duck is walking”.

opened and only the core-object can be saved . It is not recommended to create core-objects with nuclei since (1) a number of problems occur if core-objects are rough and (2) the starting position of first nuclei cannot be changed. Core-object files of rough and complex core-objects have to be corrected most of the time. This correction is explained in section 6.1.4.4. A number of different core-objects are included in the "Fringe Growth" folders on the CD-Rom. The creation of additional core-object node-files is in progress, these will be collected and can be downloaded from the Mainz-Tectonophysik WWW-site in the near future. NIH-image is freeware and can be downloaded from the NIH-image WWW-page.

6.1.4.4. Problems that can occur using "Fringe Growth"

The program "Fringe Growth" is not entirely bug-free nor does it have a security for inappropriate input. If the user enters inappropriate settings or input files the program might crash. The program checks a limited number of situations where a crash might occur and gives a warning. Once you press OK on this warning the program will exit and all data (that have not been saved) will be lost. These emergency exits have been included to prevent crashes and indefinite loops. But there might still be some situations where the program crashes without warning. If the program is in an indefinite loop (nothing happens anymore and the screen might flicker) press "ALT" "APPLE" "ESC" to exit the program (emergency exit).

Curling grains: Grains in "Fringe Growth" cannot grow into each other but they may still grow into themselves. This usually happens shortly after the nucleation in the beginning of a simulation. Curling grains will have a white colour. If this happens in the beginning the program sometimes corrects itself. If it is not doing that the simulation should be stopped since curling grains produce an error in the fringe so that grain boundaries cannot be knitted together. As long as the wrong grain boundary is in the fringe it just takes up calculation time but as soon as it approaches a suture line or the rim of the fringe nucleation will be inhibited and errors might accur so that the program crashes or stops by itself.

Fringe boundary is stationary: If the core-object has pronounced corners the fringe boundary sometimes will get locked behind corners. In order to unlock it the level4mobility should be increased (not over 50).

Memory problems: If the program draws a whole new picture of the fringe without colours the program has insufficient RAM available. In this case the memory allocated to the program should be increased and/or fewer pictures of the growing fringe should be drawn. To save the active simulation a number of windows have to be clicked away (works only if pictures are not saved automatically), the fringe has to be redrawn and can now be saved as picture. Open windows can also be saved by pressing buttons

in the combination shown in Fig. 6.19 (saves snapshots of screen or parts of screen). Dissolution/nucleation in fringe: "Fringe Growth 2.0" can dissolve grains and can

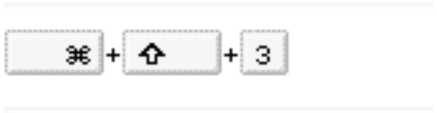

Snapshot of whole screen.

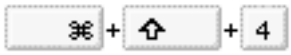

After pressing these buttons the outline of the picture to be saved can be defined by the cursor.

Combination saves picture of one window. After pressing buttons the user has to click into the window to be saved.

Pictures will be saved on the Start-Volume

Fig. 6.19 Combinations of buttons to save pictures on the screen directly with an APPLE-computer (from Apple-Help menu, MacOS 8.5).

nucleate grains inside the fringe. A number of problems exist with these routines so that sometimes simulations cannot be finished. Leaving the nucleation turned off creates less problems. Higher resolutions always create more problems and are prone to crash. It is recommended that during large simulations the pictures are saved automatically so that if the program exits not all data are lost.

Creation of core-objects: Node files created from images of complex core-objects are prone to cause errors. They have to be corrected with a text-editor. After opening the file the user has to check the node-data. The x-y coordinates of the nodes have to be in a series without major changes (normally within 1 to 4 pixel). Normally the last hundreds of nodes (complex object files contain 1000 + nodes) do not fit into the series, they have sudden changes in x-y data. These nodes have to be deleted (delete lines) and the last node in the list has to be connected to the first node.

Example of a wrong node file: (wrong data is highlighted)

20264
You can write text here and anywhere before the cross-hatch.
Do not add or delete any cross-hatch in this file. #
6 The index for the object #
0 0 400 500 The outline of the work area; last number can be changed #
3 The number of grains in this list #
The grain data (index, mineral type, number of nodes, lattice orientation) #
1 0 0 0.0
2 0 **1095** 0.0
3 0 **1095** 0.0
1095 The number of nodes in this list #
The node data (index, location, number of neighbours, 3 neighbouring nodes,3 neighbouring grains, activity status) #

1	213.00	166.00	2	**1095**	2	0	2	3	0	5
2	212.00	167.00	2	1	3	0	2	3	0	5
3	211.00	168.00	2	2	4	0	2	3	0	5
4	210.00	168.00	2	3	5	0	2	3	0	5
5	209.00	169.00	2	4	6	0	2	3	0	5
6	208.00	170.00	2	5	7	0	2	3	0	5
etc....										
1080	215.00	167.00	2	1079	1081	0	2	3	0	5
1081	214.00	167.00	2	1080	1082	0	2	3	0	5
1082	214.00	167.00	2	1081	1**083**	0	2	3	0	5
1083	**90.00**	**223.00**	**2**	**1082**	**1084**	**0**	**2**	**3**	**0**	**5**
1084	**109.00**	**210.00**	**2**	**1083**	**1085**	**0**	**2**	**3**	**0**	**5**
1085	**116.00**	**207.00**	**2**	**1084**	**1086**	**0**	**2**	**3**	**0**	**5**
1086	**121.00**	**205.00**	**2**	**1085**	**1087**	**0**	**2**	**3**	**0**	**5**
1087	**149.00**	**188.00**	**2**	**1086**	**1088**	**0**	**2**	**3**	**0**	**5**
1088	**158.00**	**183.00**	**2**	**1087**	**1089**	**0**	**2**	**3**	**0**	**5**
1089	**158.00**	**183.00**	**2**	**1088**	**1090**	**0**	**2**	**3**	**0**	**5**
1090	**75.00**	**248.00**	**2**	**1089**	**1091**	**0**	**2**	**3**	**0**	**5**
1091	**74.00**	**259.00**	**2**	**1090**	**1092**	**0**	**2**	**3**	**0**	**5**
1092	**68.00**	**355.00**	**2**	**1091**	**1093**	**0**	**2**	**3**	**0**	**5**
1093	**68.00**	**355.00**	**2**	**1092**	**1094**	**0**	**2**	**3**	**0**	**5**
1094	**0.00**	**355.00**	**2**	**1093**	**1095**	**0**	**2**	**3**	**0**	**5**
1095	**0.00**	**355.00**	**2**	**1094**	**1**	**0**	**2**	**3**	**0**	**5**

The last thirteen nodes in this file are wrong, their x-y data is not consistent (sometimes there may be more than 400 wrong nodes in large files). The x-y data of node 1082 fits to the data of the first node. Therefore 1082 can be used as last node and nodes 1083 to 1095 can be deleted. Then node 1082 has to be connected to node one and the number of nodes has to be adjusted.

Corrected node file:

20264
You can write text here and anywhere before the cross-hatch.
Do not add or delete any cross-hatch in this file. #
6 The index for the object #
0 0 400 500 The outline of the work area; last number can be changed #
3 The number of grains in this list #
The grain data (index, mineral type, number of nodes, lattice orientation) #
1 0 0 0.0
2 0 **1082** 0.0
3 0 **1082** 0.0
1082 The number of nodes in this list #
The node data (index, location, number of neighbours, 3 neighbouring nodes,3 neighbouring grains, activity status) #

1	213.00	166.00	2	**1082**	2	0	2	3	0	5
2	212.00	167.00	2	1	3	0	2	3	0	5
3	211.00	168.00	2	2	4	0	2	3	0	5
4	210.00	168.00	2	3	5	0	2	3	0	5
5	209.00	169.00	2	4	6	0	2	3	0	5
6	208.00	170.00	2	5	7	0	2	3	0	5
etc....										
1080	215.00	167.00	2	1079	1081	0	2	3	0	5
1081	214.00	167.00	2	1080	1082	0	2	3	0	5
1082	214.00	167.00	2	1081	**1**	0	2	3	0	5

If changes in the x-y coordinates occur within the list and not at the end a new node file has to be created from a new text file. For this case the core-object should be shifted or rotated by a minor amount.

6.1.5. Settings used in experiments

Simulation presented in Chapter 3 of this thesis were perfomed with "Fringe Growth 1.3", simulations presented in Chapter 4 were preformed with "Fringe Growth 2.0".

Simulations presented in Chapter 3:

(I) Simulations with straigh object-centre paths.
(II) Simulation presented in Fig. 3.7.
(III) Simulation presented in Fig. 3.8.
(IV) Simulation presented in Fig. 3.9.

simulation settings:	(I)	(II)	(III)	(IV)
Number of stages:	8000	12000	18000	14000
Distance between nodes:	5.0	5.0	3.0	5.0
Maximum growth rate:	1.0	1.0	0.5	1.0
Anisotropy in growth rate:	0.1	0.1	0.1	0.1
Open every N stages:	20	20	30	20
opening:	0.8 -1.0	1.0	0.4	1.0
opening direction:	45	45,75	starts 45	starts 45
size of nuclei:	10.0	10.0	0.8	0.8
curvature:	0.0	0.0	0.3	0.2
core-object rotation:	0.0	0.0	-0.5	-0.7
upper/lower edge into fringe:	0	0	0	50
grain boundary growth speed:	80	80	80	80

Simulations presented in Chapter 4:

Simulations presented in Chapter 4 were performed with the following settings:

Number of stages:	12000-20000
Distance between nodes:	5.0
Maximum growth rate:	1.0
Anisotropy in growth rate:	0.1
Open every N stages:	20-40
opening:	0.7-1.0
opening direction:	varies
size of nuclei:	0.6-0.8
curvature:	0.0
core-object rotation:	varies
upper/lower edge into fringe:	100-200 in the beginning, then set to 0
grain boundary growth speed:	80

about 400 to 800 fringe opening events per simulation

Object-centre paths were used for the simulations so that the opening direction and the core-object rotation relative to the fringes were adjusted manually (trace object-centre path on screen). Core-objects were rotated into the right positions and increased up to 200% in size. Nucleation in the fringe was turned on except for the simulation of object IV. Level4mobility was set to 35 to 45.

6.2. CD-ROM

A CD-ROM is attached to this thesis. It contains Quicktime movies of simulations with ”Fringe Growth” illustrating progressive fibre growth and the programs ”Fringe Growth 1.3” and ”Fringe Growth 2.0” for Macintosh PPCs.

Curriculum Vitae

Daniel Koehn

Personal details:	born 28.12.1969 married to Vera (10.10.1998) son Lennart (born 4.5.1999)
1986-1987	exchange student in Harrison, Michigan, High-School Diploma, National Honors Society
1990	German Gymnasium Diploma, Majors in Maths, Biology and English (Staatliches Gymnasium Wörth am Rhein)
1990-1991	German Army and Civil Service
1991 onwards	study of geology (Diploma) at the University of Karlsruhe
1995-1996	study at the University College Cork, Ireland, 4th and 3rd year courses with emphasis on structural geology and metamorphic petrology
1996-1997	further studies at the University of Karlsruhe
October 1997	Diploma at the University of Karlsruhe, Majors in Structural Geology and Engineering Geology, Minors in Geophysics and Petrology. Diploma thesis on the structural geology of the Lhomme valley in Belgium (Variscan fold belt). First class honors.
November 1997 till present	Phd at the University of Mainz, supervisor Cees W. Passchier, title "The kinematics of fibrous aggregates", DFG project.
Spring 1998	visit to the EPSILON Lab at the University of Monash, Australia, to program part of the program "Fringe Growth" with Paul Bons and Mark Jessell. Field work in the Flinders Ranges with Paul Bons.
Summer 1998	field work with Giancarlo Molli of the University of Pisa in Sestri Levante (Italy).
Fall 1998	attending the short course "Veins in low temperature environments" at the GSA meeting in Toronto.
Spring 1999	visit to the University of Salamanca to numerically simulate fibre growth in strain fringes from Lourdes with the program "Fringe Growth" with Domingo Aerden.